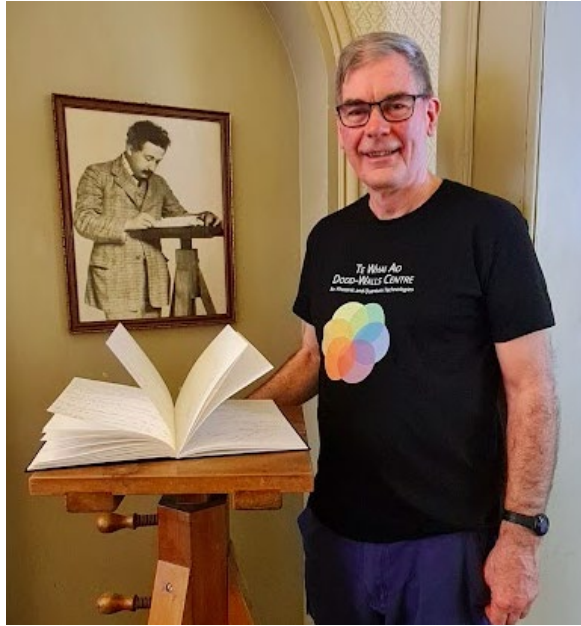


Making Sense of Rare Earth Electronic Structure. A Tutorial.



Chongqing, November 2024

Mike Reid

University of Canterbury

Christchurch

New Zealand

mike.reid@canterbury.ac.nz

<https://www2.phys.canterbury.ac.nz/~mfr24/>



TE WHAI AO
DODD-WALLS CENTRE

for Photonic and Quantum Technologies



Quantum
Technologies
Aotearoa



Fred Richardson

June 8, 1939 – April 25, 2024

ANISOTROPIC LIGAND POLARIZABILITY CONTRIBUTIONS TO LANTHANIDE $4f \rightarrow 4f$ INTENSITY PARAMETERS

Michael F. REID and Frederick S. RICHARDSON

Department of Chemistry, University of Virginia, Charlottesville, Virginia 22901, USA

Received 18 October 1982; in final form 16 December 1982

CHEMICAL PHYSICS LETTERS

18 March 1983

The $A_{fp}\Xi(t, \lambda)$ parameterization scheme of the Judd–Ofelt $4f \rightarrow 4f$ intensity model is shown to be inadequate for representing effects due to optically *anisotropic* ligand dipolar polarizations. “Extra” intensity parameters are needed when the lanthanide–ligand pairwise interactions are not cylindrically symmetric. Selection rules regarding these “extra” parameters are derived, and their possible significance to the hypersensitivity phenomenon is discussed.

Excited-State Chiral Discrimination Observed by Time-Resolved Circularly Polarized Luminescence Measurements

David H. Metcalf,^{*,†} Seth W. Snyder,[†] Shuguang Wu,[§]
Gary L. Hilmes,[§] James P. Riehl,[§] J. N. Demas,[†] and
F. S. Richardson^{*,†}

J. Am. Chem. Soc. **1989**, *111*, 3082–3083



Sergey Feofilov



François Auzel



Georges Boulon

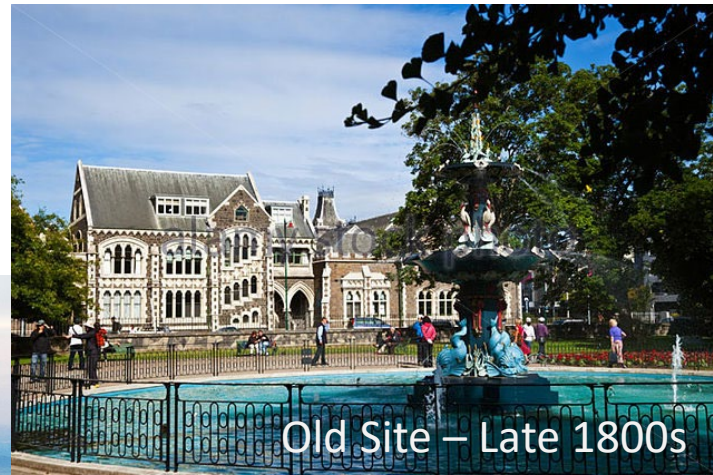


Alexander Kaplyanskii.

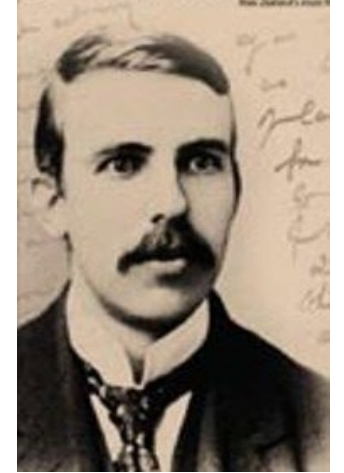
Interactions with Duan (2004) and Ma (2007)



Christchurch, New Zealand



Old Site – Late 1800s



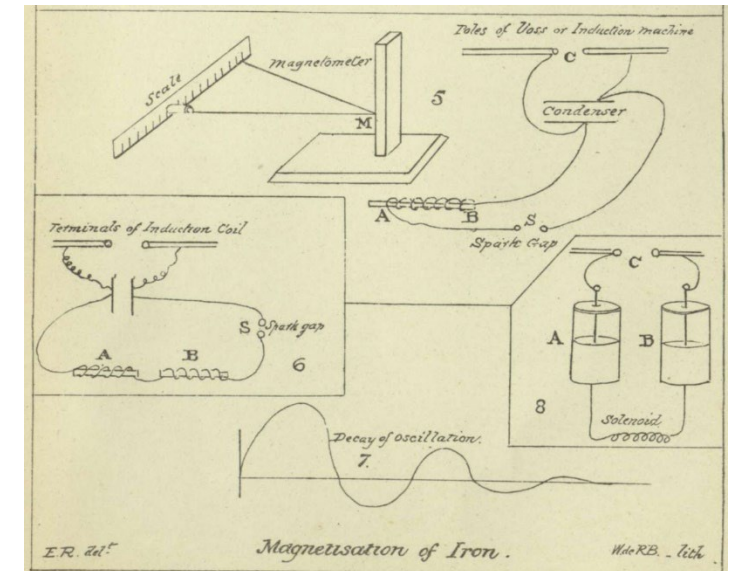
ART. LIX.—*Magnetization of Iron by High-frequency Discharges.*

By E. RUTHERFORD, M.A.

[*Read before the Philosophical Institute of Canterbury, 7th November, 1894.*]



1960s



Ernest Rutherford building, 2018



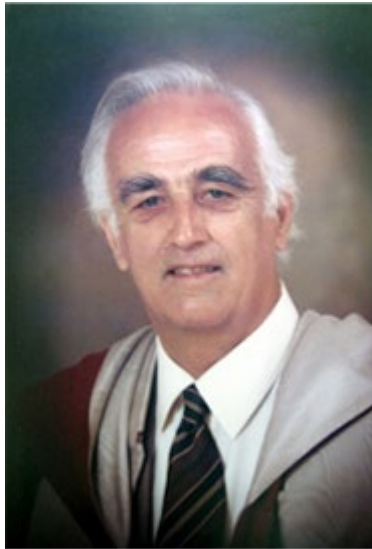
Mike Reid and Jon-Paul Wells: Our Motivation

- Develop fundamental knowledge relevant to practical applications of rare earths (lanthanides) in nano-particle imaging and quantum-information.
- Detailed understanding of spectroscopy, dynamics, electronic structure.
- Jon Wells also leads a project on ring-laser gyroscope development.



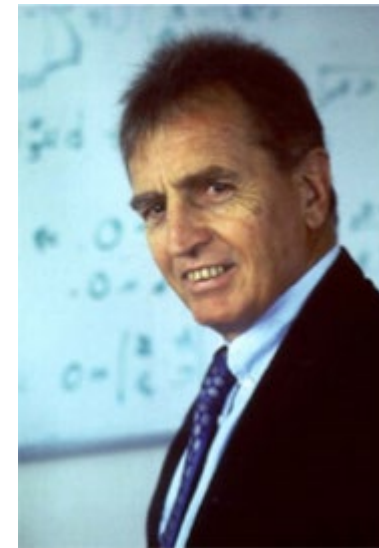
<https://www.otago.ac.nz/dodd-walls/index.html>

Jack Dodd



TE WHAI AO
DODD-WALLS CENTRE
for Photonic and Quantum Technologies

Dan Walls



Theory of Modulation of Light in a Double Resonance Experiment

J. N. Dodd and G. W. Series

Proceedings of the Royal Society of London.

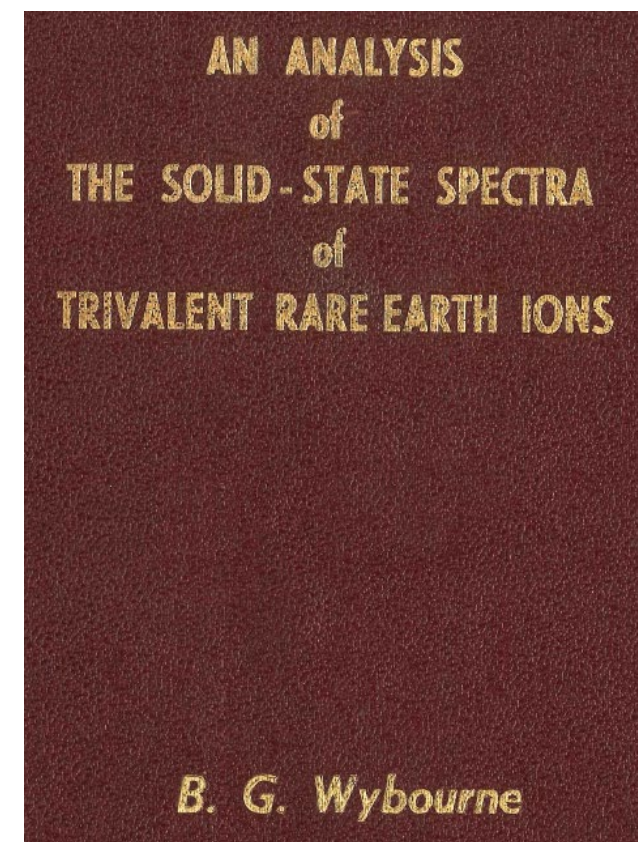
Series A, Mathematical and Physical Sciences

Vol. 263, 353 (1961)

Generation of squeezed states via degenerate four-wave mixing

M. D. Reid and D. F. Walls

Phys. Rev. A 31, 1622 (1985)



Brian Judd (1930-2023) George Ofelt (1937-2014) Brian Wybourne (1935-2003)



Roger Macfarlane



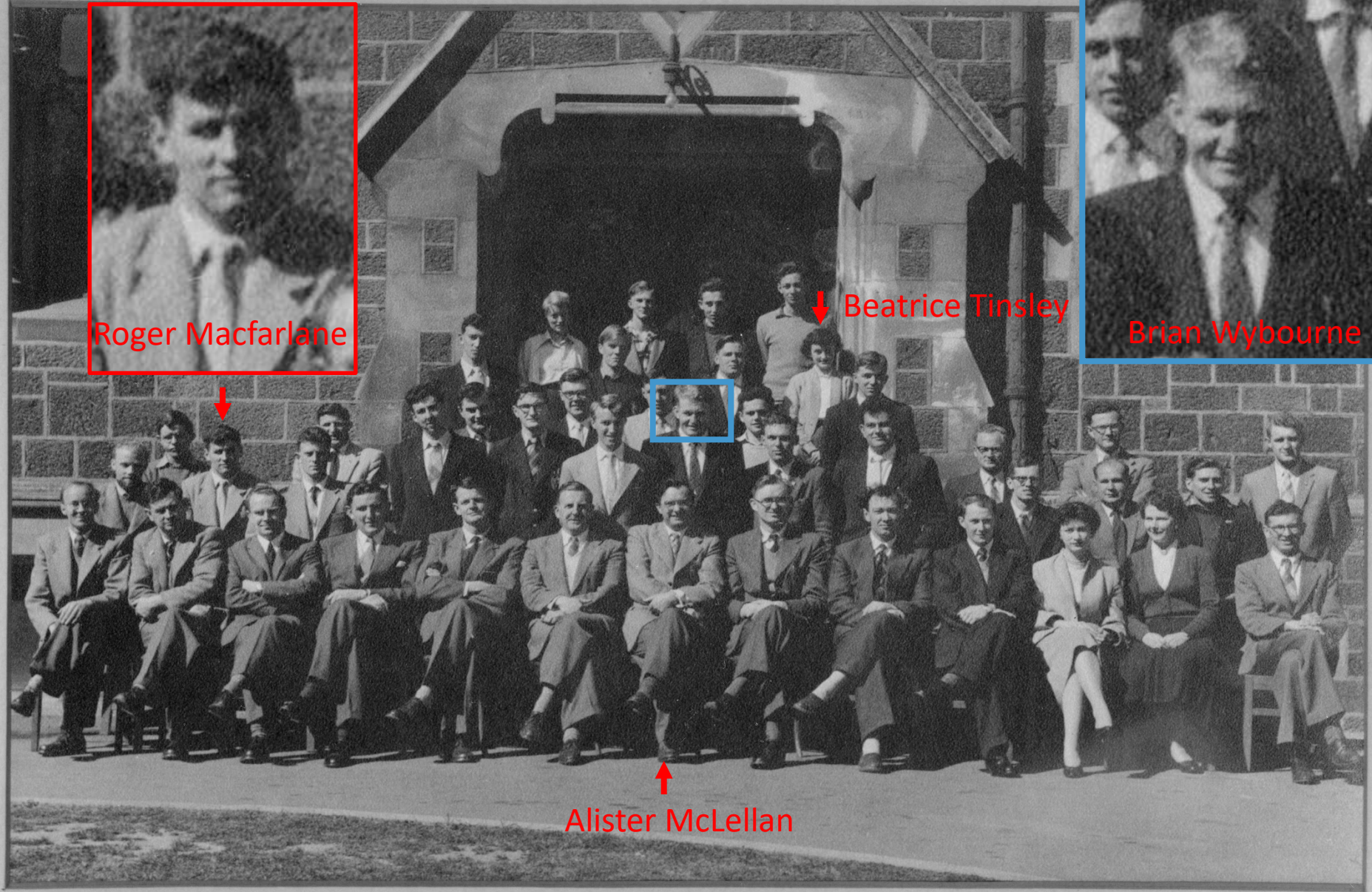
Brian Wybourne



Beatrice Tinsley



Alister McLellan



★ Physics Department ★
University of Canterbury
1959

Absent:
Glynn Jones
Rod Syme

Optical and Magnetic Properties of some Transition Ion Complexes. PhD 1963

R.M. Macfarlane

Physics Department

University of Canterbury.

R.M. Macfarlane.



SUB-KILOHERTZ OPTICAL LINEWIDTHS OF THE $^7F_0 \leftrightarrow ^5D_0$ TRANSITION IN $Y_2O_3:Eu^{3+}$

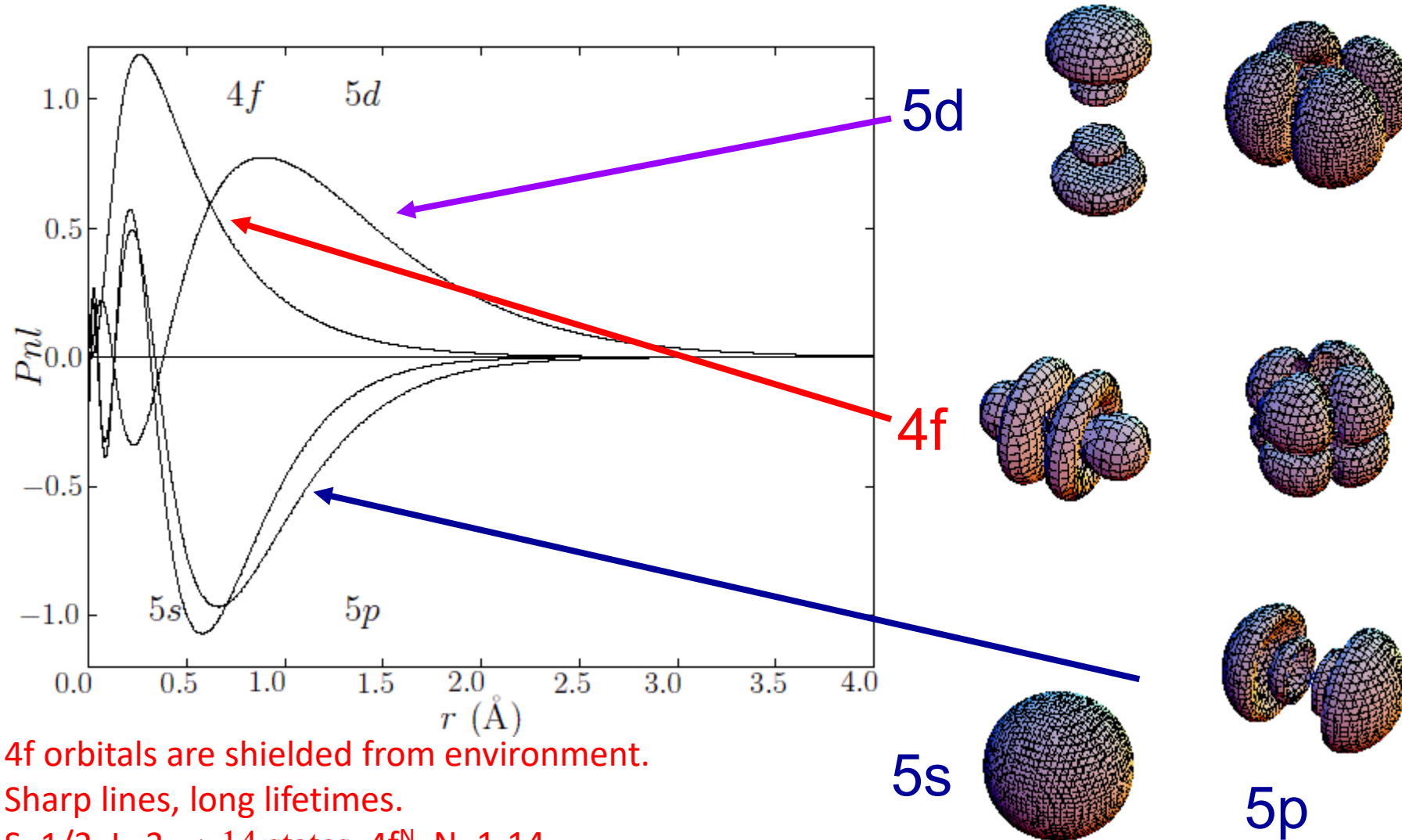
R.M. MACFARLANE and R.M. SHELBY

IBM Research Laboratory, San Jose, CA 95193, USA

Received 17 June 1981

Homogeneous optical linewidths as small as 760 Hz (fwhm) have been observed in $Y_2O_3:Eu^{3+}$ using delayed heterodyne photon echoes. Hyperfine and lifetime contributions to dephasing are estimated to contribute ≤ 300 Hz to this width, and the remainder is attributed to quasi-resonant energy transfer.

Lanthanide (Rare Earth) 3+ ground state: $5s^2 5p^6 4f^N 5d^0$



4f orbitals are shielded from environment.

Sharp lines, long lifetimes.

$S=1/2, L=3 \rightarrow 14$ states, $4f^N, N=1-14$

Many transitions available for applications.

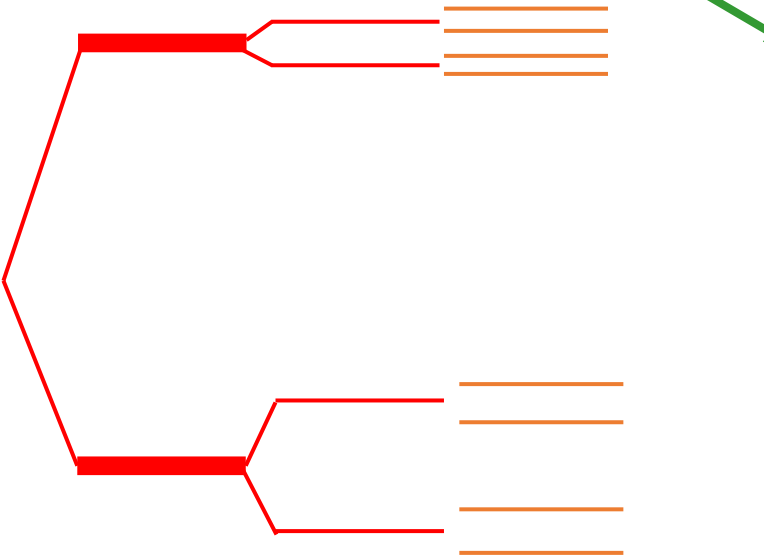
“Dieke Diagram” 1960s

Carnall, Goodman,
Rajnak, Rana, 1988

4f: $S=1/2, L=3, \rightarrow 14$ states
4f^N: N=1-14

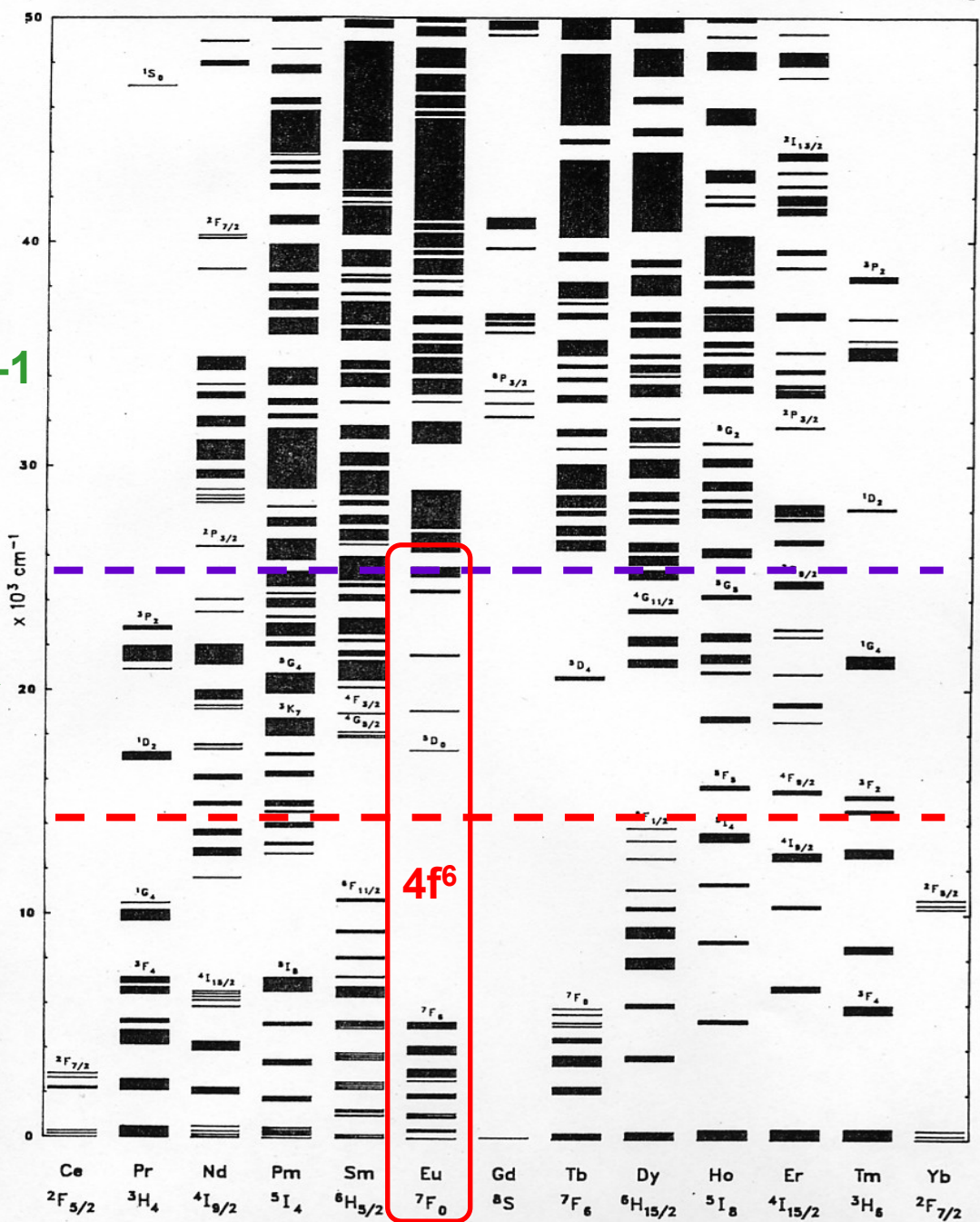
Eu³⁺, 4f⁶
3003 electronic states

20,000 cm⁻¹
500 nm
2.5 eV



Free ion Crystal Field Hyperfine/Magnetic

ENERGY LEVELS OF THE +3 LANTHANIDES IN LaF₃



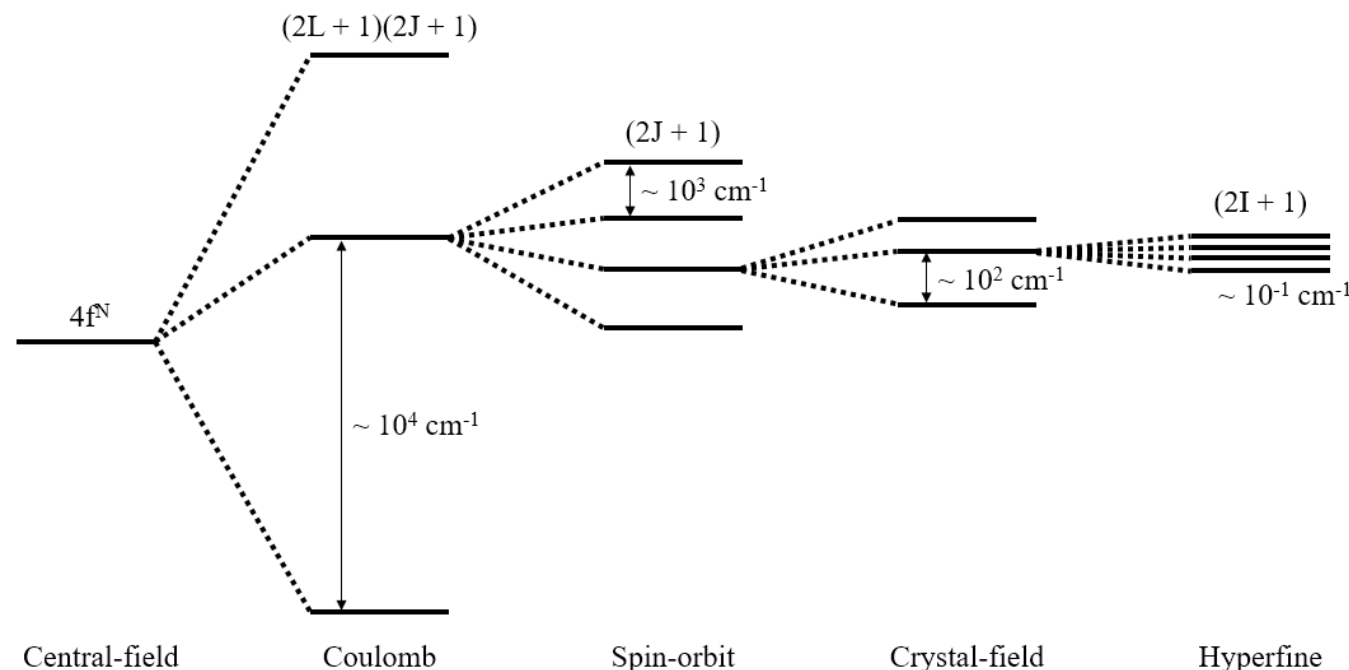
Modelling the $4f^N$ structure of rare-earth doped crystals

$$H = H_{FI} + H_{CF} + H_Z + H_{HF}$$

\swarrow Free Ion \swarrow Crystal Field \swarrow Zeeman \swarrow Hyperfine

$$H_{CF} = \sum_{k,q} B_q^k C_q^{(k)}$$

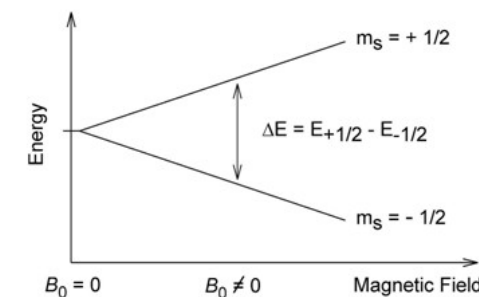
C_1 symmetry \rightarrow 27 crystal-field parameters



Zeeman

$$H_Z = \mu_B \mathbf{B} \cdot (\mathbf{L} + 2\mathbf{S})$$

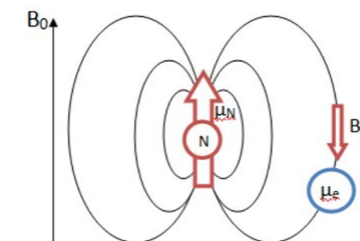
Magnetic field can be experimentally varied.



Hyperfine

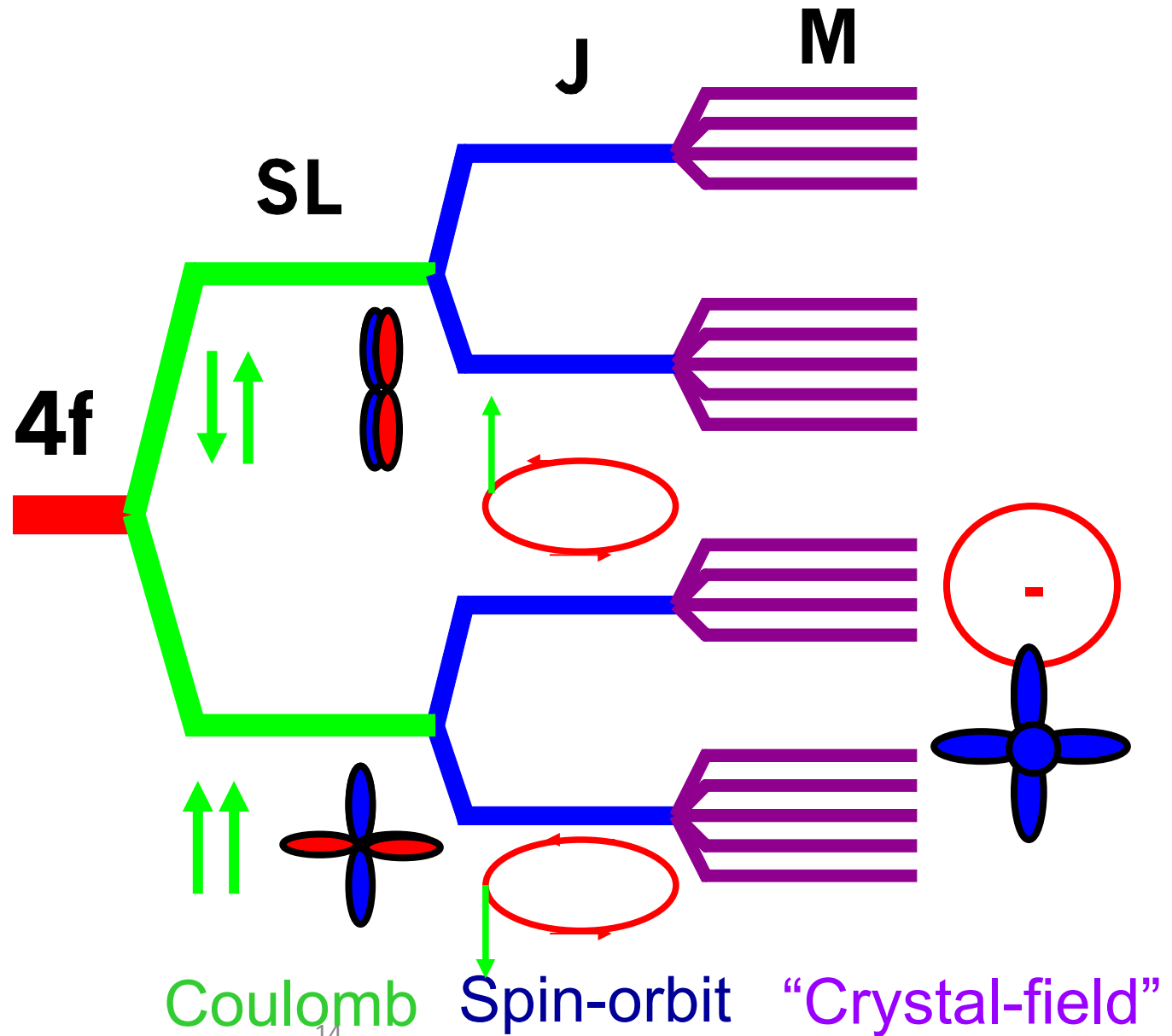
$$H_{HF} = A \mathbf{N} \cdot \mathbf{I} + Q H_Q$$

A and Q are parameters



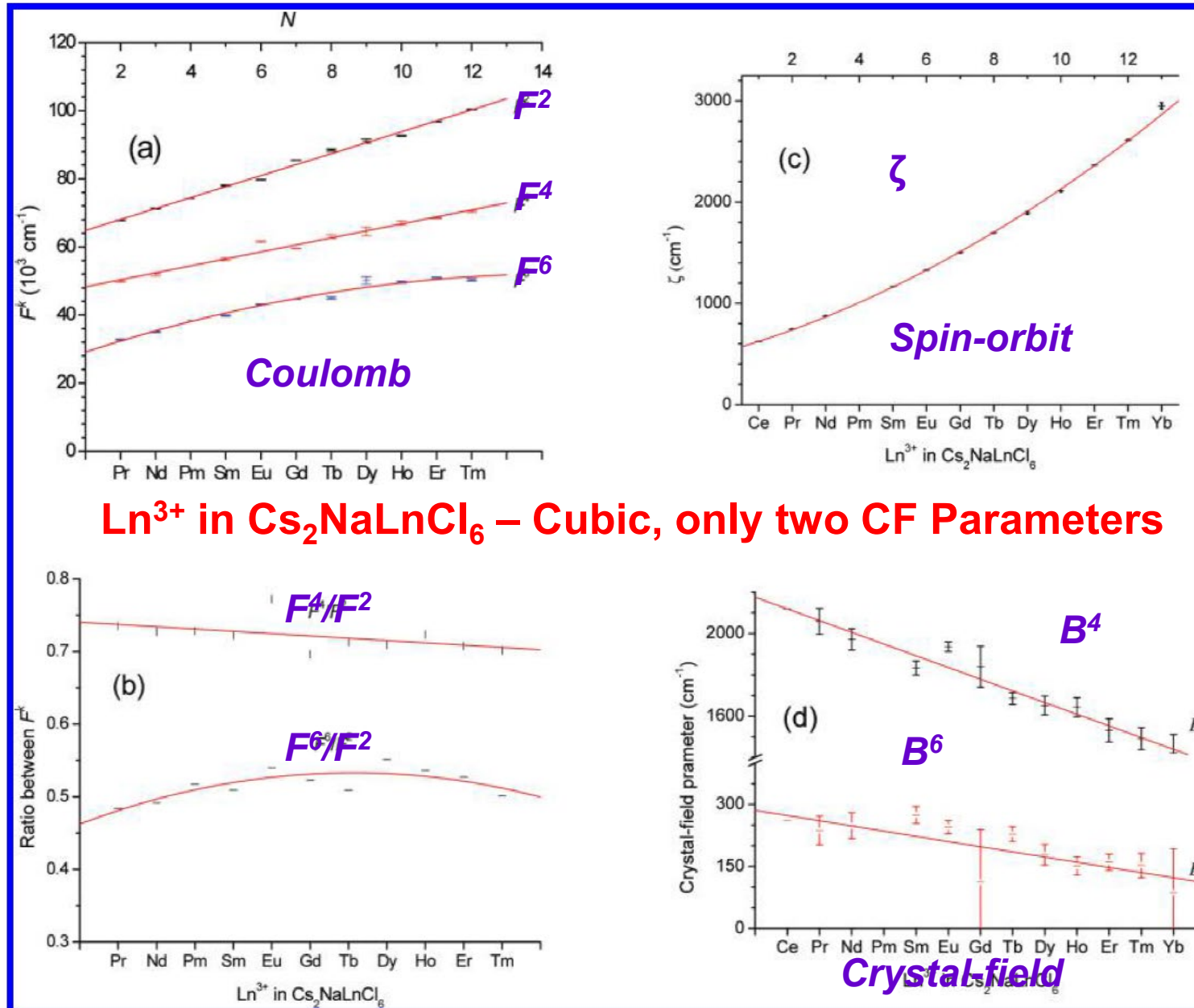
$\text{Eu}^{3+} {}^7F_0$ and 5D_0 : electronic effects are small so Direct interaction of nucleus with magnetic field and lattice are important.

Understanding the energy levels: $4f^N$



Parameter trends across the lanthanide series.

C-K Duan and P A Tanner, J. Phys. Chem. A, 2010, 114, pp 6055–6062



Ln³⁺ in Cs₂NaLnCl₆ – Cubic, only two CF Parameters

Angular momentum states and tensor operators

$$[J_x, J_y] = iJ_z, \quad \mathbf{J}^2 \equiv J_x^2 + J_y^2 + J_z^2$$

Rather than classifying states by eigenvalues and operators by commutators, it is helpful to classify both in terms of behaviour under rotations.

This is easier to relate to group representation theory.

$$J_z |jm\rangle = m |jm\rangle,$$

$$\mathbf{J}^2 |jm\rangle = j(j+1) |jm\rangle,$$

$$D(R) |jm\rangle = \sum_{m'} D_{m'm}^{(j)}(R) |jm'\rangle$$

$$[J_z, T_q^{(k)}] = q T_q^{(k)}$$

$$D(R) T_q^{(k)} D(R)^\dagger = \sum_{q'} D_{q'q}^{(k)}(R) T_{q'}^{(k)}$$

Wigner-Eckart theorem

$$\langle \alpha J M | T_q^{(k)} | \alpha' J' M' \rangle = (-1)^{J-M} \begin{pmatrix} J & k & J' \\ -M & q & M' \end{pmatrix} \langle \alpha J || T^{(k)} || \alpha' J' \rangle.$$

$$\langle \alpha J M | T_q^{(k)} | \alpha' J' M' \rangle = \langle J' M', k q | J M \rangle \frac{1}{\sqrt{2J+1}} \langle \alpha, J || T^{(k)} || \alpha', J' \rangle$$

Key idea: Matrix element = 3j symbol or Clebsch-Gordan coefficient x Reduced matrix element
“geometry” “physics”

Selection rules: $M' + q = M$ and $|J - J'| \leq k \leq J + J'$.

The easiest proof is to recall that operators transform as kets. We can therefore couple the operator and ket (up to a possible normalization):

$$|\alpha'', J'' M''\rangle \propto \sum_{q, M'} T_q^{(k)} |\alpha' J' M'\rangle \langle k q, J' M' | J'' M'' \rangle$$

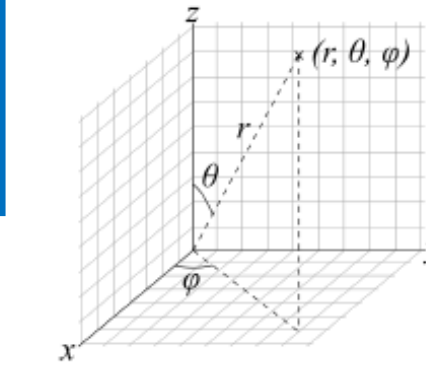
We can use orthogonality to obtain an expression for $T_q^{(k)} |\alpha' J' M'\rangle$ and derive the result.

Spherical Tensors: Potentials

$$Y_{lm}(\theta, \phi) = \sqrt{\frac{2l+1}{4\pi}} \sqrt{\frac{(l-m)!}{(l+m)!}} P_{lm}(\cos \theta) e^{im\phi}$$

$$C_q^{(k)}(\hat{\mathbf{r}}) = C_q^{(k)}(\theta, \phi) = \sqrt{\frac{4\pi}{2k+1}} Y_{kq}(\theta, \phi)$$

k	q	$C_q^{(k)}(x, y, z)$	$C_q^{(k)}(\theta, \phi)$
0	0	1	1
1	0	z/r	$\cos \theta$
1	± 1	$\mp \sqrt{\frac{1}{2}}(x \pm iy)/r$	$\mp \sqrt{\frac{1}{2}} \sin \theta e^{\pm i\phi}$
2	0	$\sqrt{\frac{1}{4}}(3z^2 - r^2)/r^2$	$\sqrt{\frac{1}{4}}(3 \cos^2 \theta - 1)$
2	± 1	$\mp \sqrt{\frac{3}{2}}z(x \pm iy)/r^2$	$\mp \sqrt{\frac{3}{2}} \cos \theta \sin \theta e^{\pm i\phi}$
2	± 2	$\sqrt{\frac{3}{8}}(x \pm iy)^2/r^2$	$\sqrt{\frac{3}{8}} \sin^2 \theta e^{\pm 2i\phi}$



Classical mechanics

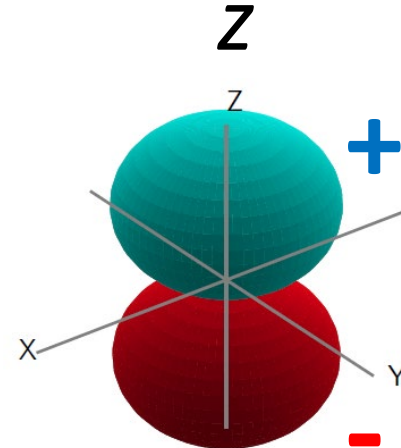
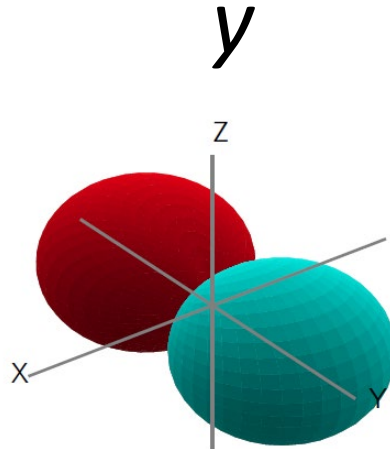
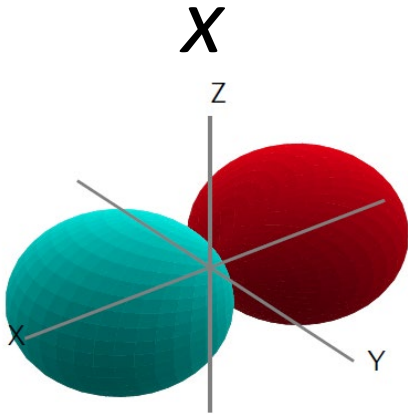


Electric and Magnetic Dipoles

$$-e\mathbf{r} = -er\mathbf{C}^{(1)}$$

$$x = r \frac{1}{\sqrt{2}} \left(-C_1^{(1)} + C_{-1}^{(1)} \right), \quad y = r \frac{i}{\sqrt{2}} \left(C_1^{(1)} + C_{-1}^{(1)} \right), \quad z = r C_0^{(1)}.$$

k	q	$C_q^{(k)}(x, y, z)$
0	0	1
1	0	z/r
1	± 1	$\mp \sqrt{\frac{1}{2}}(x \pm iy)/r$
2	0	$\sqrt{\frac{1}{4}}(3z^2 - r^2)/r^2$
2	± 1	$\mp \sqrt{\frac{3}{2}}z(x \pm iy)/r^2$
2	± 2	$\sqrt{\frac{3}{8}}(x \pm iy)^2/r^2$



$$\mathbf{B} \cdot \mathbf{J} = \sum_{i=x,y,z} B_i J_i.$$

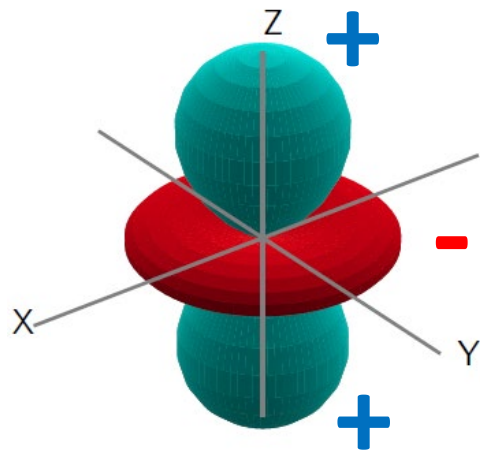
$$J_x = r \frac{1}{\sqrt{2}} \left(-J_1^{(1)} + J_{-1}^{(1)} \right), \quad J_y = r \frac{i}{\sqrt{2}} \left(J_1^{(1)} + J_{-1}^{(1)} \right), \quad J_z = r J_0^{(1)}.$$

Crystal Field Potential – Quantum Mechanical!

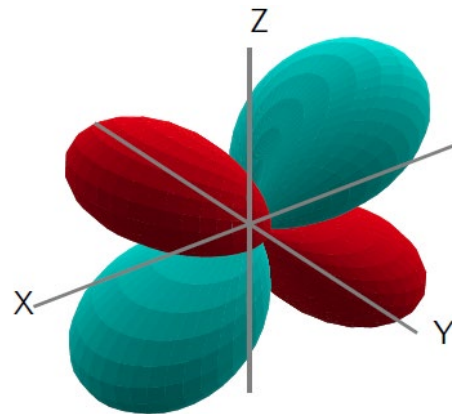
$$Y_{lm}(\theta, \phi) = \sqrt{\frac{2l+1}{4\pi}} \sqrt{\frac{(l-m)!}{(l+m)!}} P_{lm}(\cos \theta) e^{im\phi}$$

$$C_q^{(k)}(\hat{\mathbf{r}}) = C_q^{(k)}(\theta, \phi) = \sqrt{\frac{4\pi}{2k+1}} Y_{kq}(\theta, \phi)$$

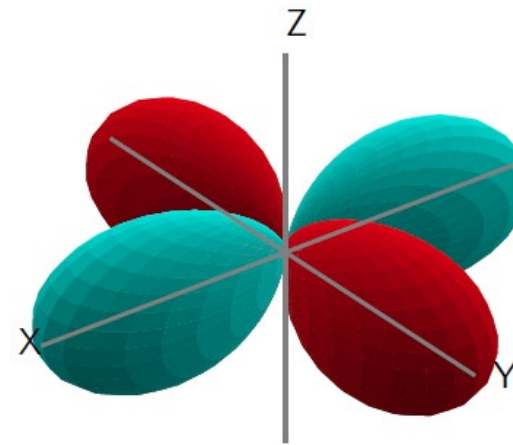
k	q	$C_q^{(k)}(x, y, z)$	$C_q^{(k)}(\theta, \phi)$
0	0	1	1
1	0	z/r	$\cos \theta$
1	± 1	$\mp \sqrt{\frac{1}{2}}(x \pm iy)/r$	$\mp \sqrt{\frac{1}{2}} \sin \theta e^{\pm i\phi}$
2	0	$\sqrt{\frac{1}{4}}(3z^2 - r^2)/r^2$	$\sqrt{\frac{1}{4}}(3 \cos^2 \theta - 1)$
2	± 1	$\mp \sqrt{\frac{3}{2}}z(x \pm iy)/r^2$	$\mp \sqrt{\frac{3}{2}} \cos \theta \sin \theta e^{\pm i\phi}$
2	± 2	$\sqrt{\frac{3}{8}}(x \pm iy)^2/r^2$	$\sqrt{\frac{3}{8}} \sin^2 \theta e^{\pm 2i\phi}$



$C_0^2(r)$



$C_1^2(r) - C_{-1}^2(r)$

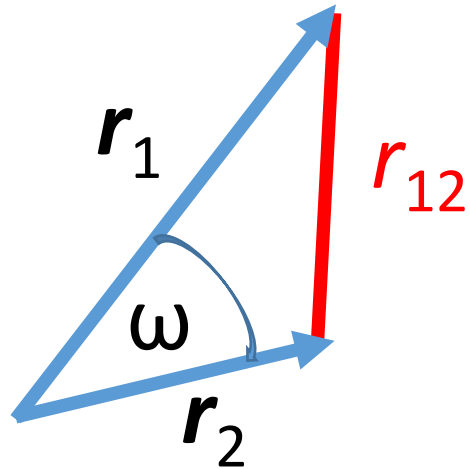


$C_2^2(r) + C_{-2}^2(r)$

$$H_{CF} = \sum_{k,q} B_q^k C_q^{(k)}$$

Note: Potential is **real**.
Phases of parameters
determine **orientation**,
e.g. $e^{iq\phi}$

Coulomb interaction and crystal field: Addition theorem



$$\begin{aligned} \frac{1}{r_{12}} &= \sum_{k=0}^{\infty} \frac{r_{<}^k}{r_{>}^{k+1}} P_k(\cos \omega) \quad \text{cos } \omega: -1..1 \\ &= \sum_{k=0}^{\infty} \frac{r_{<}^k}{r_{>}^{k+1}} C^{(k)}(\hat{\mathbf{r}}_1) \cdot C^{(k)}(\hat{\mathbf{r}}_2) \\ &= \sum_{k=0}^{\infty} \frac{r_{<}^k}{r_{>}^{k+1}} \sum_{q=-k}^{+k} C_q^{(k)}(\hat{\mathbf{r}}_1) C_{-q}^{(k)}(\hat{\mathbf{r}}_2) (-1)^q. \end{aligned}$$

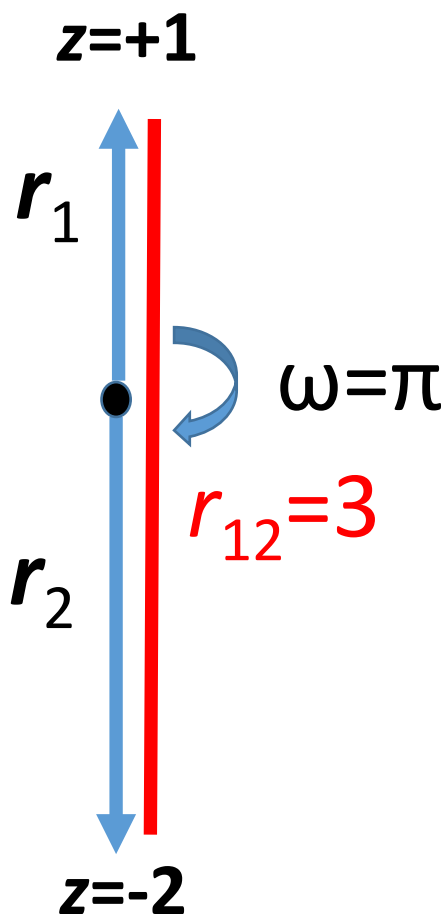
Key idea:
 $1/r_{12}$ is a function
of r_1 and r_2

Legendre Polynomials
orthogonal: -1..1

k	P_k
0	1
1	x
2	$(3x^2 - 1)/2$

k	q	$C_q^{(k)}(x, y, z)$
0	0	1
1	0	z/r
1	± 1	$\mp \sqrt{\frac{1}{2}}(x \pm iy)/r$
2	0	$\sqrt{\frac{1}{4}}(3z^2 - r^2)/r^2$
2	± 1	$\mp \sqrt{\frac{3}{2}}z(x \pm iy)/r^2$
2	± 2	$\sqrt{\frac{3}{8}}(x \pm iy)^2/r^2$

Addition Theorem - Example



$$1/r_{12} = 1/3 \quad \cos \omega = \cos \pi = -1$$

$$\begin{aligned} \frac{1}{r_{12}} &= \sum_{k=0}^{\infty} \frac{r_{<}^k}{r_{>}^{k+1}} P_k(\cos \omega) \\ &= \frac{1^0}{2^1} \times (1) + \frac{1^1}{2^2} \times (-1) + \frac{1^2}{2^3} \times \left(\frac{1}{2} (3 \times (-1)^2 - 1) \right) + \dots \\ &= \frac{1}{2} - \frac{1}{4} + \frac{1}{8} + \dots \end{aligned}$$

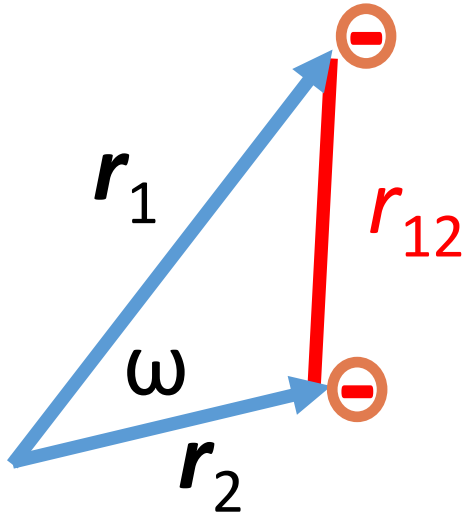
$$\begin{aligned} \frac{1}{r_{12}} &= \sum_{k=0}^{\infty} \frac{r_{<}^k}{r_{>}^{k+1}} \sum_{q=-k}^{+k} C_q^{(k)}(\hat{\mathbf{r}}_1) C_{-q}^{(k)}(\hat{\mathbf{r}}_2) (-1)^q \\ &= \frac{1^0}{2^1} \times 1 \times 1 + \frac{1^1}{2^2} \times (+1) \times (-1) + \frac{1^2}{2^3} \times \left(\left(\sqrt{\frac{1}{4}}(3-1) \right) \times \left(\sqrt{\frac{1}{4}}(3-1) \right) \right) + \dots \\ &= \frac{1}{2} - \frac{1}{4} + \frac{1}{8} + \dots \end{aligned}$$

Legendre Polynomials
orthogonal: -1..1

k	P_k
0	1
1	x
2	$(3x^2 - 1)/2$

k	q	$C_q^{(k)}(x, y, z)$
0	0	1
1	0	z/r
1	± 1	$\mp \sqrt{\frac{1}{2}}(x \pm iy)/r$
2	0	$\sqrt{\frac{1}{4}}(3z^2 - r^2)/r^2$
2	± 1	$\mp \sqrt{\frac{3}{2}}z(x \pm iy)/r^2$
2	± 2	$\sqrt{\frac{3}{8}}(x \pm iy)^2/r^2$

Coulomb Interaction



$$\begin{aligned}
 \frac{1}{r_{12}} &= \sum_{k=0}^{\infty} \frac{r_{<}^k}{r_{>}^{k+1}} P_k(\cos \omega) \\
 &= \sum_{k=0}^{\infty} \frac{r_{<}^k}{r_{>}^{k+1}} C^{(k)}(\hat{\mathbf{r}}_1) \cdot C^{(k)}(\hat{\mathbf{r}}_2) \\
 &= \sum_{k=0}^{\infty} \frac{r_{<}^k}{r_{>}^{k+1}} \sum_{q=-k}^{+k} C_q^{(k)}(\hat{\mathbf{r}}_1) C_{-q}^{(k)}(\hat{\mathbf{r}}_2) (-1)^q.
 \end{aligned}$$

$$\begin{aligned}
 H_{\text{Coulomb}} &= \frac{e^2}{4\pi\epsilon_0} \sum_k^{\text{even}} \sum_{i<j} \frac{r_{<}^k}{r_{>}^{k+1}} [C^{(k)}(\hat{\mathbf{r}}_i) \cdot C^{(k)}(\hat{\mathbf{r}}_j)] \\
 &= \sum_k^{\text{even}} F^k \left[\sum_{i<j} C^{(k)}(\hat{\mathbf{r}}_i) \cdot C^{(k)}(\hat{\mathbf{r}}_j) \right] \\
 &= \sum_k^{\text{even}} F^k f_k.
 \end{aligned}$$

Two-centre addition theorem: Ligand polarization(dynamic coupling) and energy transfer

Ionic transitions hypersensitive to environment

B. R. Judd

Physics Department, The Johns Hopkins University, Baltimore, Maryland 21218

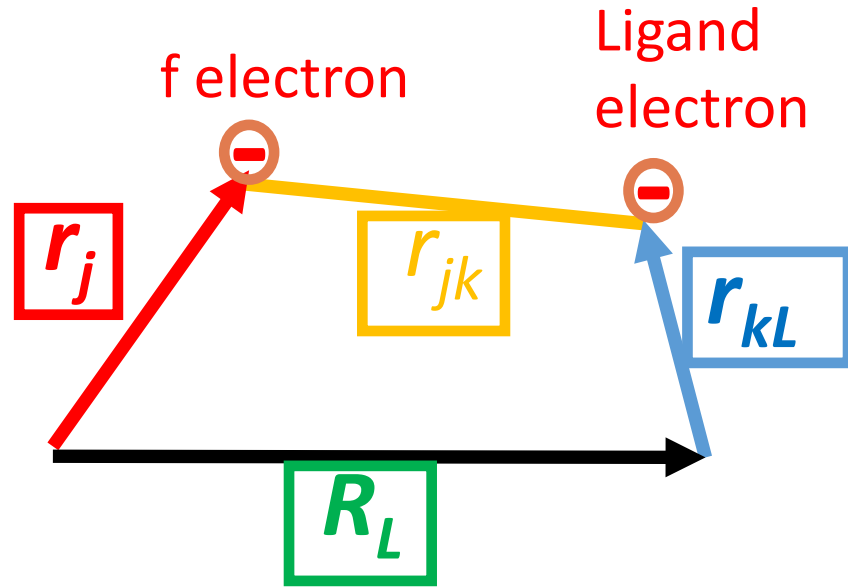
(Received 5 February 1979)

$$r_{jk}^{-1} = \sum_{l,t} r_j^l r_{kL}^t R_L^{-l-t-1} [(2l+2t)! / (2l)!(2t)!]^{1/2} \\ \times (-1)^t (C_j^{(l)} C_{kL}^{(t)})^{(l+t)} \cdot C_L^{(l+t)}.$$

Interaction between f electron and Ligand electron

Energy transfer

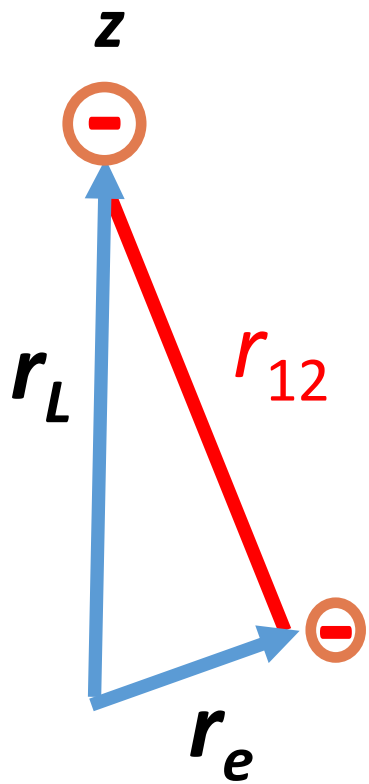
In this case there is an interaction between f electrons on two ions. Dipole-dipole is $l=t=1$, so we have $1/R^3$. Square gives $1/R^6$. Exchange interaction gives a different distance dependence.



Key idea:

$1/r_{jk}$ is a function
of r_j , r_{kL} , and R_L .

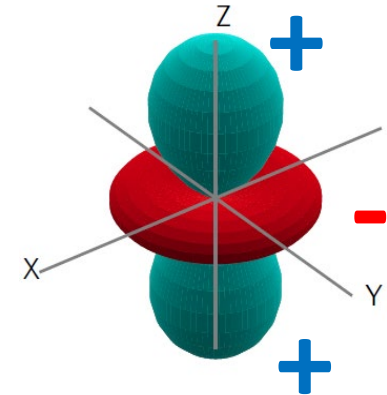
Electrostatic Crystal Field



$$\begin{aligned}
 V &= \frac{e^2}{4\pi\epsilon_0} \sum_{kq} \langle r^k \rangle C_q^{(k)}(\theta_e, \phi_e) \frac{1}{r_L^{k+1}} C_{-q}^{(k)}(\theta_L, \phi_L) (-1)^q \\
 &= \sum_{kq} \left[\frac{e^2}{4\pi\epsilon_0} \langle r^k \rangle \frac{1}{r_L^{k+1}} C_{-q}^{(k)}(\theta_L, \phi_L) (-1)^q \right] [C_q^{(k)}(\theta_e, \phi_e)] \\
 &= \sum_{kq} B_q^k C_q^{(k)}.
 \end{aligned}$$

$$\begin{aligned}
 C_0^{(2)} &= \sqrt{\frac{1}{4}} (3z^2 - r^2) / r^2 = 1, \\
 r_L &= 3 \text{ \AA} = 3 \times 10^{-10} \text{ m}, \\
 \langle r^2 \rangle &= 0.2 \text{ \AA} = 0.2 \times 10^{-20} \text{ m}^2.
 \end{aligned}$$

$$\begin{aligned}
 \frac{1}{r_{12}} &= \sum_{k=0}^{\infty} \frac{r_{<}^k}{r_{>}^{k+1}} P_k(\cos \omega) \\
 &= \sum_{k=0}^{\infty} \frac{r_{<}^k}{r_{>}^{k+1}} C^{(k)}(\hat{\mathbf{r}}_1) \cdot C^{(k)}(\hat{\mathbf{r}}_2) \\
 &= \sum_{k=0}^{\infty} \frac{r_{<}^k}{r_{>}^{k+1}} \sum_{q=-k}^{+k} C_q^{(k)}(\hat{\mathbf{r}}_1) C_{-q}^{(k)}(\hat{\mathbf{r}}_2) (-1)^q.
 \end{aligned}$$



$C_0^{(2)}(r)$

$$B_0^2 = \frac{e^2}{4\pi\epsilon_0} \times \frac{1}{r_L^3} C_0^{(2)}(0,0) (-1)^0 = \frac{(1.6 \times 10^{-19})^2}{4\pi \times 8.85 \times 10^{-12}} \times \frac{0.2 \times 10^{-20}}{(3 \times 10^{-10})^3} = 1.7 \times 10^{-20} \text{ J}.$$

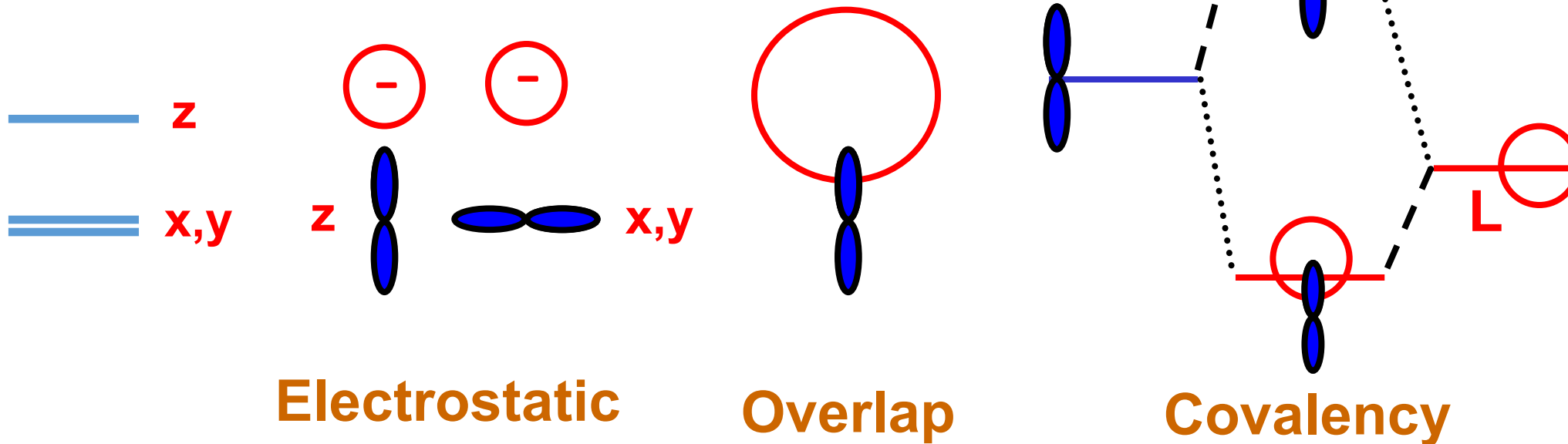
We can convert to eV by dividing by $1.6 \times 10^{-19} \text{ C}$, and multiply by 8066 to convert to cm^{-1} .
So B_0^2 is 0.11 eV, or 860 cm^{-1} .

“Crystal Field” $\sum_{k,q} B_q^k C_q^{(k)}$

[Diagrams use p orbitals for simplicity.]

*Do the “Ligand Field”
Parameters in Lanthanides
Represent Weak Covalent
Bonding?*

C.K. Jorgensen, R.
Pappalardo, H.H. Schmidtke
J. Chem. Phys. 1963



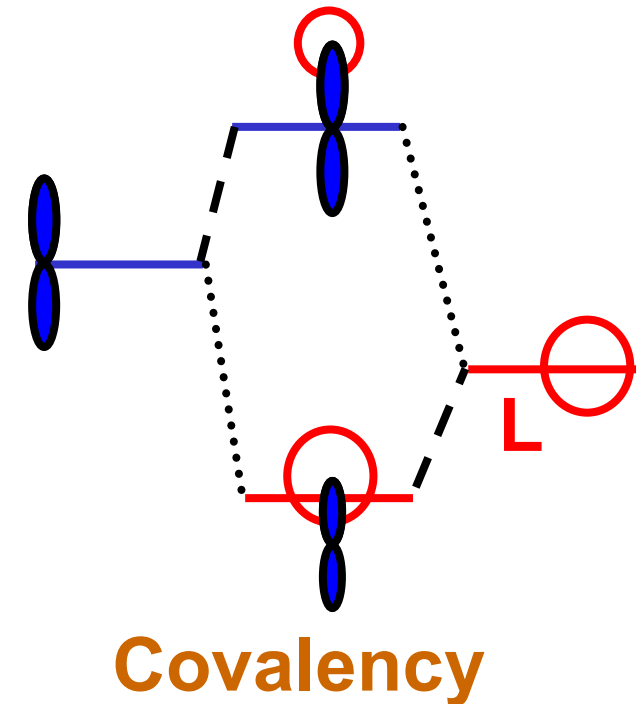
All increase energy of z orbital more than x,y

Orbital energies or Hamiltonian matrix \leftrightarrow crystal-field parameters

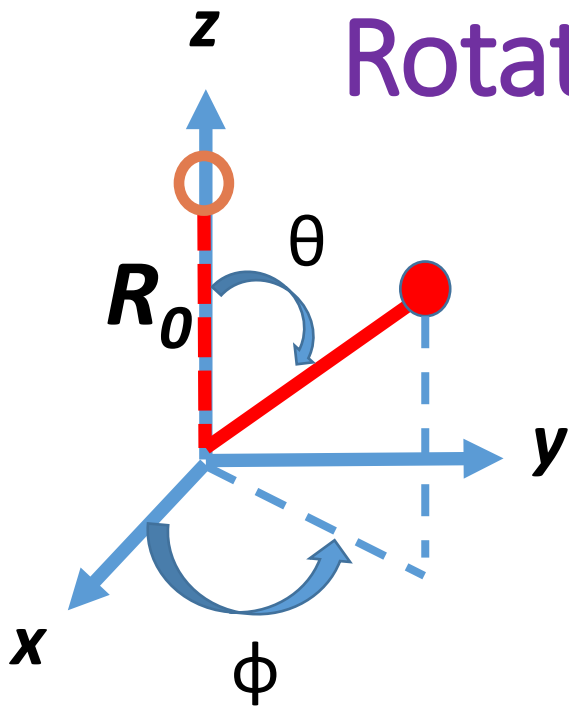
Do the ``Ligand Field'' Parameters in Lanthanides Represent Weak Covalent Bonding?

C.K. Jorgensen, R. Pappalardo, H.H. Schmidtke, J. Chem. Phys. 1963

Abstract: Instead of explaining the seven different f-orbital energies or five different d-orbital energies by parameters $A_{nm} \langle r_n \rangle$ of the electrostatic ligand field model, we propose to classify the energy levels according to the actual one-electron energies and to interpret these quantities by the weak effects of σ antibonding on the partly filled shell. Calculations of the relative angular dependence of such effects are made in a simple model and compared with experimental data for nine- and eight-coordinated lanthanide compounds. The agreement is judged to be much more satisfactory than when the electrostatic model is applied, and the number of freely chosen parameters is much smaller.



Rotations and the Superposition Model



Electrostatic model:

$$B_q^k = \frac{e^2}{4\pi\epsilon_0} \langle r^k \rangle \sum_L \frac{1}{r_L^{k+1}} C_{-q}^{(k)}(\theta_L, \phi_L) (-1)^q$$

Rotation matrix is related to the spherical tensors:

$$D_{q'0}^{(j)}(\alpha = \phi, \beta = \theta, \gamma = 0) = (-1)^{q'} C_{-q'}^{(K)}(\theta, \phi).$$

Rotate from Z and change the distance to build up CF in terms of single ligand CF (“intrinsic parameters”):

$$B_q^k = \bar{B}_k(R_0) \sum_L C_{-q}^{(k)}(\theta_L, \phi_L) (-1)^q \left(\frac{R_0}{R_L} \right)^{t_k}$$

$$B_0^k(R_L) \equiv \bar{B}_k(R_L)$$

Table A.1. The Wigner rotation matrices $D_{m',m}^1(\alpha, \beta, \gamma)$.

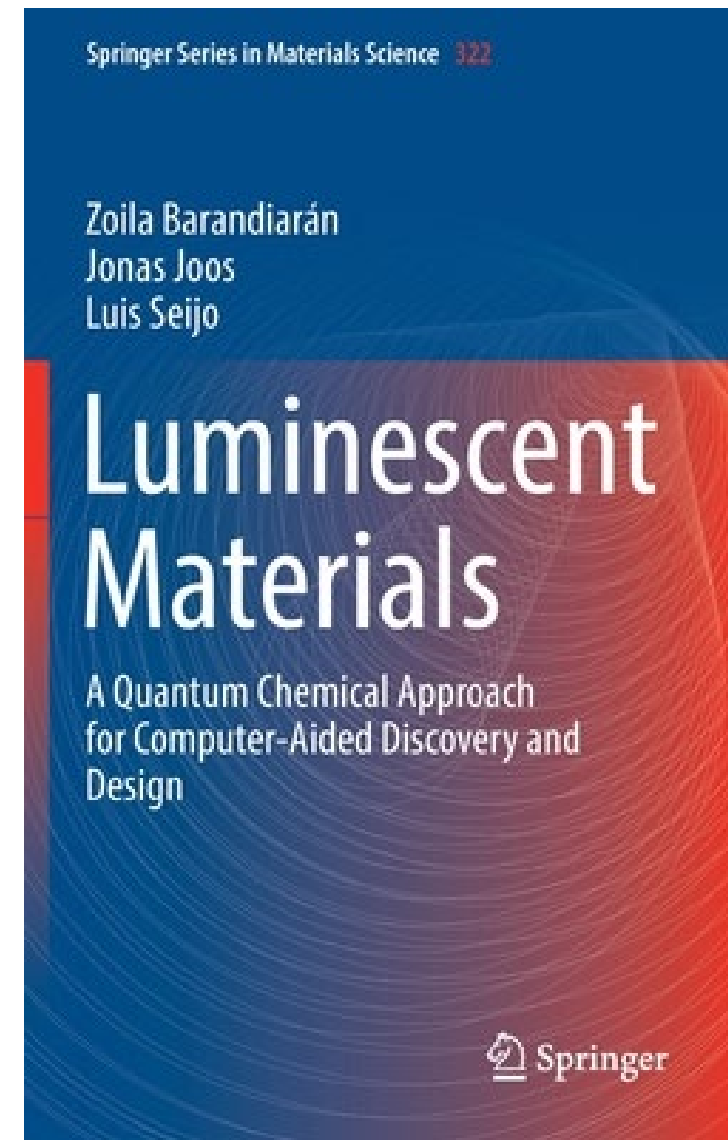
m'	m		
	1	0	-1
1	$\frac{1+\cos\beta}{2} e^{-i(\alpha+\gamma)}$	$-\frac{1}{\sqrt{2}} \sin\beta e^{-i\alpha}$	$\frac{1-\cos\beta}{2} e^{-i(\alpha-\gamma)}$
0	$\frac{1}{\sqrt{2}} \sin\beta e^{-i\gamma}$	$\cos\beta$	$-\frac{1}{\sqrt{2}} \sin\beta e^{i\gamma}$
-1	$\frac{1-\cos\beta}{2} e^{i(\alpha-\gamma)}$	$\frac{1}{\sqrt{2}} \sin\beta e^{i\alpha}$	$\frac{1+\cos\beta}{2} e^{i(\alpha+\gamma)}$

Key idea: Crystal-field parameters are a product of single-ligand interaction (“intrinsic parameters”) and geometry (distances and angles).

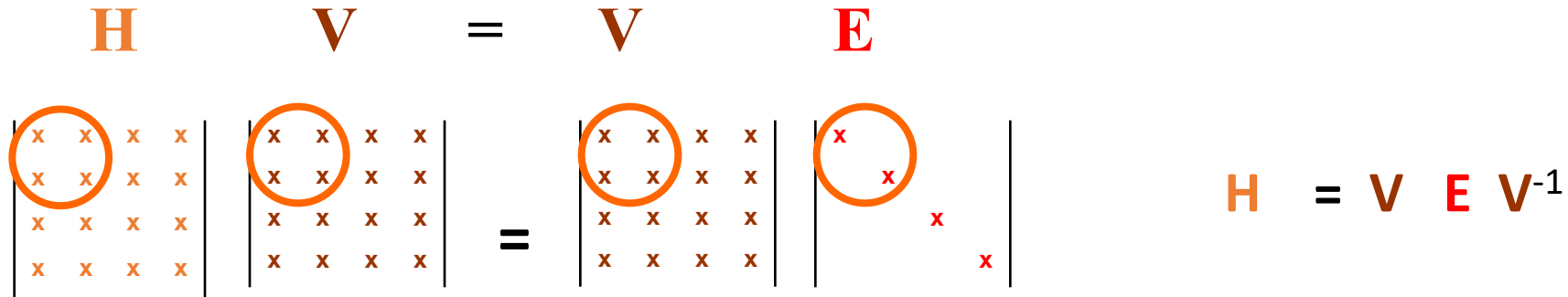
k	q	$C_q^{(k)}(x, y, z)$	$C_q^{(k)}(\theta, \phi)$
0	0	1	1
1	0	z/r	$\cos\theta$
1	± 1	$\mp \sqrt{\frac{1}{2}}(x \pm iy)/r$	$\mp \sqrt{\frac{1}{2}} \sin\theta e^{\pm i\phi}$

Relating ab-initio (first principles) calculations to crystal-field calculations

- Modern quantum-chemistry calculations for rare-earth materials:
 - DFT calculation using VASP.
 - 4f energies (without spin-orbit) using AIMP embedded cluster approach
 - [Seijo et al J. Chem. Phys. 114, 118 (2001).]
 - SA-CASSCF calculation using MOLCAS.
- Use calculations for Ce^{3+} to estimate parameters for the series.
 - For high symmetry we can just fit the energy levels of the ab-initio calculation.
 - Not possible in low symmetries such as D_2 (YAG), C_1 (YSO)
 - Need to relate the matrices.
 - Project the Hamiltonian into the model space.
(Hurtubise and Freed, Adv. Chem. Phys. 83, 465, 1993).



Relate H_{eff} to full H

$$\mathbf{H} \mathbf{V} = \mathbf{V} \mathbf{E}$$


$$\mathbf{H} = \mathbf{V} \mathbf{E} \mathbf{V}^{-1}$$

Use a subset of energies and eigenvectors from ab-initio calculation:

$$\mathbf{H}_{\text{eff}}^{\text{NH}} = \mathbf{V}_p \mathbf{E}_p \mathbf{V}_p^{-1} \quad (\text{non-Hermitian}) \quad [\text{'p' is the small, 'projected' matrix}]$$

$$\mathbf{V}_k = (\mathbf{V}_p \mathbf{V}_p^+)^{-1/2} \mathbf{V}_p \quad (\text{orthonormal})$$

$$\mathbf{H}_{\text{eff}} = \mathbf{V}_k \mathbf{E}_p \mathbf{V}_k^{-1} \quad (\text{Hermitian})$$

Can Solve: $\mathbf{H}_{\text{eff}} = \sum_{\alpha} \mathbf{P}_{\alpha} \mathbf{T}_{\alpha}$ for parameters \mathbf{P}_{α}

Reid MF., Duan CK. and Zhou HW. (2009) Crystal-field parameters from ab initio calculations. Journal of Alloys and Compounds 488: 591-594.

Alternative approach

The above approach can be hard to implement if there is more than one f electron as it is hard to work out the quantum numbers.

An alternative is use ab-initio calculations of expectation values of angular momentum operators ($J_x J_y J_z$ etc) and use those to determine the quantum numbers.

Nicholas Chilton's group use this approach:

Gould et al., Science, 2022, 375, 198 (supplementary material)

Example: $\text{LiYF}_4\text{:Ce}^{3+}$ J. Phys. Chem. C 2012, 116, 20513–20521

A Theoretical Study on the Structural and Energy Spectral Properties of Ce^{3+} Ions Doped in Various Fluoride Compounds

Jun Wen,[†] Lixin Ning,[‡] Chang-Kui Duan,^{*,†} Yonghu Chen,[†] Yongfan Zhang,[§] and Min Yin[†]

DFT calculation using VASP.
4f energies (without spin-orbit) using AIMP
embedded cluster approach
[Seijo et al J. Chem. Phys. 114, 118 (2001).]
SA-CASSCF calculation using MOLCAS.

LiYF ₄					
			CF	CF + SO	exptl ^b
4f ¹			0	0	0
			196	247	
			196	481	
			297	2214	
			504	2255	
			504	2409	
			1321	3016	
5d ¹			32389	33378	33433
			40274	41142	41101
			48640	49404	48564
			48640	50144	50499
			52213	53520	52790
			32 44431	45518	45277

(4f from Pr³⁺)

Parameter	Experiment	Theory
$B_0^2(4f)$	481	310
$B_0^4(4f)$	−1150	−1104
$B_4^4(4f)$	−1228	−1418
$B_0^6(4f)$	−89	−70
$B_4^6(4f)$	−1213	−1140 + 237i
$B_0^2(5d)$	4673	4312
$B_0^4(5d)$	−18649	−18862
$B_4^4(5d)$	−23871	−23871

Temperature dependent infrared absorption, crystal-field and intensity analysis of Ce^{3+} doped LiYF_4

Jon-Paul R. Wells^{a,b,*}, S. P. Horvath^a, Michael F. Reid^{a,c}

Optical Materials, **47**, 33 (2015)



Table 1: Experimental, fitted, and ab-initio [21] energy levels ($\text{cm}^{-1} \pm 0.1$), ground state g -values for Ce^{3+} in LiYF_4 .

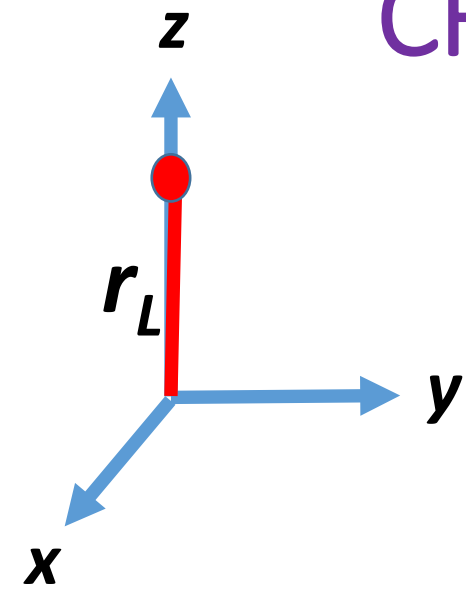
State	Experiment	Fitted	Ab-initio
$Z_1\gamma_{7,8}$	0.0	1.5	0
$Z_2\gamma_{5,6}$	216	213.8	247
$Z_3\gamma_{7,8}$	-	414.4	481
$Y_1\gamma_{5,6}$	2216.1	2215.5	2214
$Y_2\gamma_{7,8}$	2312.8	2312.1	2255
$Y_3\gamma_{5,6}$	2428.8	2430.1	2409
$Y_4\gamma_{7,8}$	3157.8	3158.6	3016
g_{\parallel}	2.765	2.751	
g_{\perp}	1.473	1.514	

Table 2: Fitted and ab-initio [21] spin-orbit and S_4 symmetry crystal-field parameters (cm^{-1}) for Ce^{3+} in LiYF_4 .

Parameter	Fitted	Ab-initio
ζ	626	-
B_0^2	298	310
B_0^4	-1328	-1104
B_4^4	-1282	-1418
B_0^6	-192	-70
B_4^6	-1743	-1140
$B_4^{6'}$	693	237

Note use of magnetic splittings in crystal-field fit. We now expand on this idea.

CF calculations with magnetic splittings



$$B_q^k = \bar{B}_k(R_0) \sum_L C_{-q}^{(k)}(\theta_L, \phi_L) (-1)^q \left(\frac{R_0}{R_L} \right)^{t_k}$$

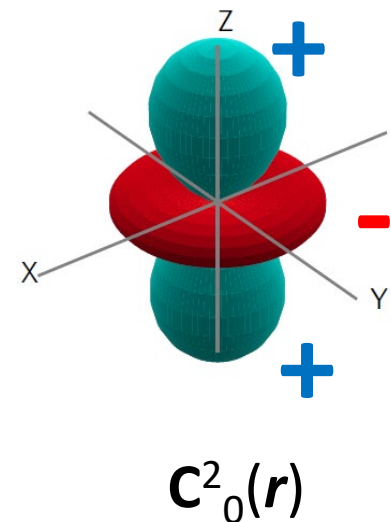
Consider the $^4F_{3/2}$ multiplet of Nd^{3+} .
We only need B_q^2 in this case.

E.g. Single ligand on Z, $B_0^2 = 500 \text{ cm}^{-1}$

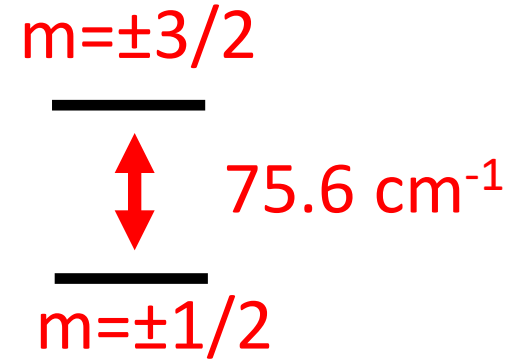
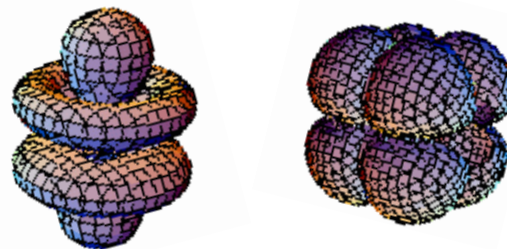
But there are many sets of parameters that would give the same splitting.

We can use magnetic splittings to determine the orientation of the potential...

Potential



f orbitals:

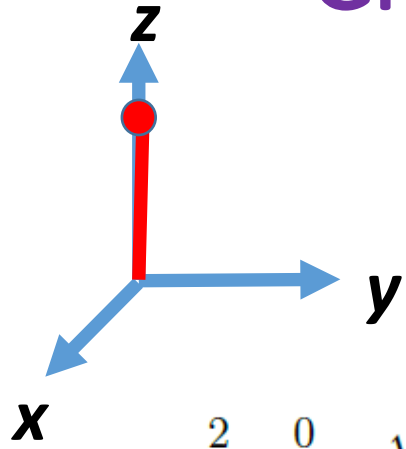


k	q	$C_q^{(k)}(x, y, z)$
0	0	1
1	0	z/r
1	± 1	$\mp \sqrt{\frac{1}{2}}(x \pm iy)/r$
2	0	$\sqrt{\frac{1}{4}}(3z^2 - r^2)/r^2$
2	± 1	$\mp \sqrt{\frac{3}{2}}z(x \pm iy)/r^2$
2	± 2	$\sqrt{\frac{3}{8}}(x \pm iy)^2/r^2$

CF calculations with magnetic splittings

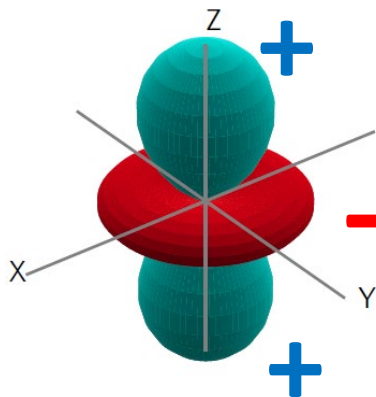
Single ligand on Z, $B^2_0 = 500 \text{ cm}^{-1}$

Calculate magnetic splitting of upper state: $B=4T$

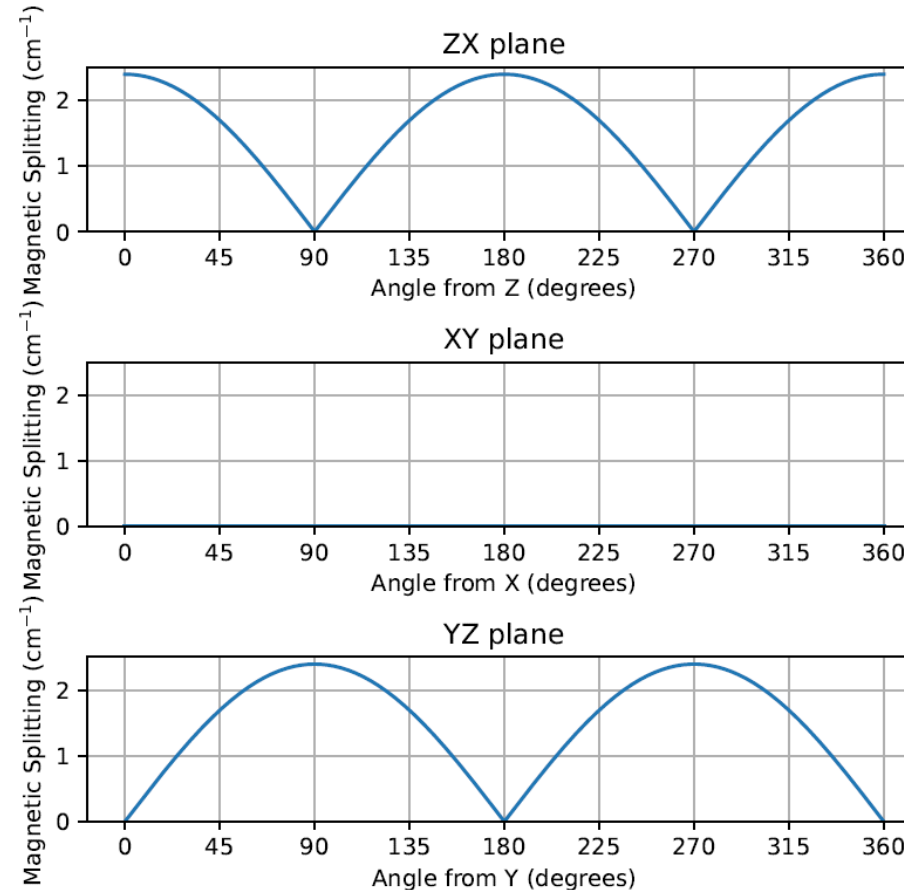


2	0	$\sqrt{\frac{1}{4}}(3z^2 - r^2)/r^2$
2	± 1	$\mp \sqrt{\frac{3}{2}}z(x \pm iy)/r^2$
2	± 2	$\sqrt{\frac{3}{8}}(x \pm iy)^2/r^2$

Potential



$C^2_0(r)$

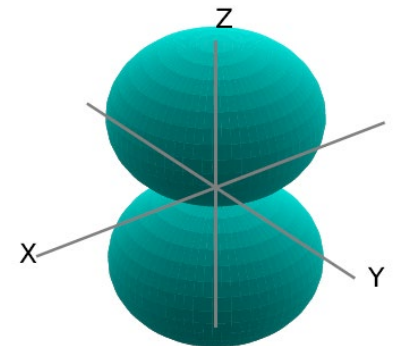


$m=\pm 3/2$

$\updownarrow 75.6 \text{ cm}^{-1}$

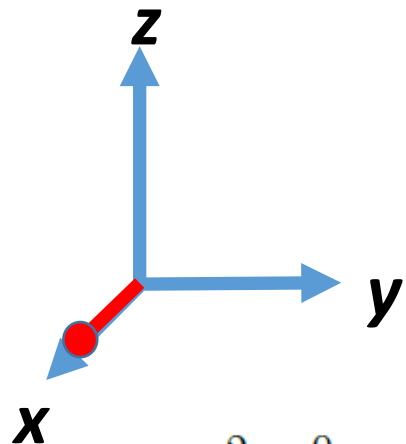
$m=\pm 1/2$

Magnetic Splitting



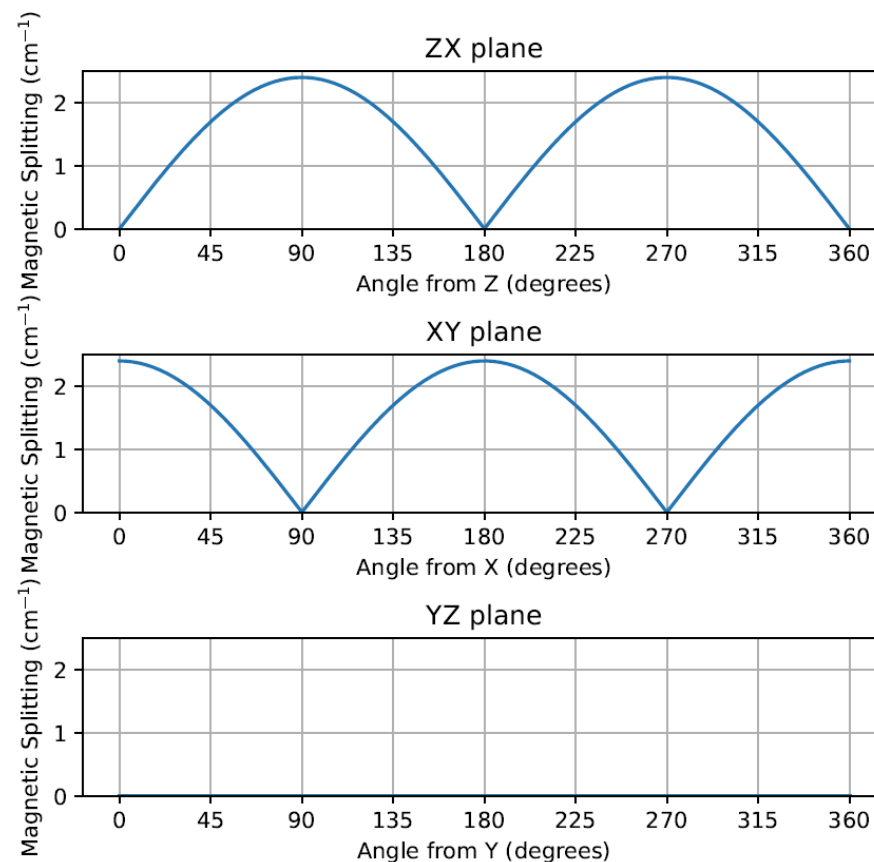
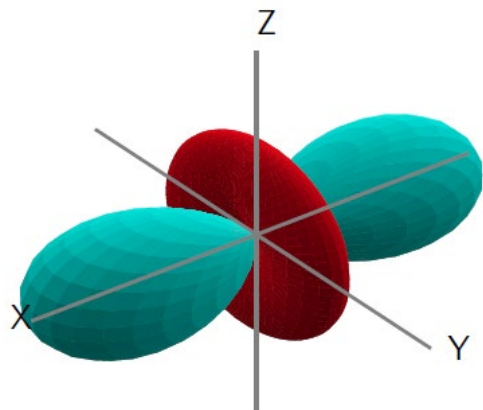
Change orientation!

Single ligand on X, $B^2_0 = -250 \text{ cm}^{-1}$ $B^2_2 = +306 \text{ cm}^{-1}$
 Calculate magnetic splitting of upper state: $B=4\text{T}$



2	0	$\sqrt{\frac{1}{4}}(3z^2 - r^2)/r^2$
2	± 1	$\mp \sqrt{\frac{3}{2}}z(x \pm iy)/r^2$
2	± 2	$\sqrt{\frac{3}{8}}(x \pm iy)^2/r^2$

Potential



$m=\text{mixture}$

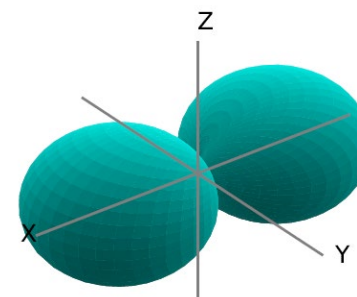


75.6 cm^{-1}



$m=\text{mixture}$

Magnetic Splitting



Transition Intensities

- Electric Dipole, Magnetic Dipole, ...
- ED between $4f^N$ and $4f^{N-1}5d$ can be calculated directly
 - But require modelling of vibronic bands.
- ED within $4f^N$ are parity forbidden.
 - “Forced electric dipole” transitions.
 - Construct Effective electric dipole operator that accounts for mixing of configurations of opposite parity on ion or ligand.
 - First detailed treatment: Judd, Ofelt, 1962.

Effective Electric Dipole Operator

$$D_{\text{eff},q} = D_q^{(1)} + D_q^{(1)} \sum_{\beta \notin M} \frac{|\beta\rangle\langle\beta|V}{E_0 - E_\beta^{(0)}} + \sum_{\beta \notin M} \frac{V|\beta\rangle\langle\beta|}{E_0 - E_\beta^{(0)}} D_q^{(1)} + \dots$$

If all denominators are the same then the sum over $|\beta\rangle\langle\beta|$ is 1. Couple the operators:

$$T_\ell^{(\lambda)} = \sum_{q,t,p} D_q^{(1)} V_p^{(t)} \langle 1 q, t p | \lambda \ell \rangle$$

Our parametrization. $\lambda=2,4,6$, $t=\lambda\pm 1$, λ

$$D_{\text{eff},q} = \sum_{\lambda,t,p} A_{tp}^\lambda U_{p+q}^{(\lambda)} (-1)^q \langle \lambda(p+q), 1-q | tp \rangle$$

Dipole strength

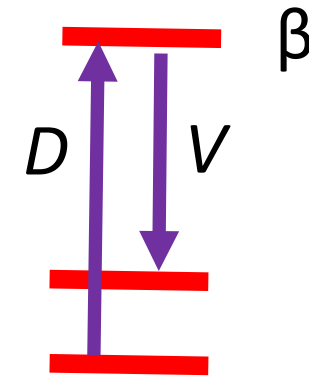
$$S_{FI,q}^{\text{ED}} = \sum_i \sum_f e^2 \left| \langle F f | D_q^{(1)} | I i \rangle \right|^2$$

Oscillator strength

$$f_{FI,q}^{\text{ED}} = \frac{2m\omega}{\hbar e^2} \frac{\chi_L}{n} \frac{1}{g_I} S_{FI,q}^{\text{ED}}$$

Einstein A coefficients ($1/\tau$)

$$A_{FI,q}^{\text{ED}} = \frac{1}{4\pi\epsilon_0} \frac{4\omega^3}{\hbar c^3} n \chi_L \frac{1}{g_I} S_{FI,q}^{\text{ED}}$$



Key idea:

Couple

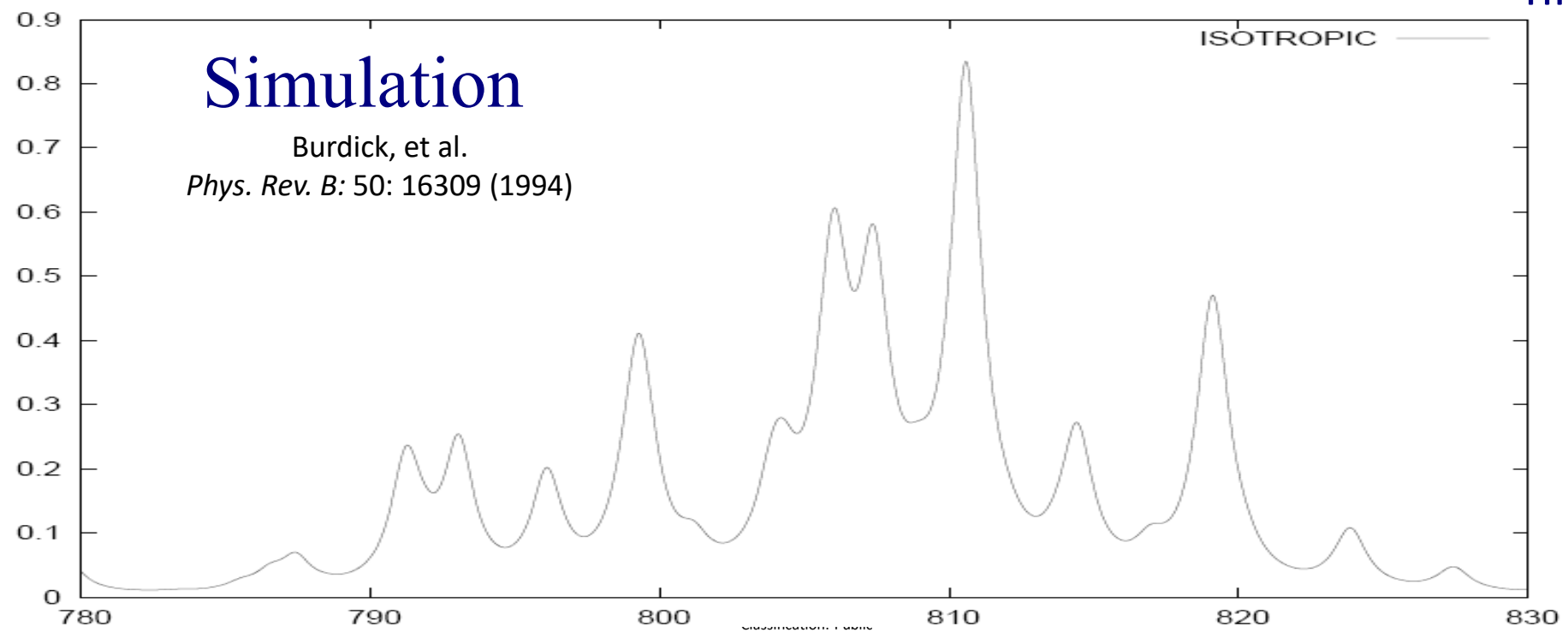
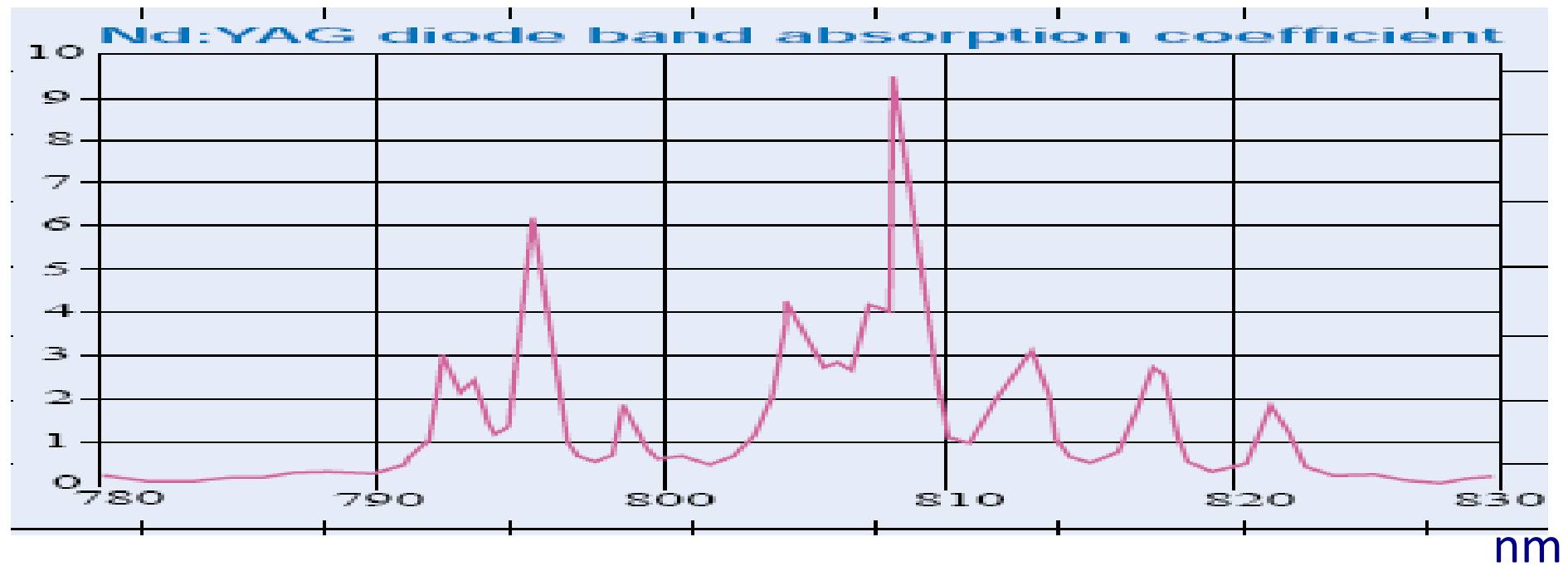
electric dipole operator: D

and

perturbing potential: V

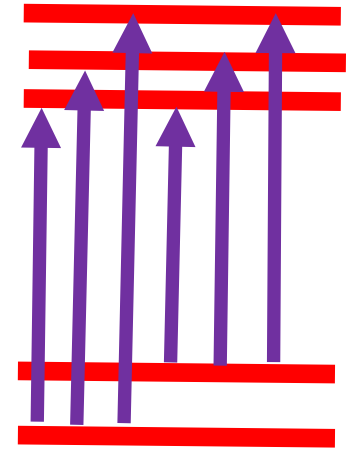
to obtain:

effective electric dipole operator: D_{eff}



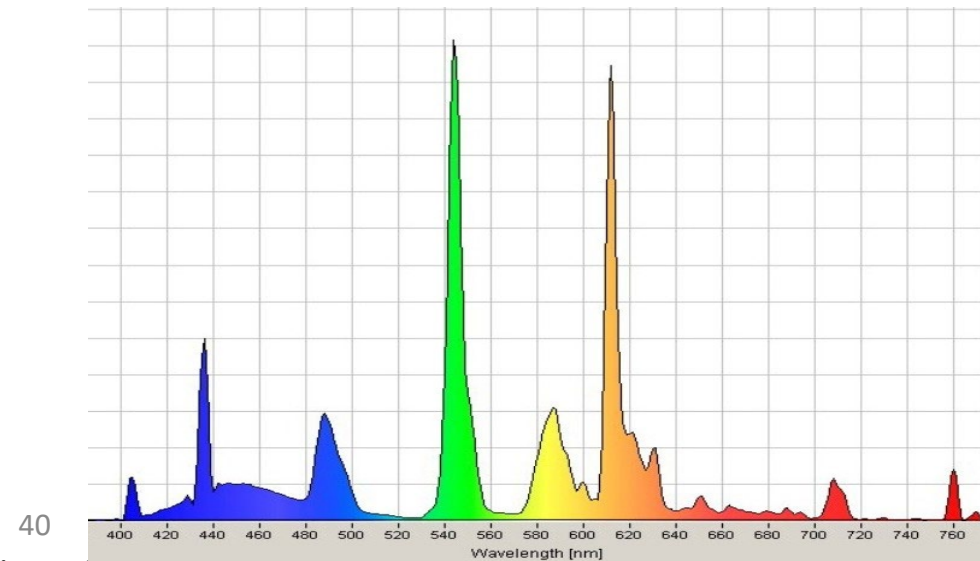
Multiplet-Multiplet transitions

- Judd 1962
 - For solutions and glasses at room temperature.
 - Sum over all states in a multiplet and all polarizations.
 - Reduces to three-parameter *linear* fit. ← huge simplification!
 - Ω_λ parameters with $\lambda=2,4,6$
 - 1000s of citations!



$$\bar{S}_{\alpha_F J_F, \alpha_I J_I}^{\text{ED}} = \frac{1}{3} e^2 \sum_{\lambda} \Omega_{\lambda} \langle \alpha_F J_F \| \mathbf{U}^{(\lambda)} \| \alpha_I J_I \rangle^2$$

$$\Omega_{\lambda} = \sum_{t,p} \frac{1}{2\lambda + 1} |A_{tp}^{\lambda}|^2$$



Reminiscencies of a quenched luminescence investigatory ☆

George Blasse

University Utrecht, Debye Institute, P.O. Box 80 000, 3508 TA Utrecht, The Netherlands

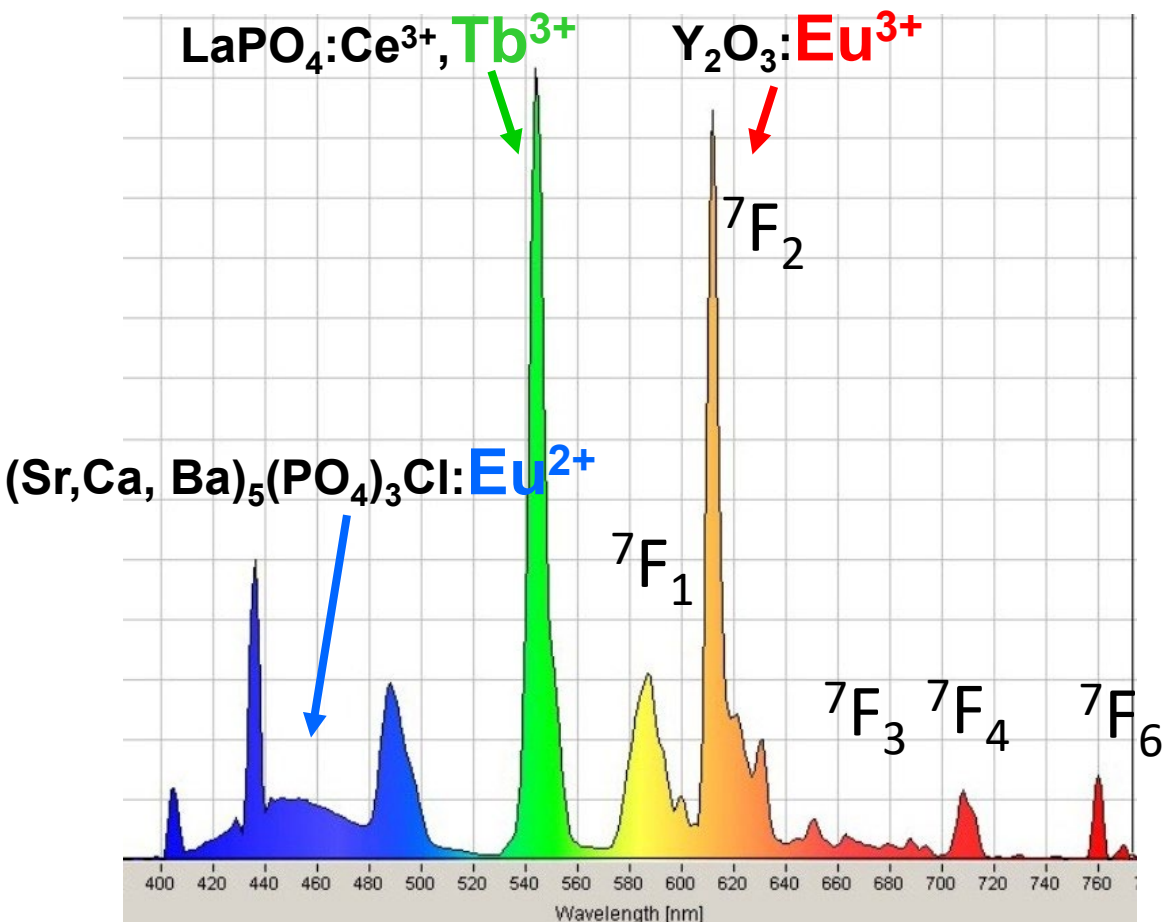
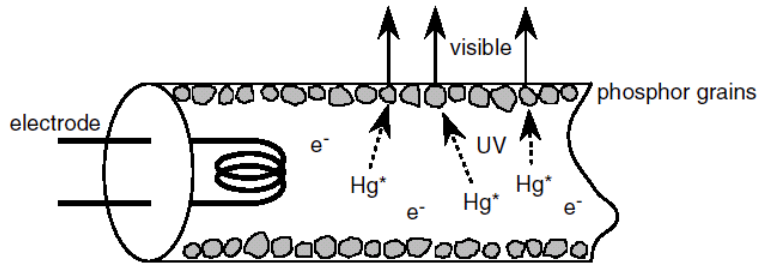
Journal of Luminescence 100 (2002) 65–67

Hypersensitivity: The emission of Eu^{3+} consists of an orange allowed magnetic-dipole transition ($^5\text{D}_0\text{--}^7\text{F}_1$), a red parity—forbidden electric-dipole (ED) transition ($^5\text{D}_0\text{--}^7\text{F}_2$), and further infrared ED transitions. For application, the emission should consist of as much $^5\text{D}_0\text{--}^7\text{F}_2$ emissions as possible. This requires Eu^{3+} to occupy a site without inversion symmetry. This, however, induces also the infrared emission. Fortunately, the rare-earth transitions with $\Delta J = 2$ are hypersensitive to the surroundings, i.e. a small deviation from inversion symmetry induces strong red emission whereas the infrared emission is still weak. By comparing many systems I found that a certain amount of covalency is a condition for this hypersensitivity. Later calculations by others confirmed this, but to me they are not transparent. It remains striking that the high quality of colour displays like in TV is due to this hypersensitivity effect.

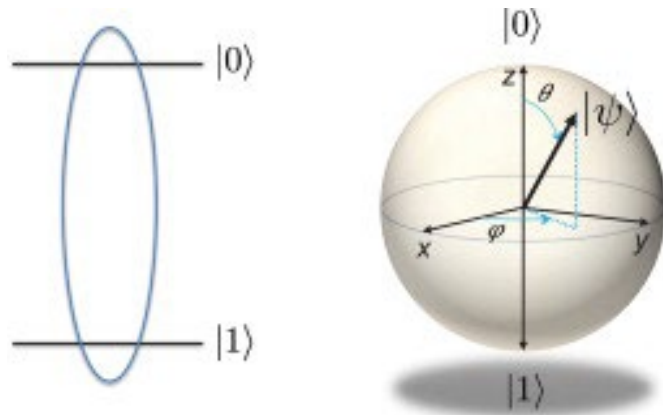
Classification: Public



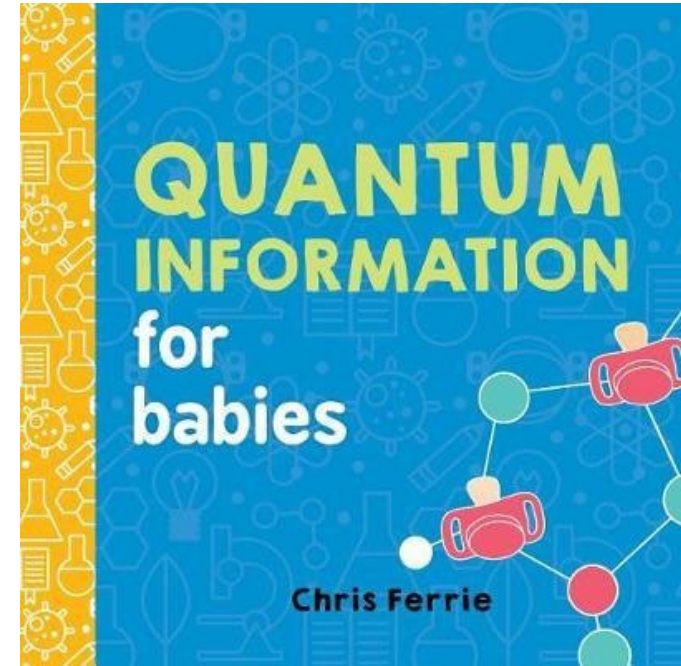
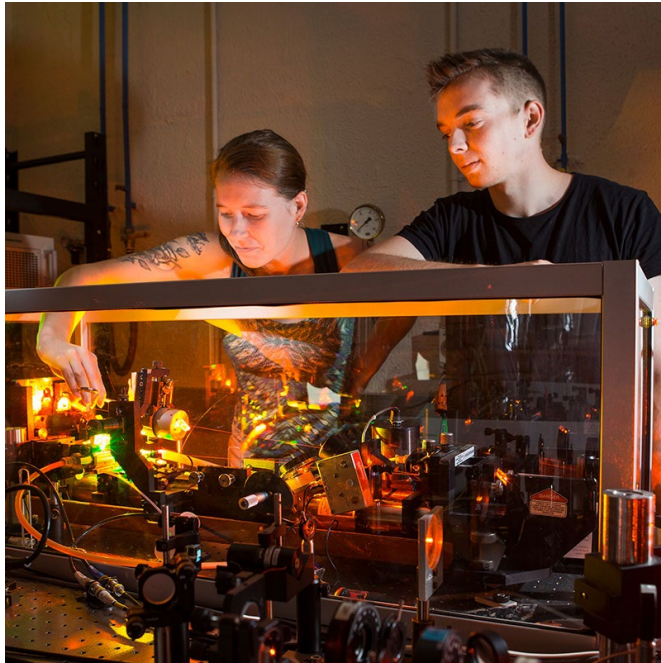
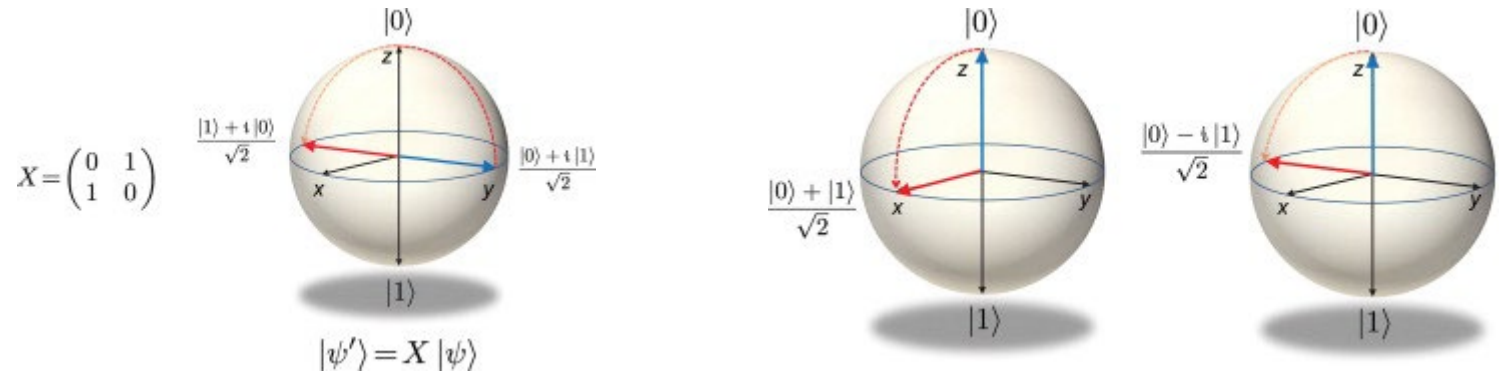
George Blasse
1934–2020



Quantum Information Applications?



$$|\psi\rangle = \cos(\theta/2) |0\rangle + e^{i\phi} \sin(\theta/2) |1\rangle$$



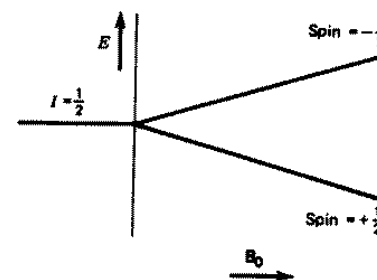
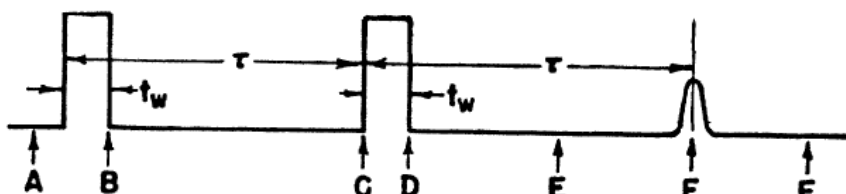


Spin Echoes*†

E. L. HAHN†

Physics Department, University of Illinois, Urbana, Illinois

(Received May 22, 1950)

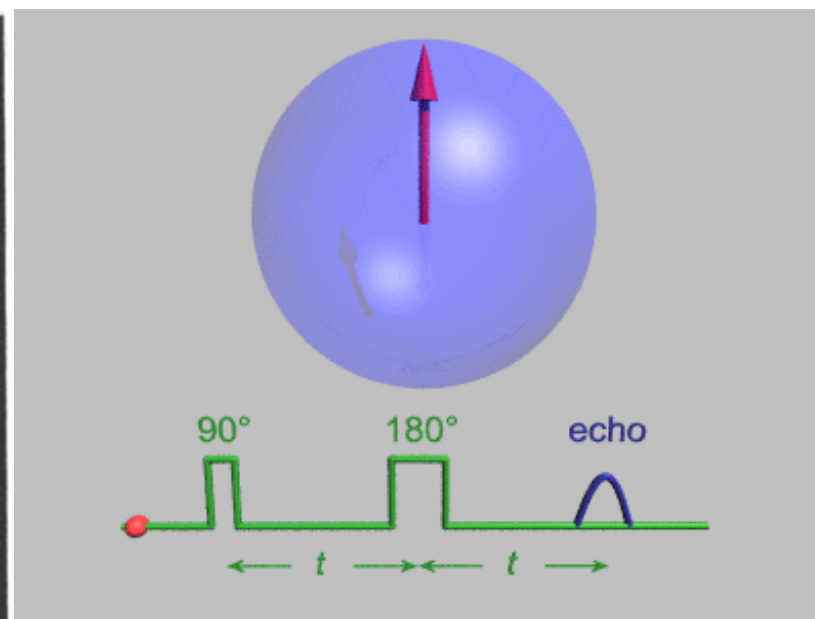
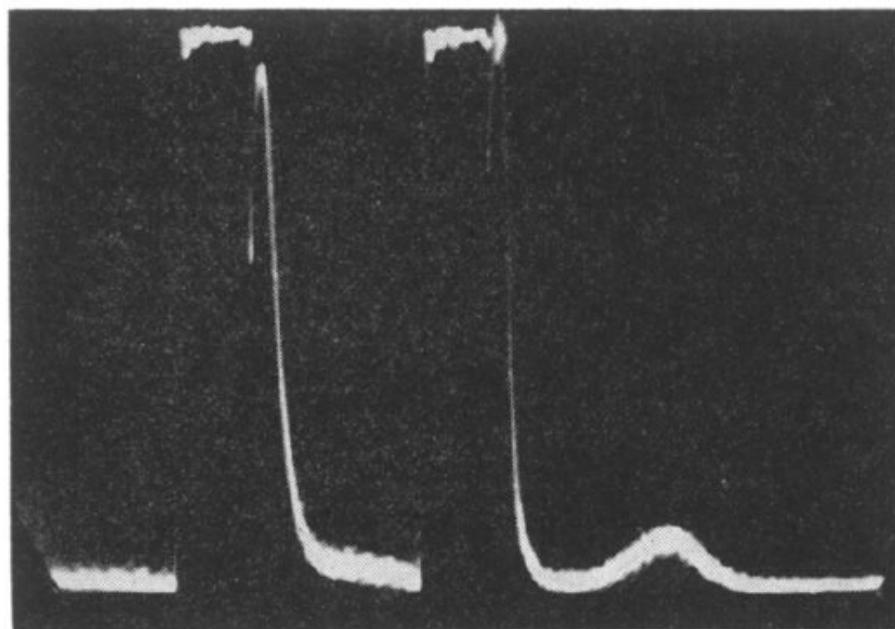


30MHz/0.7T

$\tau \approx 100\mu\text{s}$

Modern NMR

600MHz/14T



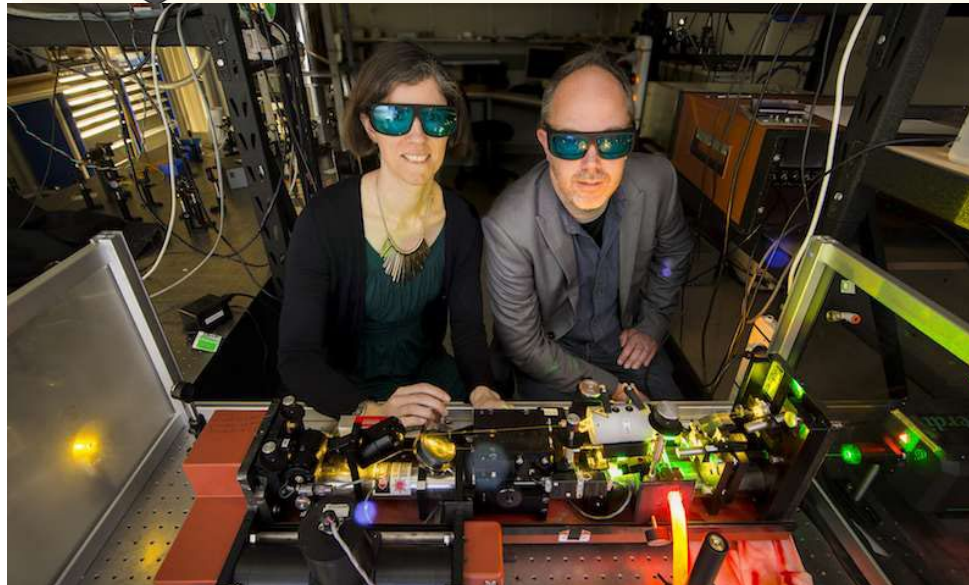
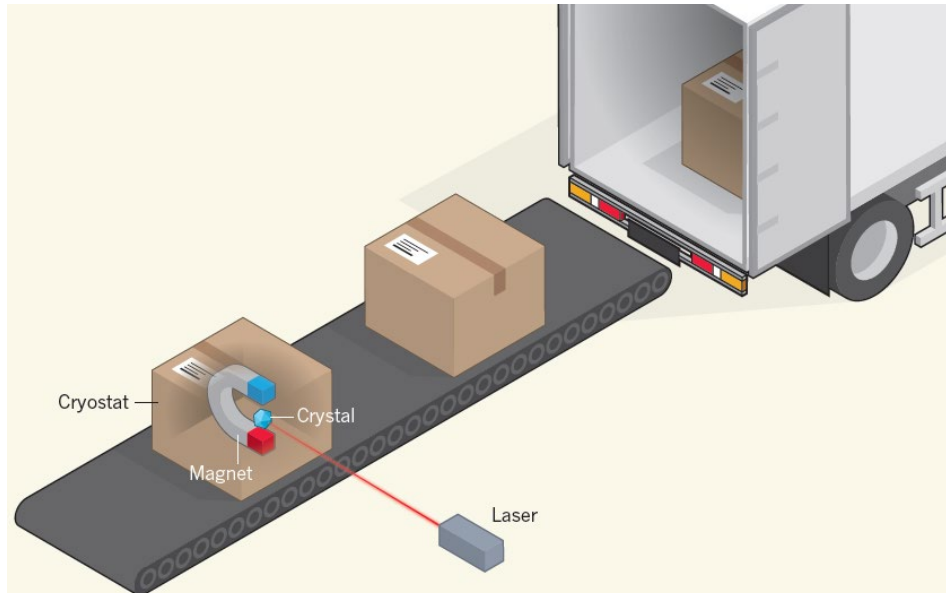
(N)MRI



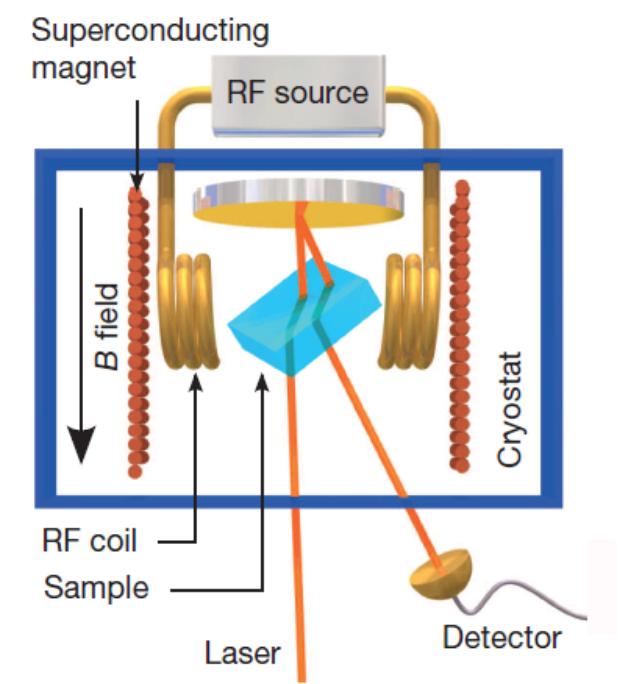
FIG. 11. Free induction signals for protons in paraffin. The echo lasts for $\sim 1.4 \times 10^{-5}$ sec. The r-f pulses, about $25 \mu\text{sec.}$ wide, cause some blocking of the i.f. amplifier. The echo envelope decay time is also of the order of the single echo lifetime.

Spin Echo: Wikipedia

Six-Hour Coherence: $^{151}\text{Eu}^{3+}$



Rose Ahlefeldt, Matt Sellars, ANU, Australia.



Manjin Zhong, SUSTech, Shenzhen

(Note that recent work has re-ordered the states relative to those shown on the left.)

Crystal-Field Calculations for Y_2SiO_5 (YSO)

In low symmetry the use of magnetic measurements to fix the orientation of the crystal-field potential is crucial.

Sebastian Horvath worked on this problem during his PhD and we have since extended this work to several rare-earth ions.

Y1 and Y2 sites are six and seven-coordinate respectively.

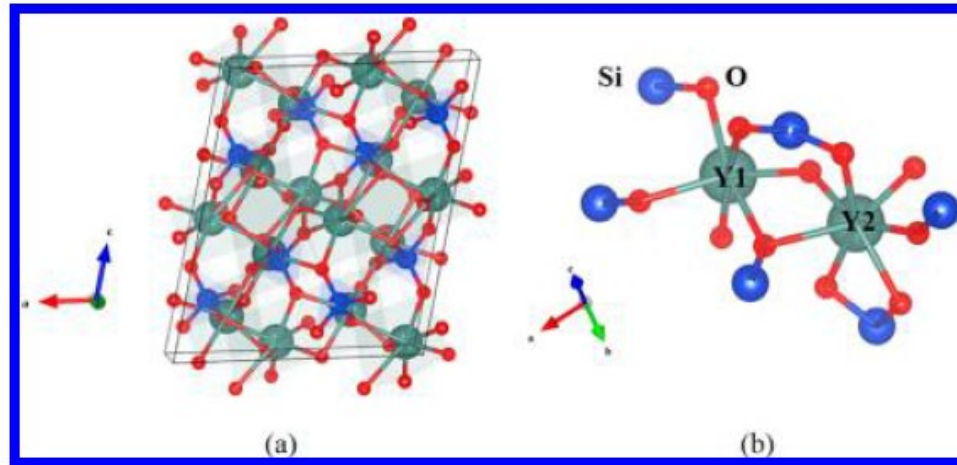


Figure 1. Schematic representations of local atomic structures around the two types of yttrium (Y1 and Y2) sites along with the unit cell of X2-YSO.

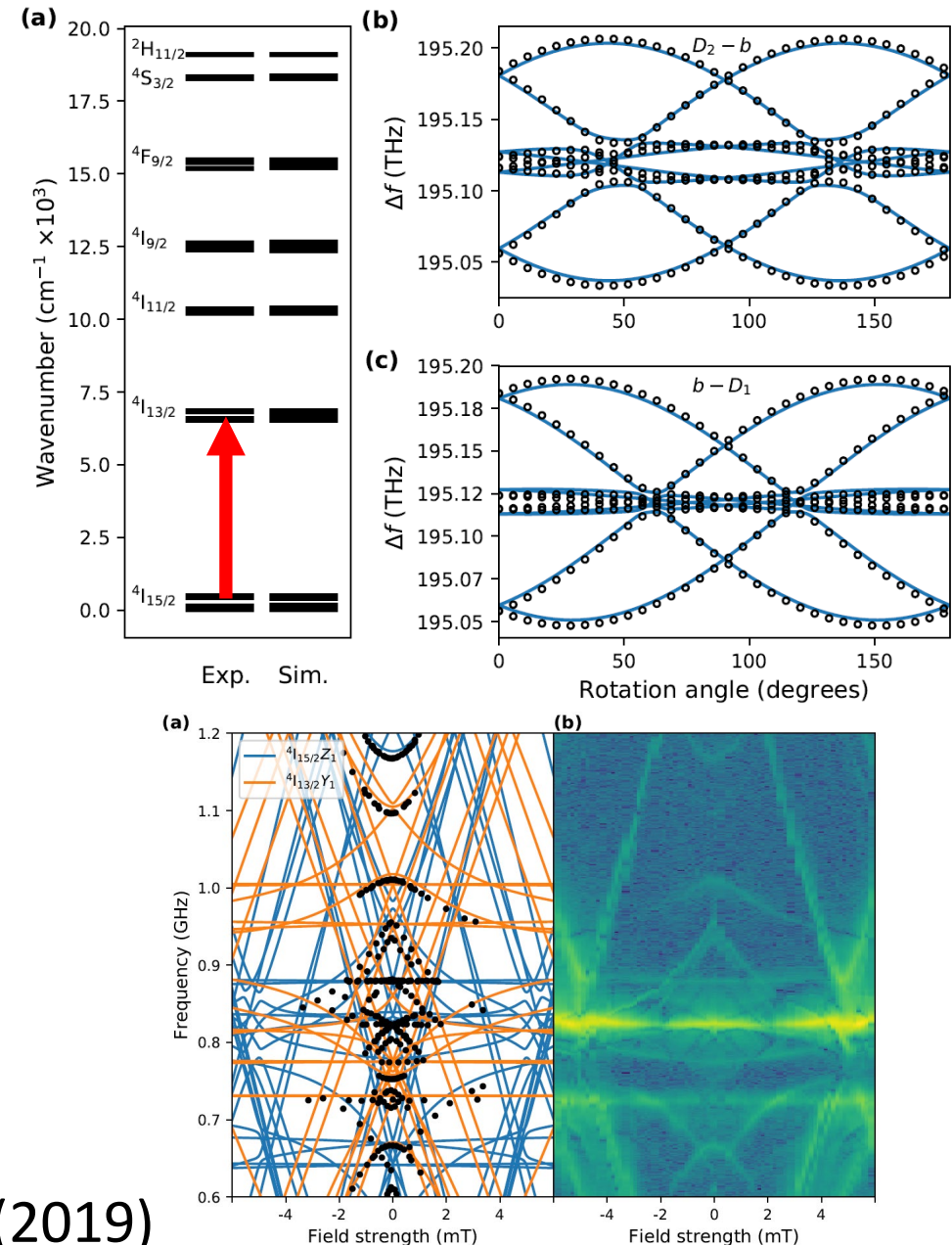


Crystal-Field Calculation for $^{167}\text{Er}^{3+}:\text{YSO}$ Site 1

$$H = H_{\text{FI}} + H_{\text{CF}} + H_{\text{Z}} + H_{\text{HF}} + H_{\text{Q}}.$$

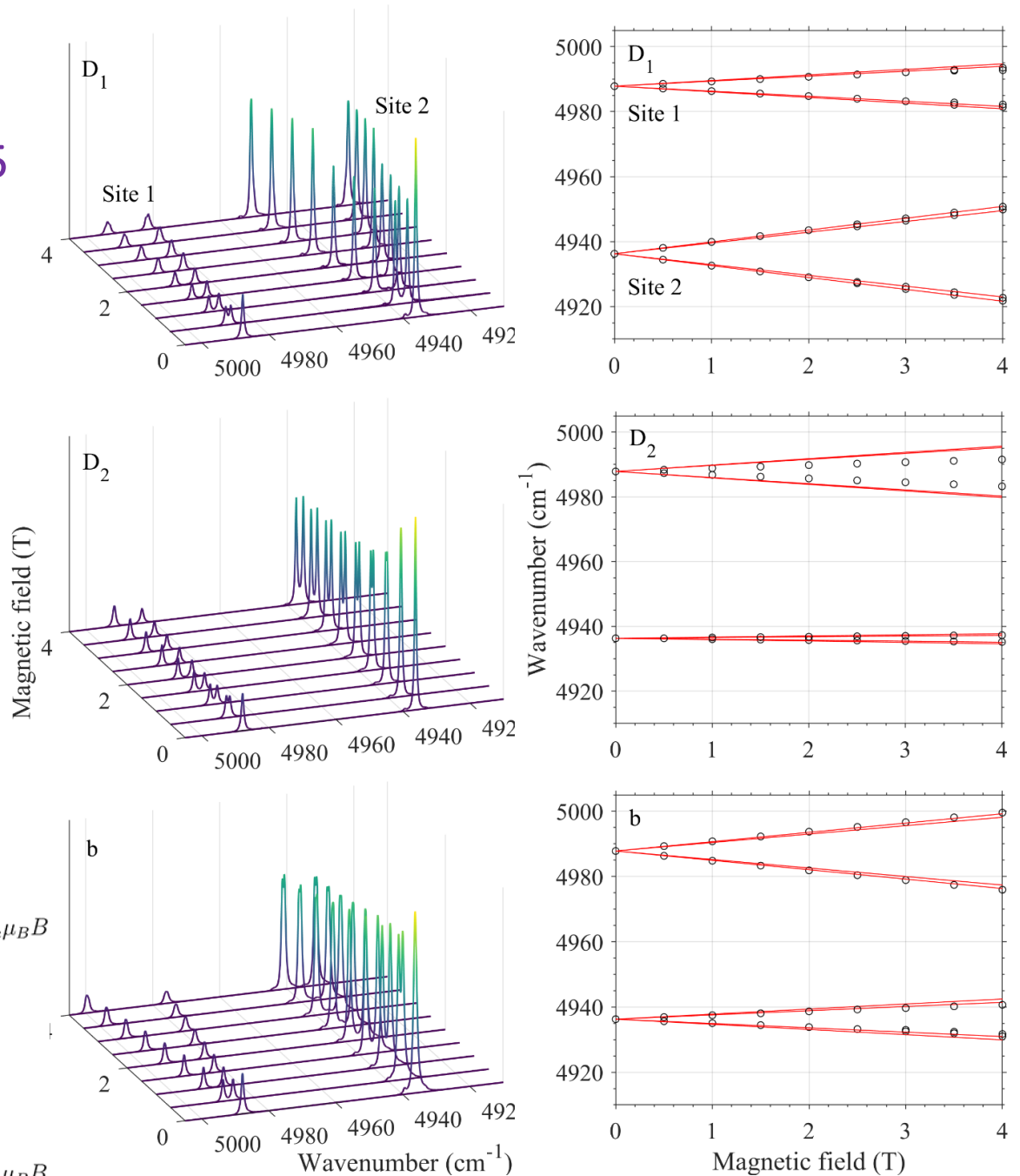
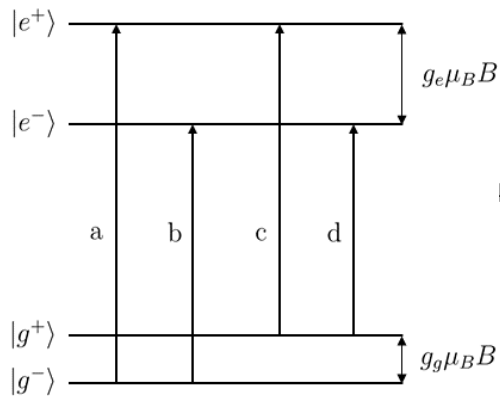
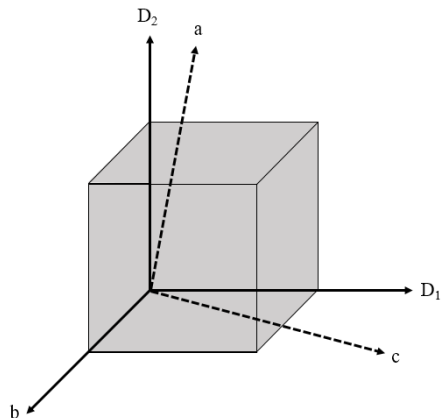
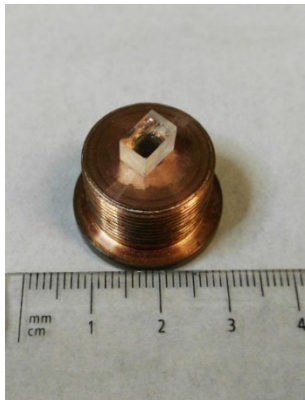
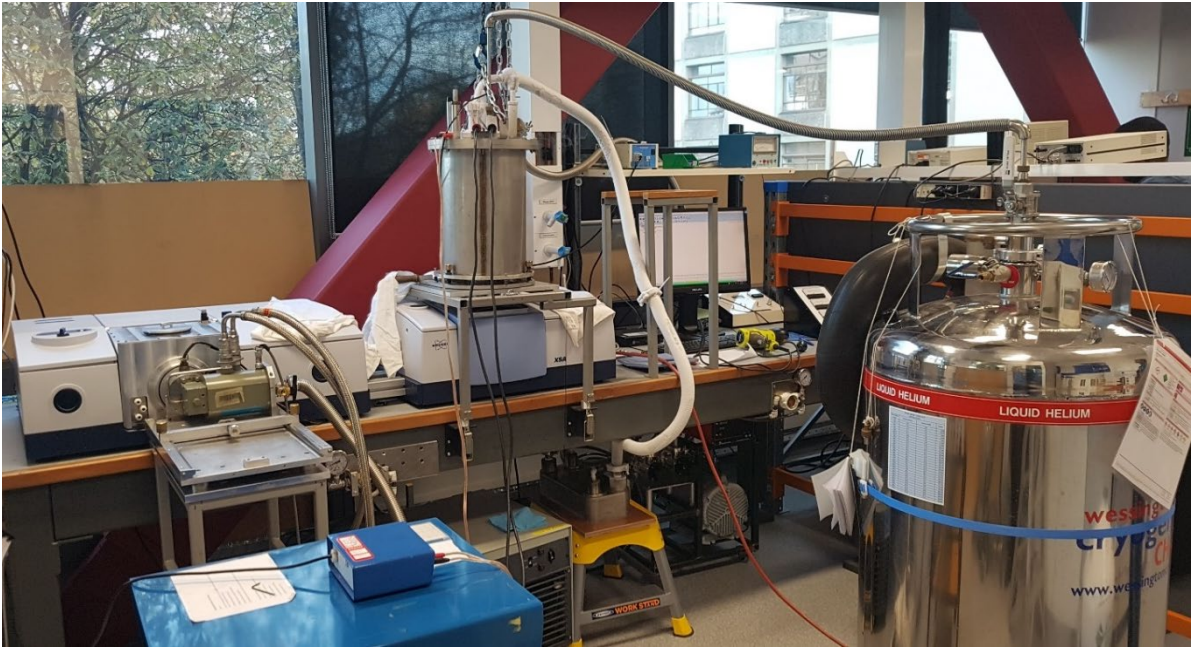
- Use literature and new data for electronic energy levels, magnetic, and hyperfine splitting.
- Directional magnetic data is crucial to fixing orientation of CF Hamiltonian for low-symmetry sites.
- Separately calculate:
 - Electronic energy levels
 - Magnetic splitting for various field orientations
 - Hyperfine splitting.
- Data (Effectively 95 data points)
 - 35 Electronic energies
 - 12 Ground-state hyperfine levels
 - 12 Zeeman rotation points
 - Raman heterodyne hyperfine data (15 MHz accuracy)
- 34 Parameters (similar to spin-Hamiltonian parameter number...)

Sebastian Horvath et al. Phys. Rev. Lett. **123**, 057401 (2019)



Extension to other ions: Zeeman spectroscopy of $\text{Sm}^{3+}:\text{Y}_2\text{SiO}_5$

N.L. Jobbitt et al. J. Phys. Condensed Matter 34:325502 (2022)



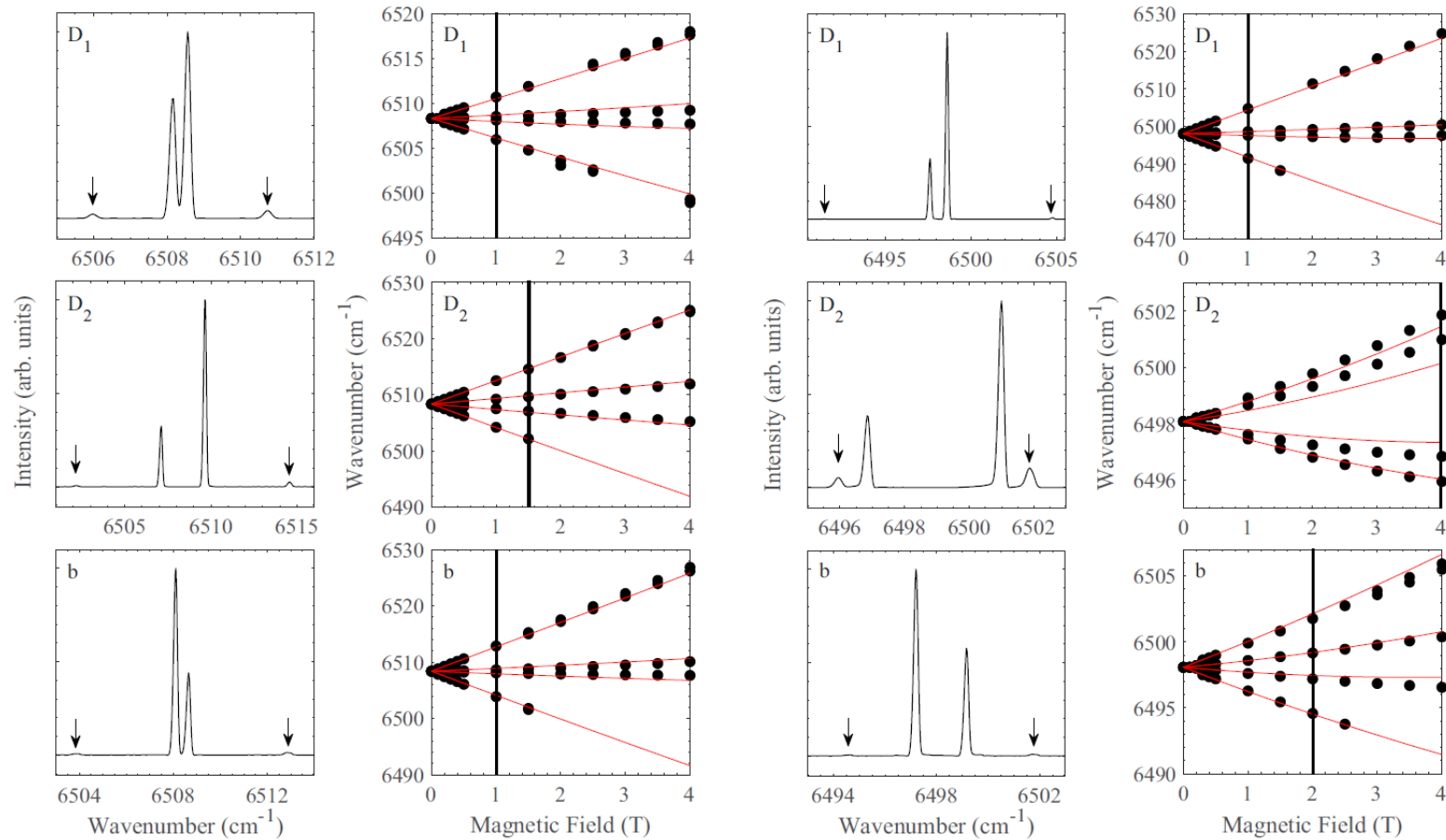
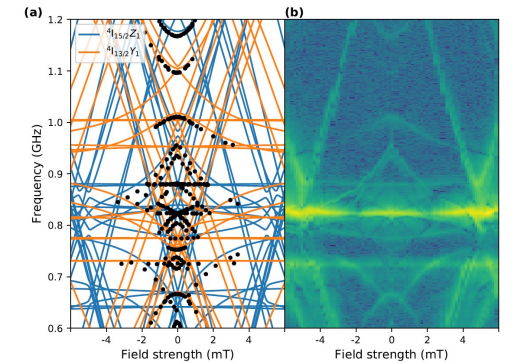
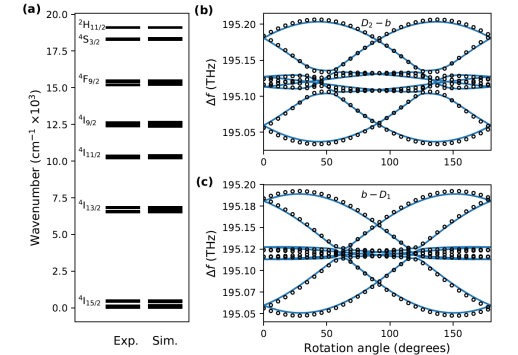


FIG. 2. Magnetic splittings of the site 1 $Z_1 \rightarrow Y_1$ transition for magnetic fields applied along the three crystallographic axes of Y_2SiO_5 . The top, middle, and bottom panels shows $B \parallel D_1$, $B \parallel D_2$, and $B \parallel b$, respectively. The left panels show 4.2-K Zeeman absorption spectra at magnetic field strengths represented by the vertical lines in the right panels. The weak outer transitions are labeled with arrows to assist the reader. The right panels show the experimental splittings, represented by the circles, and the calculated splittings are represented by the red lines.

Site 1

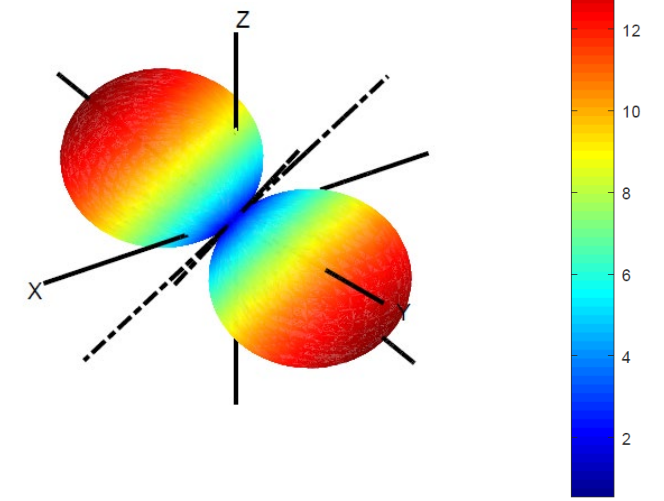
FIG. 3. Magnetic splittings of the site 2 $Z_1 \rightarrow Y_1$ transition for magnetic fields applied along the three crystallographic axes of Y_2SiO_5 . The top, middle and bottom panels shows $B \parallel D_1$, $B \parallel D_2$, and $B \parallel b$, respectively. The left panels show 4.2-K Zeeman absorption spectra at magnetic field strengths represented by the vertical lines in the right panels. The weak outer transitions are labeled with arrows to assist the reader. The right panels show the experimental splittings, represented by the circles, and the calculated splittings are represented by the red lines.

Site 2



Site 1 ground state magnetic splitting

g value max: 14



Er³⁺:YSO Nick Jobbitt et al. Phys. Rev. B 104, 155121 (2021)

TABLE III. Fitted values for the free-ion, crystal-field and hyperfine parameters and their related uncertainties of site 1 and site 2 in Er³⁺:Y₂SiO₅. All values are in cm⁻¹. Parameters determined by Horvath *et al.* are also included for comparison [16,18].

Parameter	Site 1				Site 2		
	This study	Uncertainty	Ref. [16]	Ref. [18]	This study	Uncertainty	Ref. [18]
E_{avg}	35491.3	0.1	35503.5	—	35507.5	0.1	—
F^2	95805.7	1.0	96029.6	95346	96121.9	1.3	95721
F^4	67869.7	3.4	67670.6	68525	67722.4	4.5	68564
F^6	53148.2	2.5	53167.1	52804	53241.2	3.1	52999
ζ	2360.5	0.1	2362.9	2358	2362.3	0.1	2356
B_0^2	−479.6	6.1	−149.8	−563	389.0	3.7	354
B_1^2	471.4+143.8i	2.9 + 3.0i	420.6+396.0i	558+280i	−325.7 − 95.8i	2.7 + 3.0i	498.6807+274i
B_2^2	125.5−2.0i	2.8 + 2.3i	−228.5+27.6i	143−121i	−368.5+53.7i	1.8 + 2.0i	−75.8028+60i
B_0^4	−640.6	31.3	1131.2	−125	17.2	15.5	226
B_1^4	288.8+924.1i	7.2 + 25.3i	985.7+34.2i	225−831i	−378.7 − 519.5i	5.1 + 9.3i	−657.8381+593i
B_2^4	−273.9+320.9i	11.1 + 16.7i	296.8+145.0i	−48 − 945i	−72.0 − 146.0i	5.7 + 6.7i	335.7827+253i
B_3^4	−873.7 − 367.8i	20.7 + 9.7i	−402.3 − 381.7i	−615 − 688i	−890.8+570.4i	9.5 + 7.3i	−71.3262 − 46i
B_4^4	−600.8+1210.5i	23.7 + 9.2i	−282.3+1114.3i	744−102i	−198.7 − 567.9i	7.8 + 5.2i	−813.9654+64i
B_0^6	145.7	13.2	−263.2	−28	73.4	4.3	219
B_1^6	−105.9 − 329.0i	2.9 + 4.0i	111.9+222.9i	49+199i	−37.5+49.9i	3.4 + 5.7i	−127+197i
B_2^6	−119.9+164.1i	7.7 + 8.8i	124.7+195.9i	120−107i	135.5+60.6i	4.5 + 1.5i	−36 − 47i
B_3^6	1.1+133.3i	6.7 + 4.5i	−97.9+139.7i	195−55i	−166.7+131.8i	2.6 + 4.0i	17−108i
B_4^6	−84.6+36.9i	5.0 + 4.5i	−93.7 − 145.0i	−287 − 161i	227.2+47.6i	1.2 + 3.0i	−100+77i
B_5^6	75.5+6.9i	4.3 + 6.6i	13.9+109.5i	−117+162i	119.5+64.3i	3.7 + 3.2i	−263+103i
B_6^6	−48.5+118.0i	6.2 + 4.2i	3.0−108.6i	136+186i	37.6−41.3i	3.5 + 2.8i	12−26i
S^2	386.6	—	399.0	483.0	363.1	—	397.9
S^4	948.2	—	862.9	824.6	653.3	—	607.5
S^6	183.8	—	189.6	218.6	151.5	—	171.4
a_I	0.005306	0.000008	0.005466	0.0059	0.005389	0.000012	0.0069
a_Q	0.0554	0.0020	0.0716	0.0800	0.0240	0.0024	0.0808

Note that 34 parameters is the same as the number of spin Hamiltonian parameters for Z1 and Y1.

g, A, Q tensors: (6+6+5)*2



Er³⁺:Y₂SiO₅ predictions: Polarization Measurements

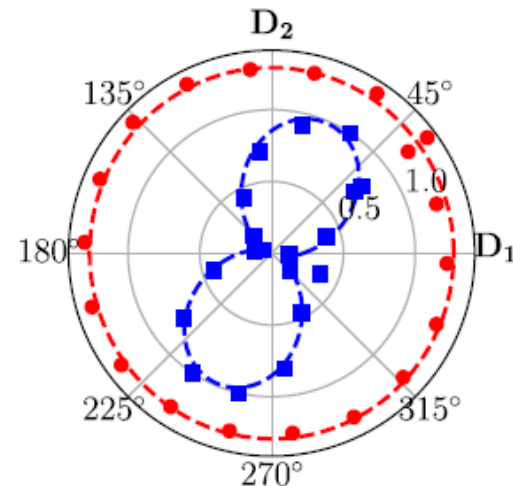
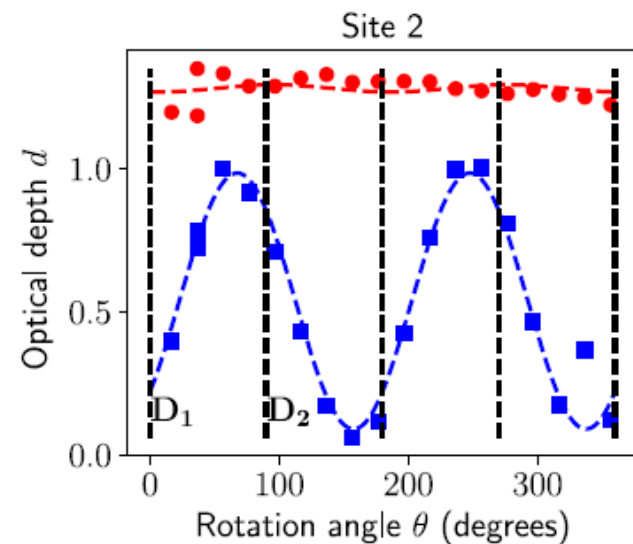
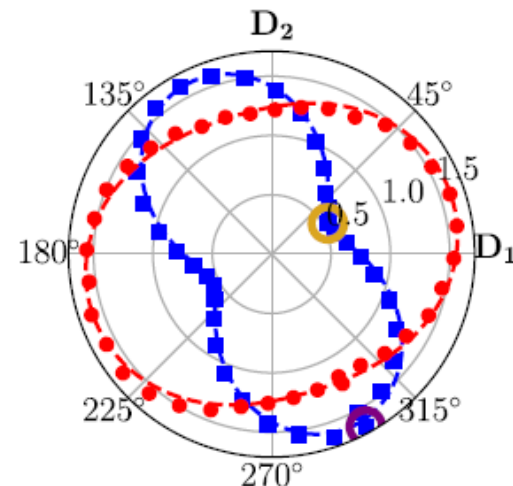
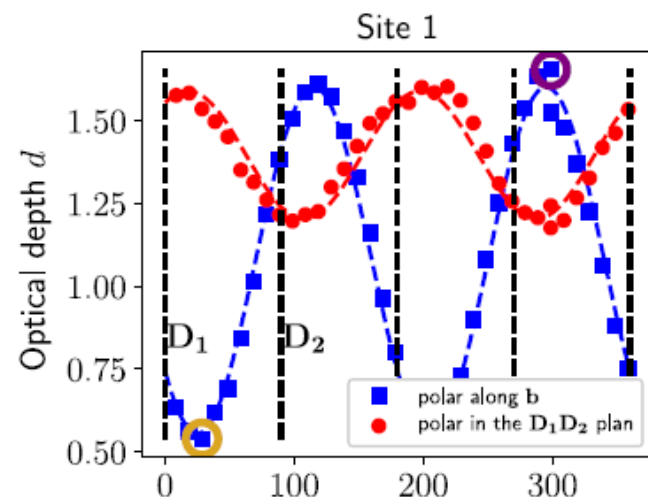
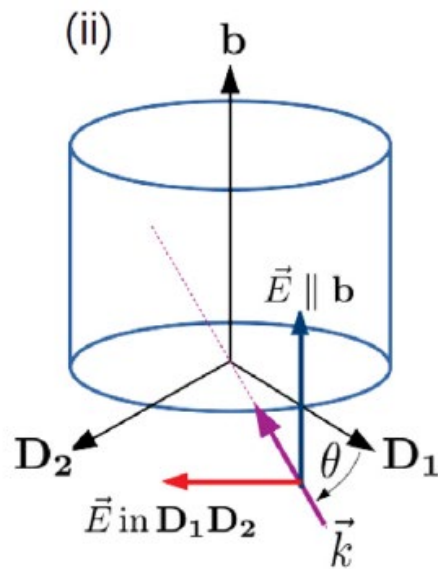
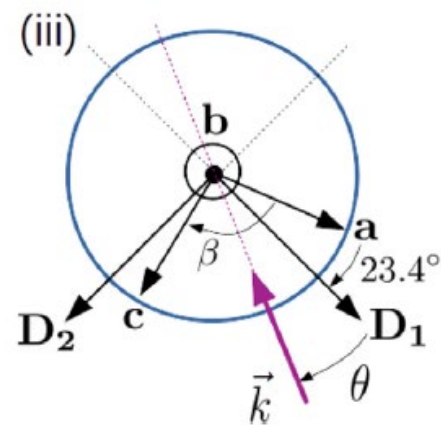
Polarization measurements for 1550 μm transitions

Y. Petit et al. Opt. Mater. X, **8**, 100062 (2020)

Blue: $E \parallel b \rightarrow$ Magnetic dipole variation.

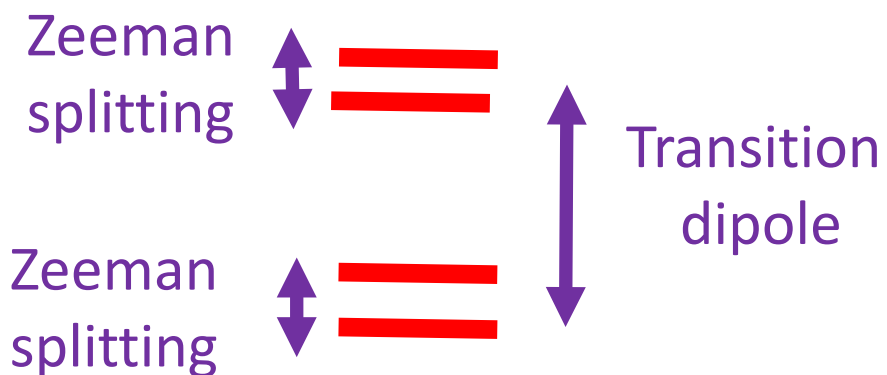
Red: $M \parallel b \rightarrow$ Electric dipole variation.

Y. Petit et al.

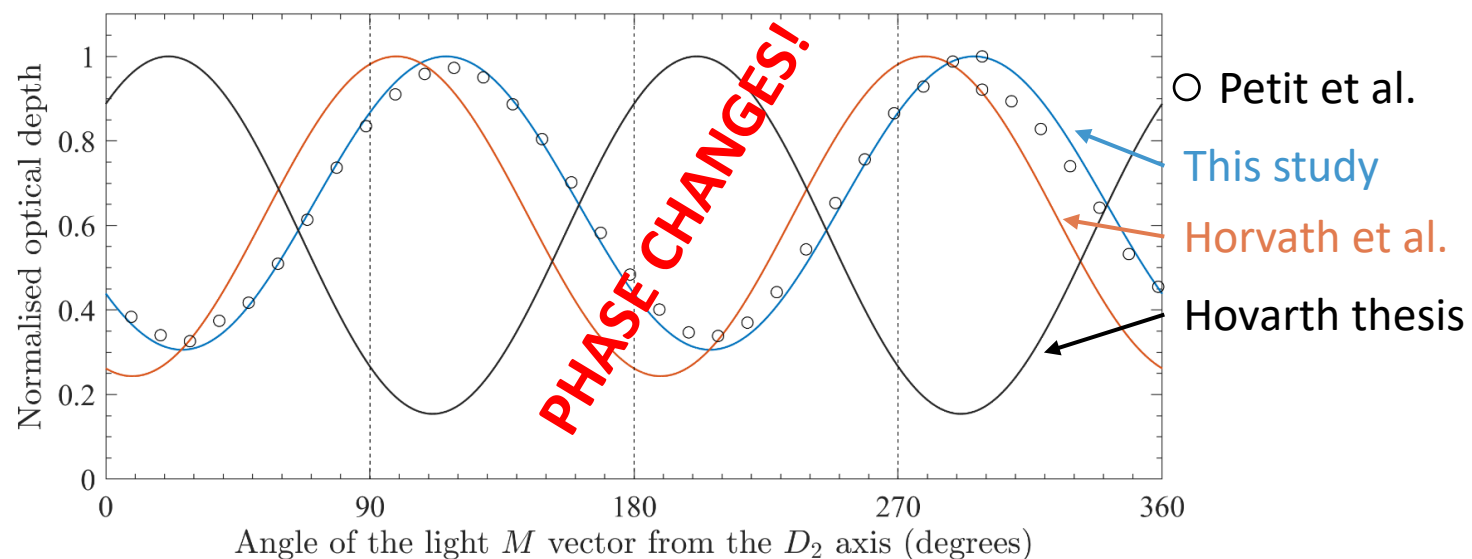


Er³⁺:Y₂SiO₅ Predictions: Polarization

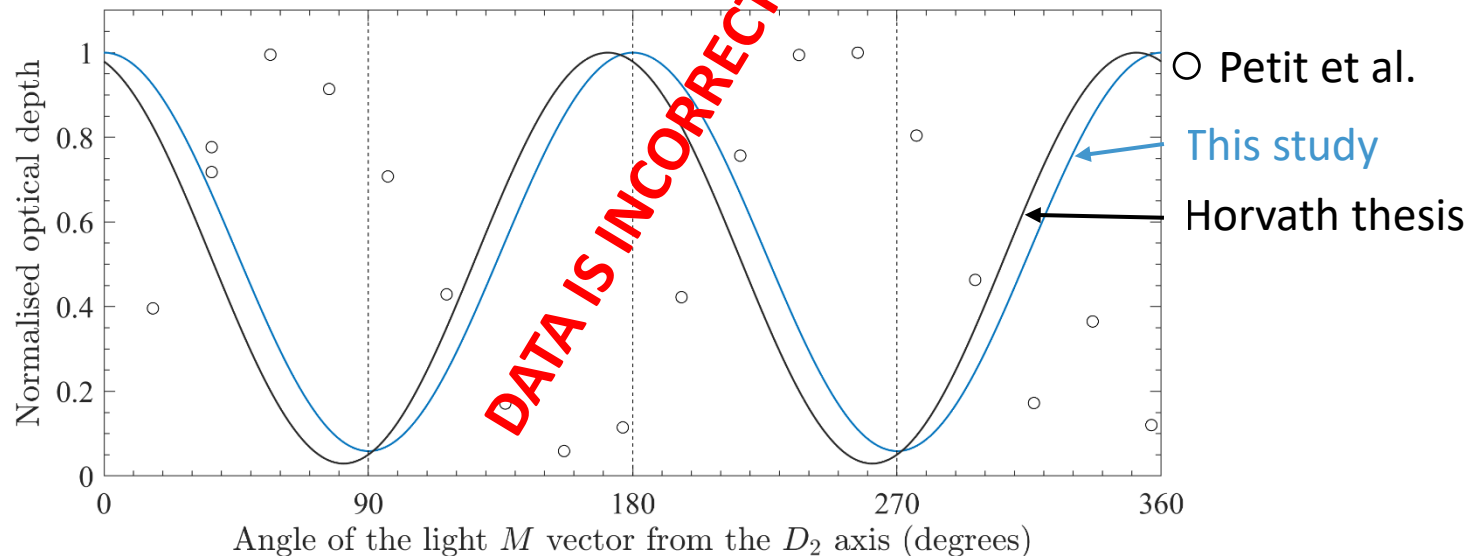
- We cannot (yet) calculate electric-dipole moments in low symmetry, but can calculate magnetic dipole moments (same matrix elements as Zeeman).
- Our predictions for Site 1 have improved with more data.
- Site 2 is still out of phase...
Calculation or measurement?
- Interesting that all fits reproduce Zeeman splitting, but not dipole moments **between** states.



Site 1 – magnetic dipole



Site 2 – magnetic dipole



Er³⁺:Y₂SiO₅ predictions: high-field hyperfine

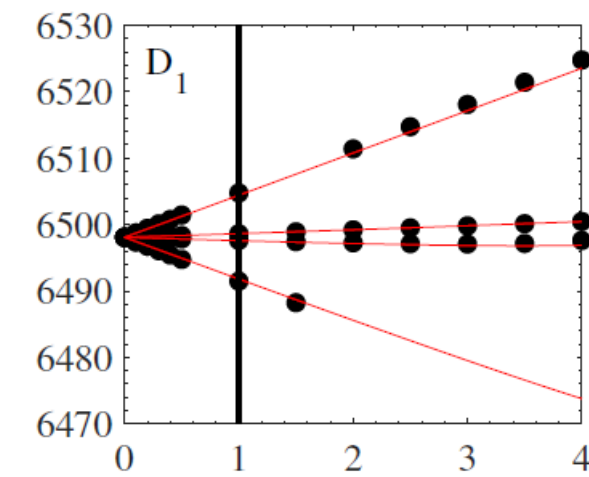
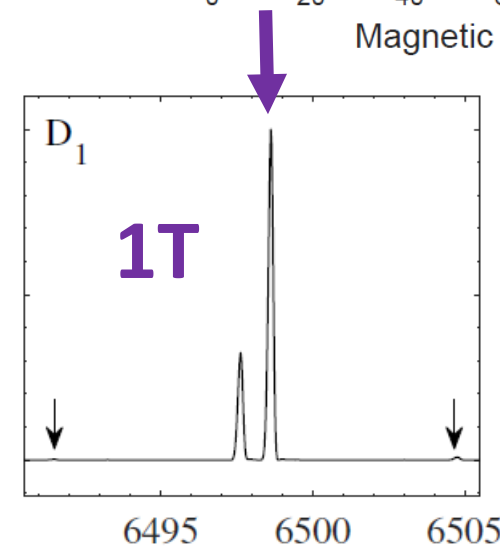
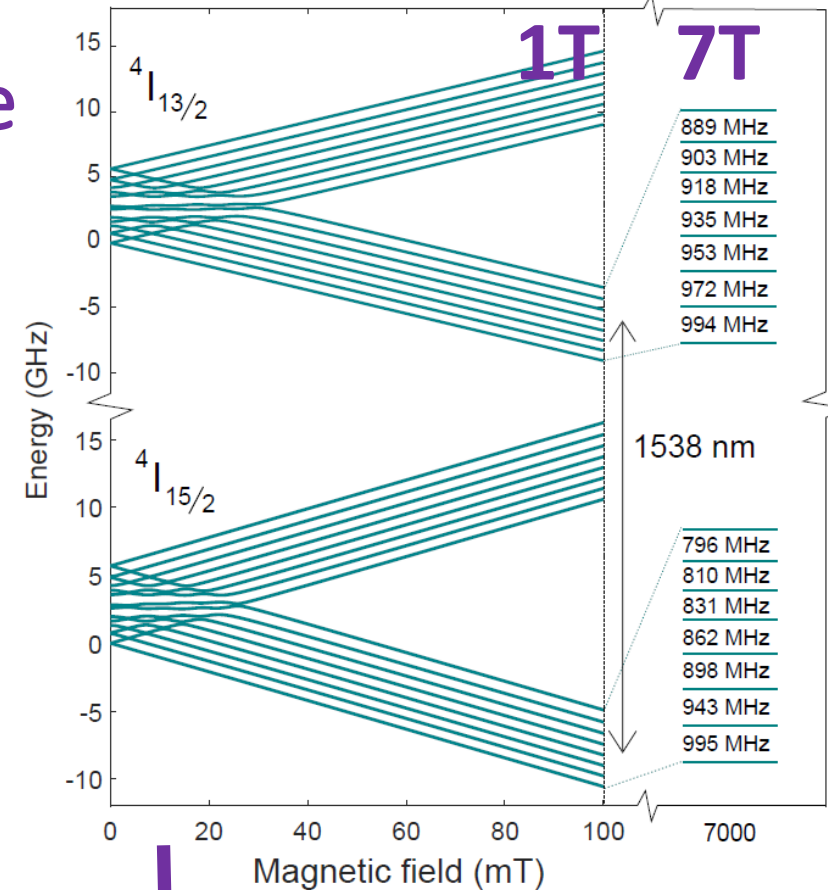
Hyperfine structure of Site 2 1.5μm transition:
7T along D₁.

Miloš Rančić et al. Nat. Phys., **4**, 50-54 (2018)

Non-linear regime where spin-Hamiltonian approach breaks down.

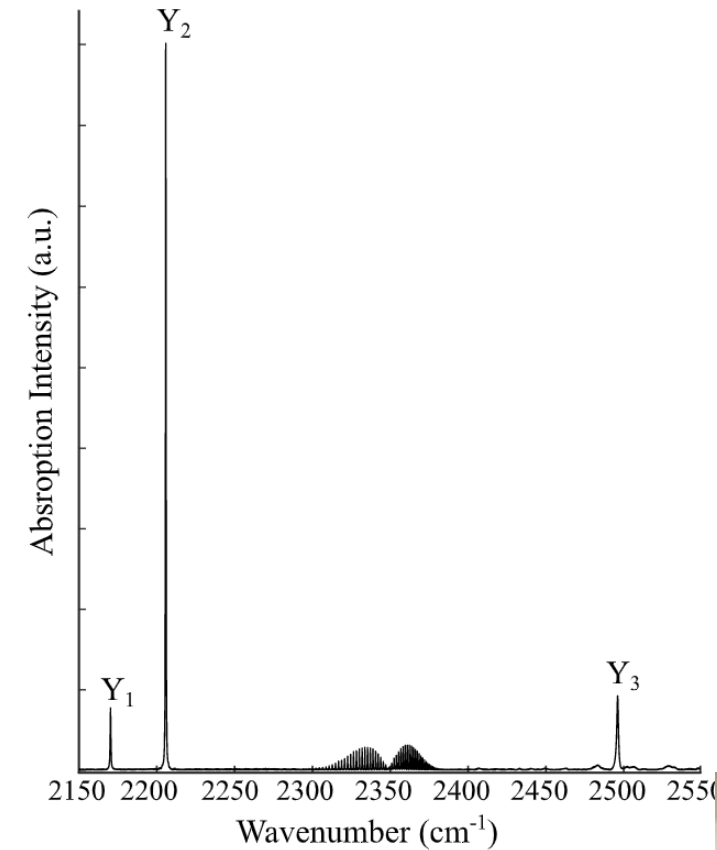
Unlike Site 1, our Site 2 fit does not include Y₁ hyperfine data – this is a *prediction*.

Splittings ΔE	⁴ I _{15/2} Z ₁		⁴ I _{13/2} Y ₁	
	This study	Ref. [5]	This study	Ref. [5]
Δ(1, 2)	897	995	928	994
Δ(2, 3)	881	943	912	972
Δ(3, 4)	865	898	895	953
Δ(4, 5)	849	862	879	935
Δ(5, 6)	833	831	863	918
Δ(6, 7)	817	810	847	903
Δ(7, 8)	801	796	831	889

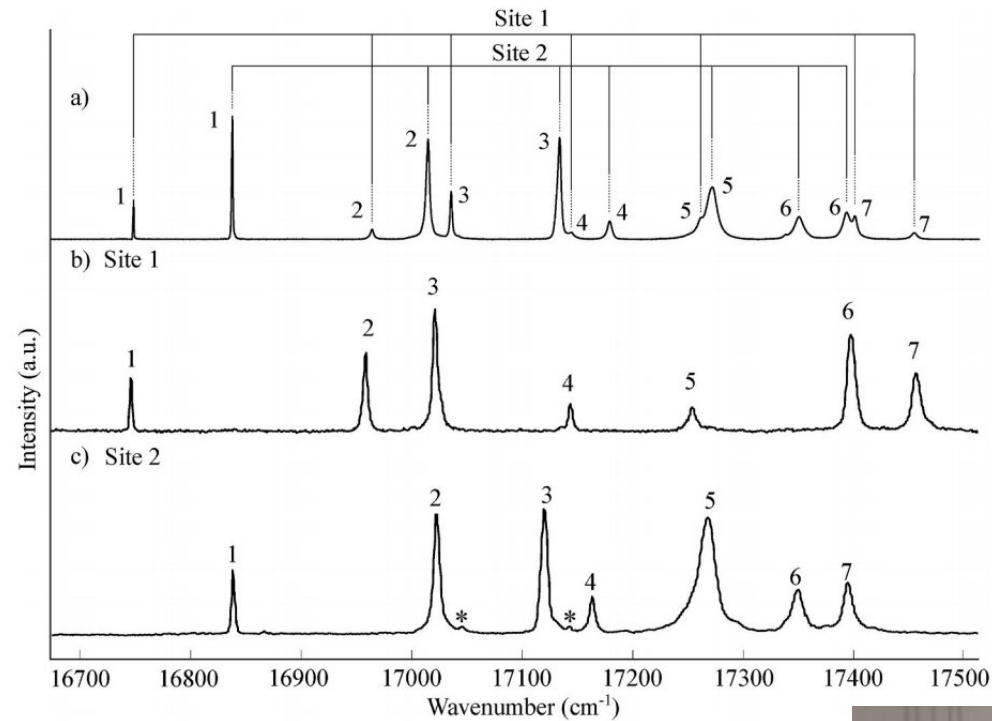


Other work by our group on Y_2SiO_5

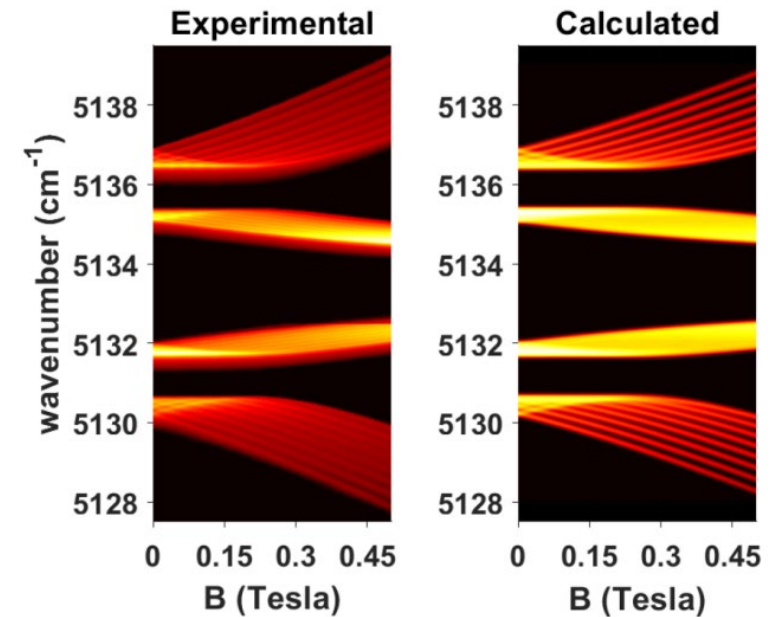
$\text{Ce}^{3+}:\text{Y}_2\text{SiO}_5$



$\text{Nd}^{3+}:\text{Y}_2\text{SiO}_5$

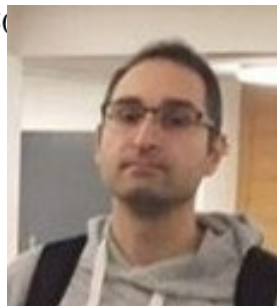


$\text{Ho}^{3+}:\text{Y}_2\text{SiO}_5$



Yashar Alizadeh et al.

Opt. Mater., **117**, 111114 (2021)



Yashar Alizadeh et al.

J. Lumin., **234**, 117959 (2021)



Sagar Mothkuri et al.

Phys. Rev. B, **103**, 104109 (2021)

Summary of spectroscopic work on Y_2SiO_5

We have shown that we can do crystal-field fits on low-symmetry systems.

But:

Proving that our fits are **unique** is still an open question.

Comparing fits with 27 parameters is difficult!

Perhaps ab-initio calculations are good enough to guide the fits?

The Journal of Physical Chemistry A, 2014, 118.

Spectroscopic Distinctions between Two Types of Ce^{3+} Ions in $\text{X}_2\text{-Y}_2\text{SiO}_5$: A Theoretical Investigation

Jun Wen,^{*,†} Chang-Kui Duan,[‡] Lixin Ning,^{*,§} Yucheng Huang,[§] Shengbao Zhan,[†] Jie Zhang,[†] and Min Yin[‡]

Table 5. Calculated Principal Values of the g-Tensors for Ce^{3+} Ions in $\text{X}_2\text{-YSO}$ in Comparison with the Experimental Values for Ce^{3+} Ions in LSO

principal values	site 1 (CN = 6)		site 2 (CN = 7)	
	calcd	exptl ^a	calcd	exptl ^a
g_x	0.015	0	0.394	0.55
g_y	1.317	1.3	1.743	1.69
g_z	2.297	2.3	2.216	2.25

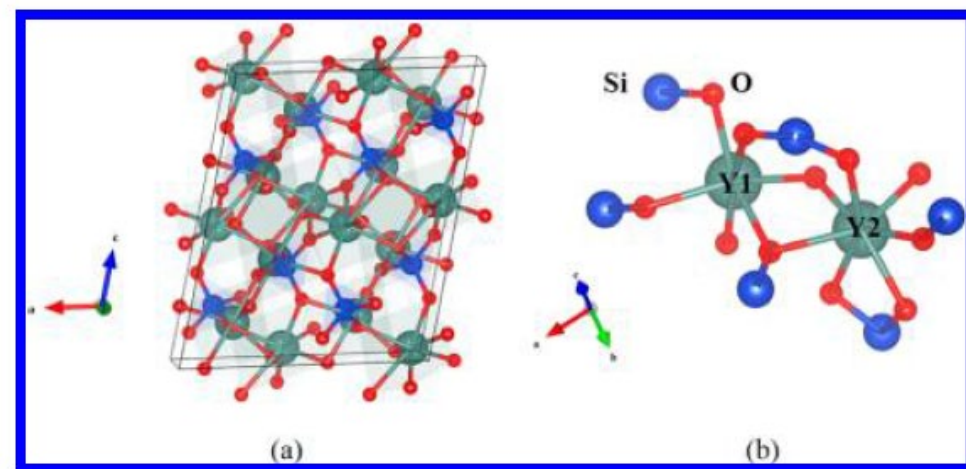


Figure 1. Schematic representations of local atomic structures around the two types of yttrium (Y1 and Y2) sites along with the unit cell of $\text{X}_2\text{-YSO}$.

Ce³⁺ in X₂-YSO

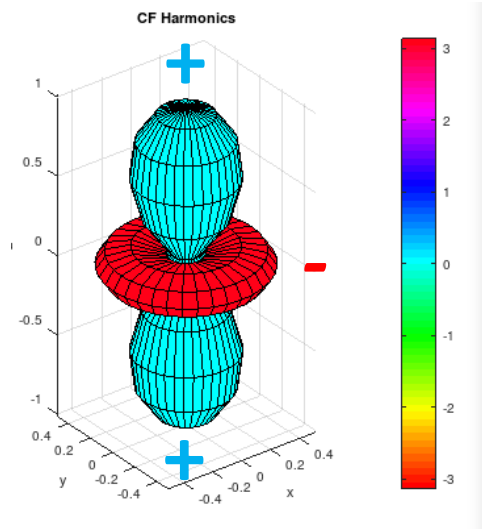
郝锐杰 (Ruijie HAO), 景伟国 (Weiguo JING)*

Chang-Kui Duan

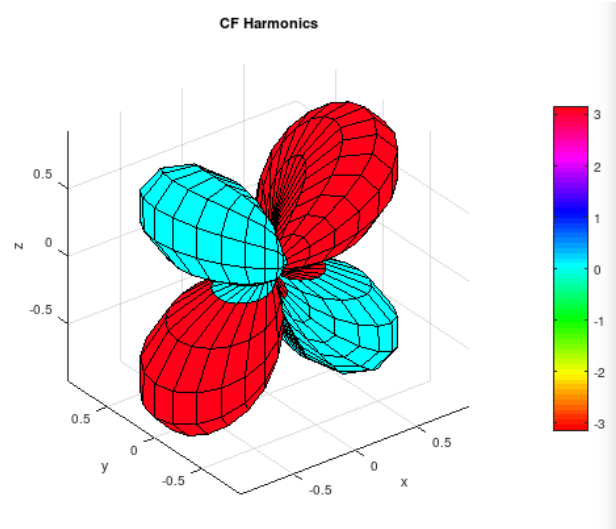
USTC, Hefei, China



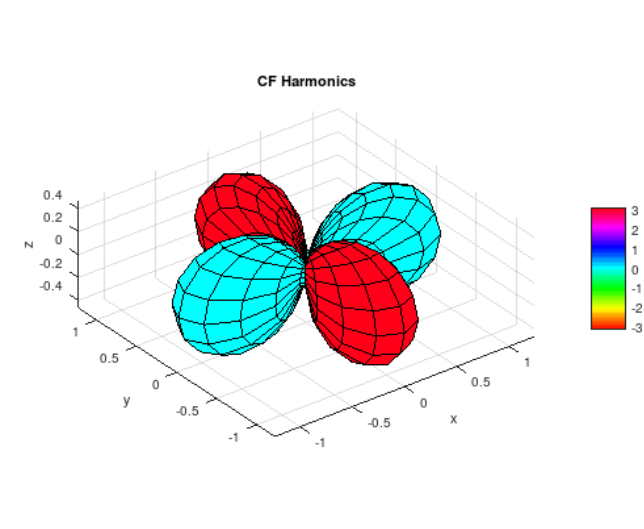
K=2 Spherical Harmonics - Potential



$$C^2_0(r)$$



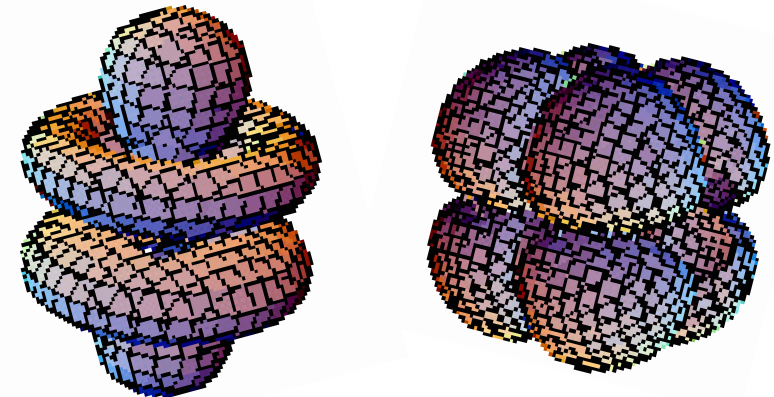
$$C^2_1(r) - C^2_{-1}(r)$$



$$C^2_2(r) + C^2_{-2}(r)$$

$$C^2_0(r) \sim 3z^2 - r^2 \sim 3\cos^2\theta - 1, \text{ etc.}$$

Potential acts on 4f orbitals:

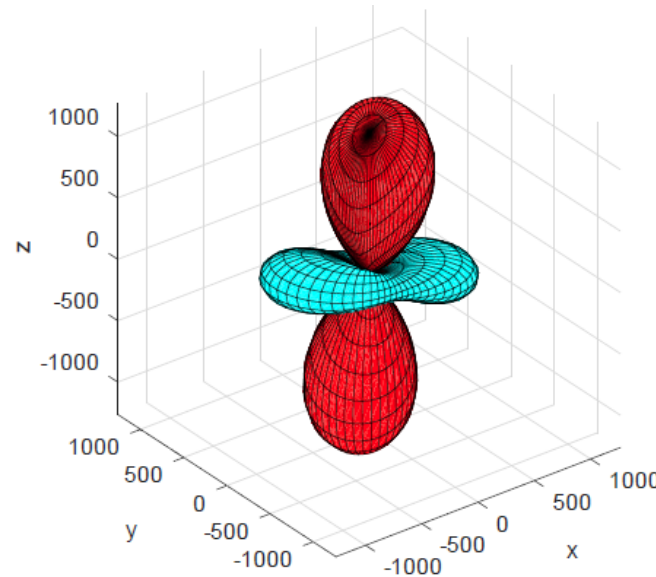
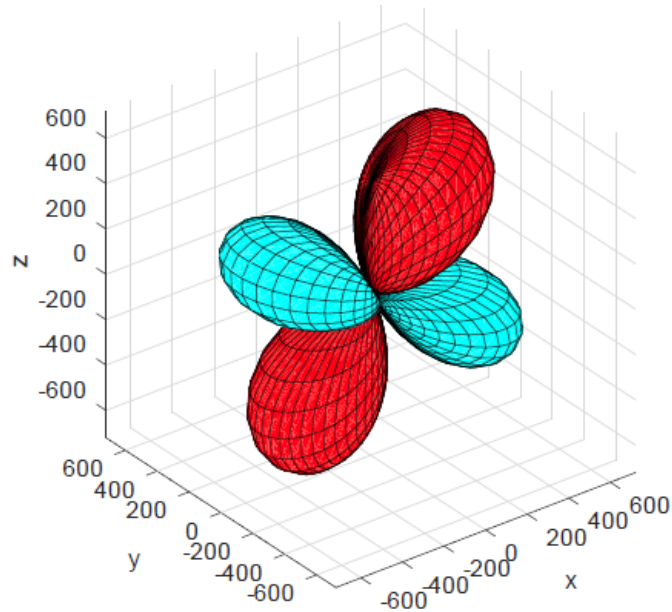


Fitted and ab-initio parameters for the k=2 part of the crystal-field **potential** (Er³⁺:YSO, site 1).

$$H_{CF} = \sum_{k,q} B_q^k C_q^{(k)}$$

Parameter fit

Ab-initio calculation



Parameter fit for Er³⁺

$$B_{20} = -479.6$$

$$B_{21} = 471.4 + 143.8i$$

$$B_{22} = 125.5 - 2.0i$$

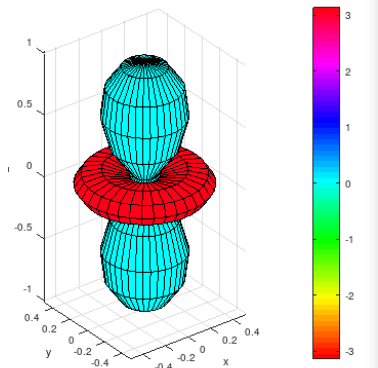
Ab-initio calculation for Ce³⁺

$$B_{20} = -1162;$$

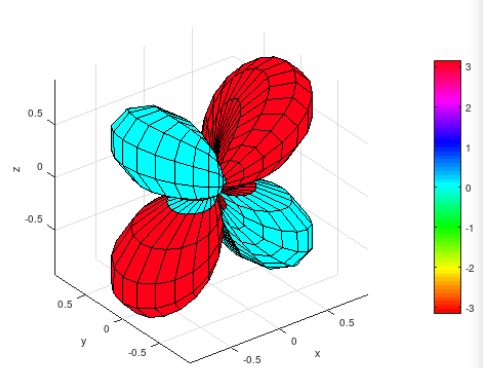
$$B_{21} = 362 - 198i;$$

$$B_{22} = 129 + 76i;$$

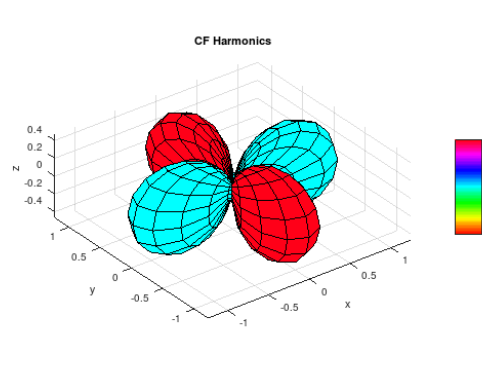
$C_0^2(r)$



$C_1^2(r) - C_{-1}^2(r)$



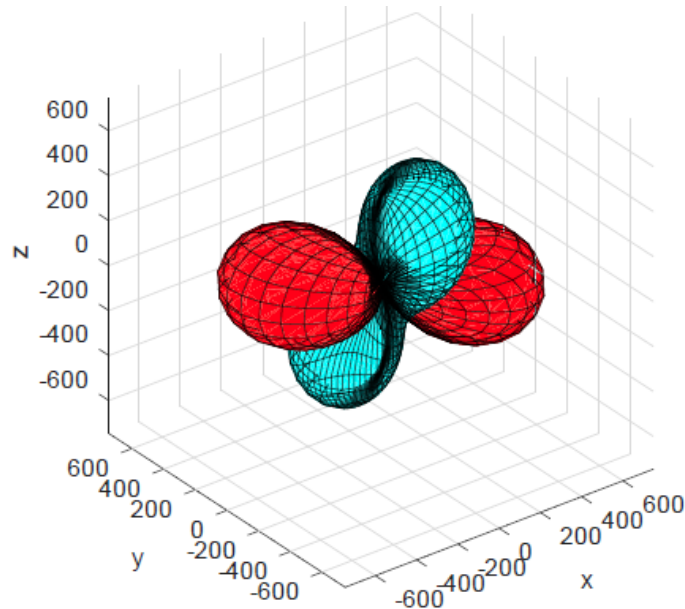
$C_2^2(r) + C_{-2}^2(r)$



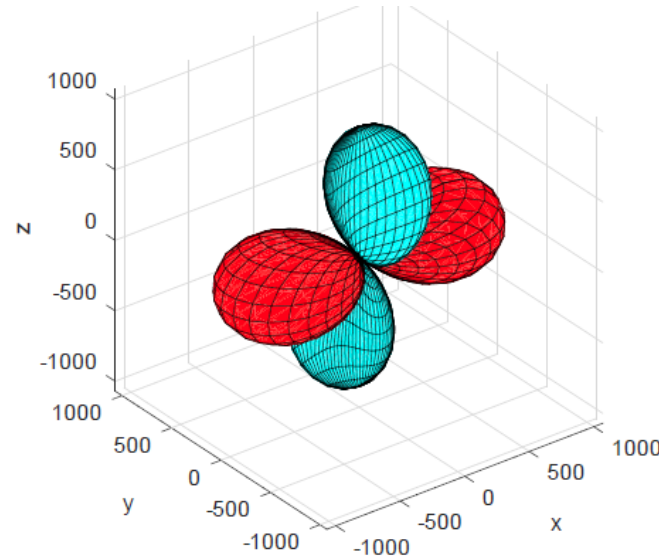
Fitted and ab-initio parameters for the k=2 part of the crystal-field potential (Er³⁺:YSO, site 2).

$$H_{CF} = \sum_{k,q} B_q^k C_q^{(k)}$$

Parameter fit



Ab-initio calculation



Parameter fit for Er³⁺

$$B_{20} = 389$$

$$B_{21} = -325.7 - 95.8i$$

$$B_{22} = -368.5 + 53.7i$$

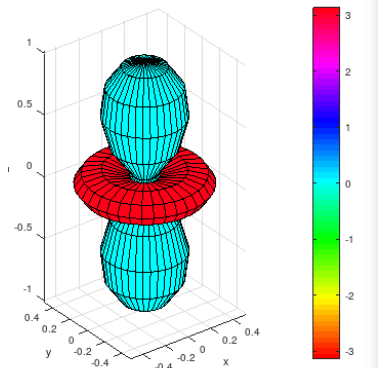
Ab-initio calculation for Ce³⁺

$$B_{20} = 925;$$

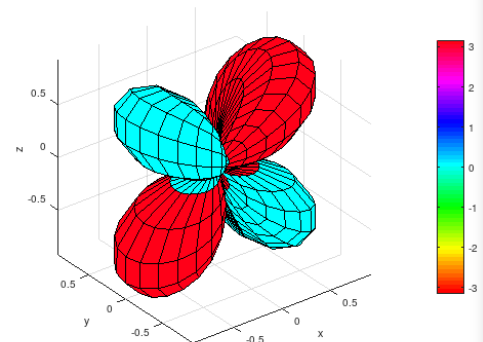
$$B_{21} = -30 - 219i$$

$$B_{22} = -496 + 46i$$

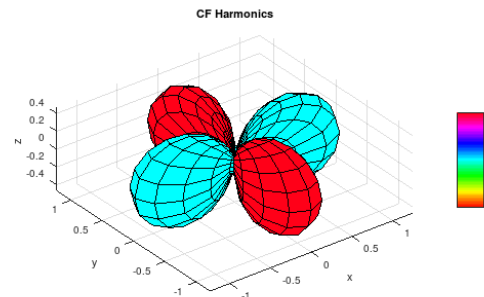
$C_0^2(r)$



$C_1^2(r) - C_{-1}^2(r)$

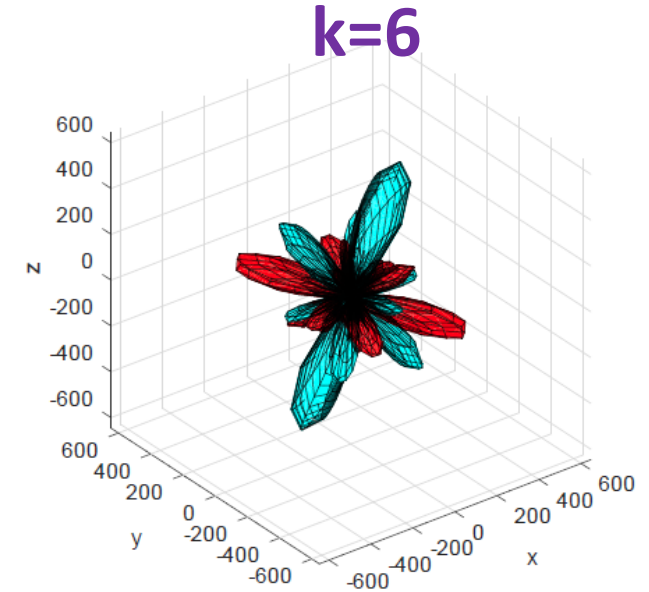
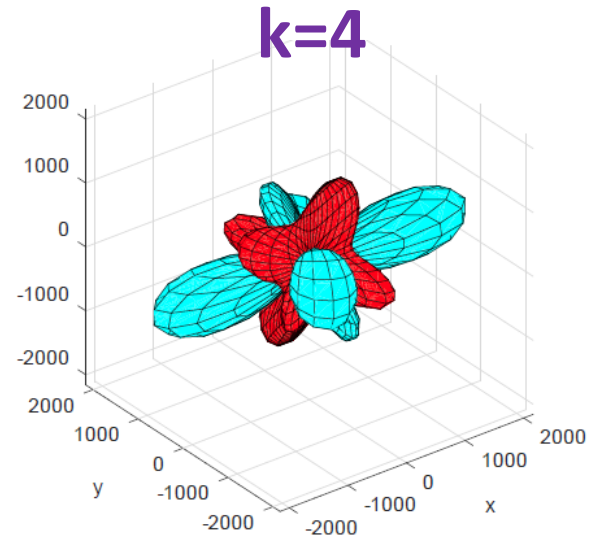
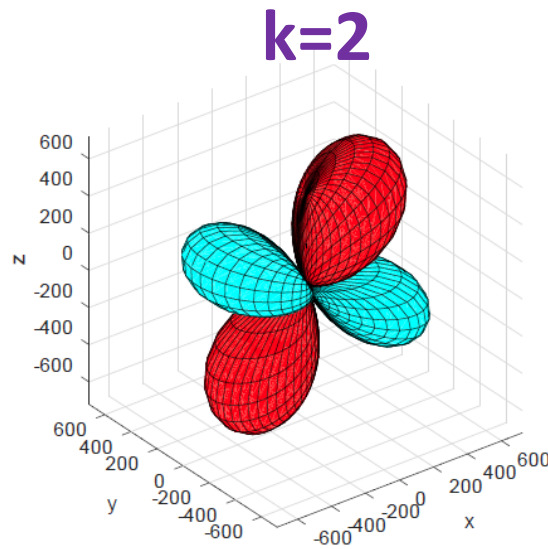


$C_2^2(r) + C_{-2}^2(r)$

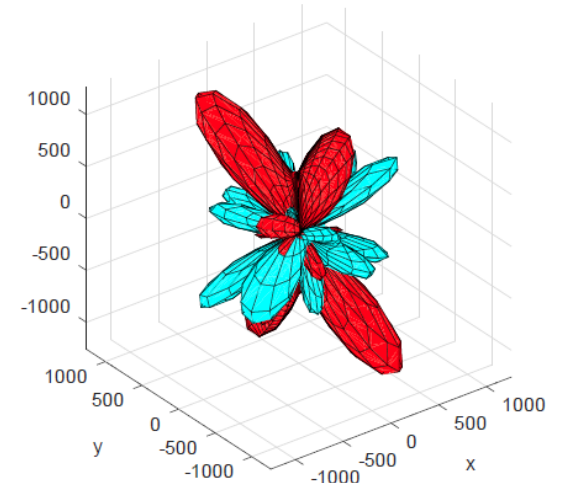
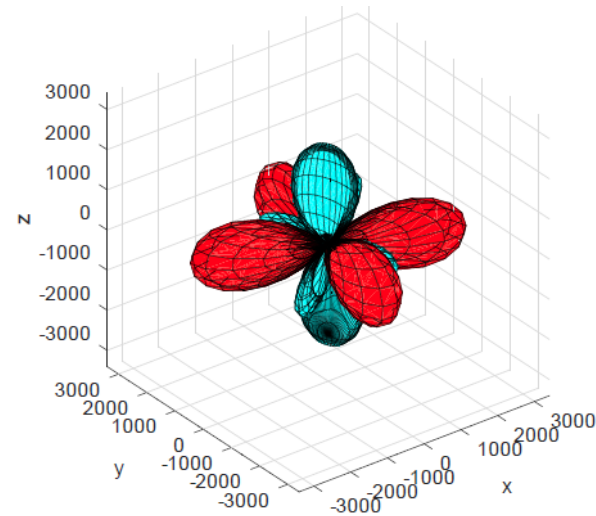
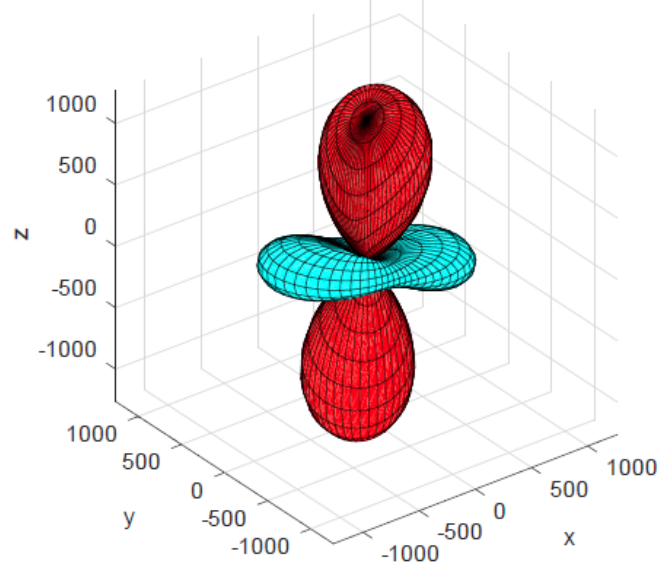


Fitted and ab-initio parameters for the $k=2,4,6$ parts of the crystal-field potential ($\text{Er}^{3+}:\text{YSO}$, site 1).

Parameter fit

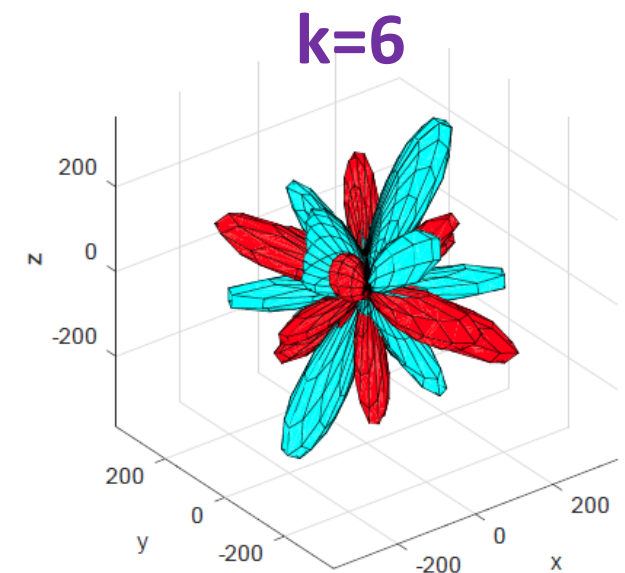
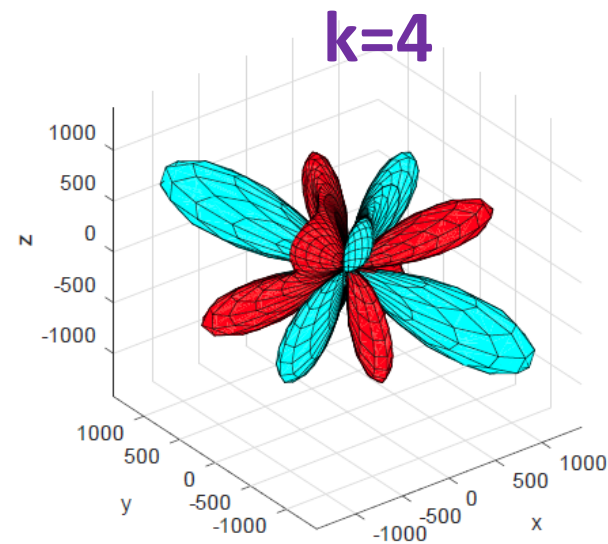
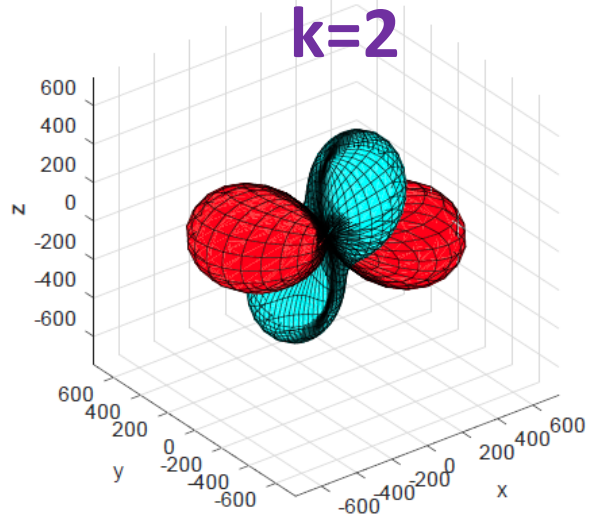


Ab-initio

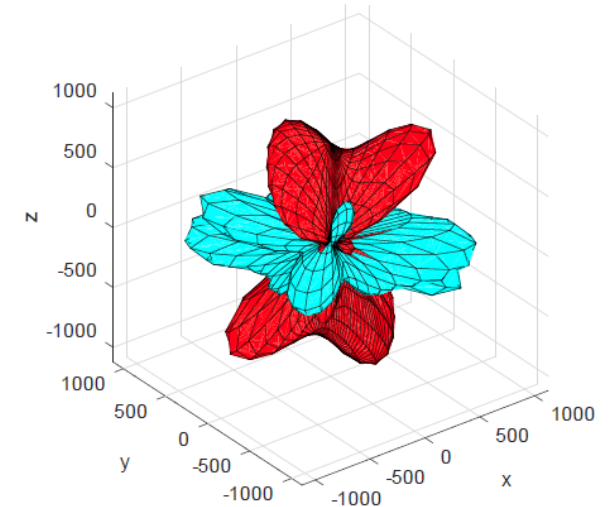
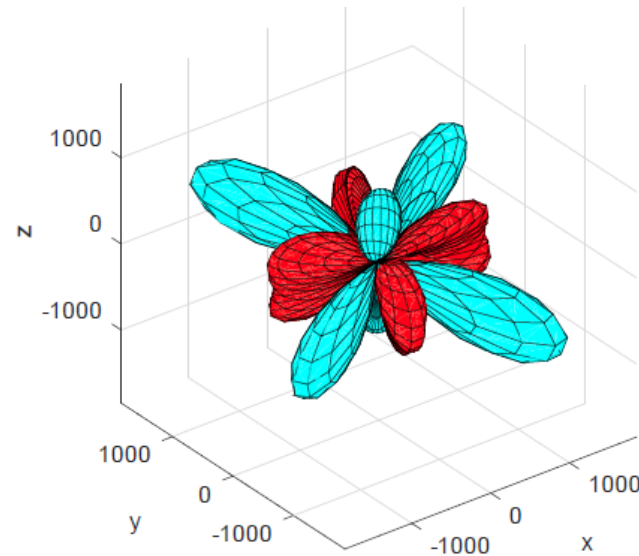
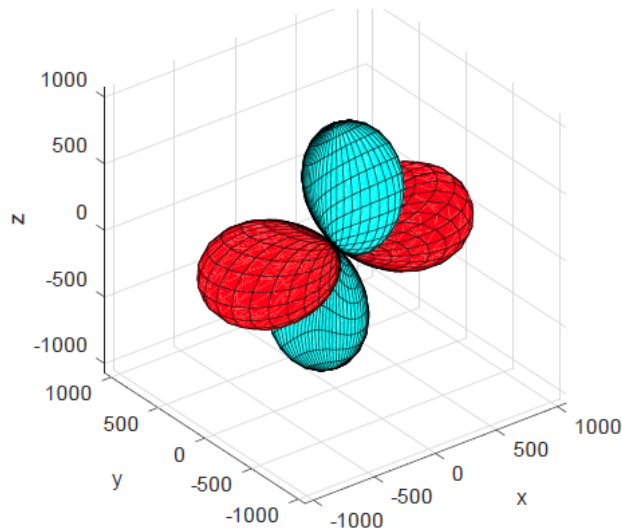


Fitted and ab-initio parameters for the $k=2,4,6$ part of the crystal-field potential ($\text{Er}^{3+}:\text{YSO}$, site 2).

Parameter fit



Ab-initio



In Progress: Prediction of the hyperfine structure of $^{151}\text{Eu}^{3+}:\text{Y}_2\text{SiO}_5$

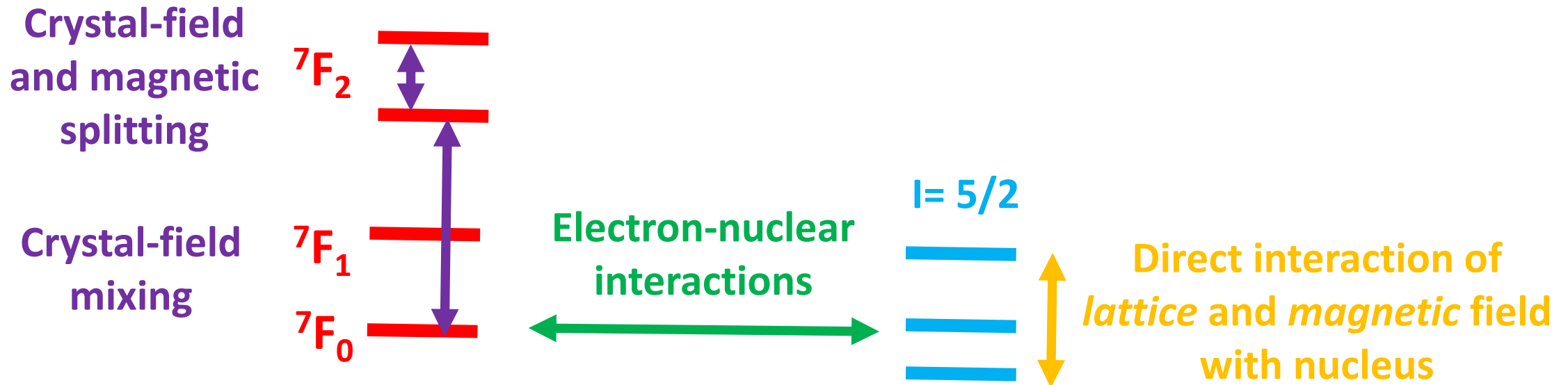
The $\text{Sm}^{3+}:\text{Y}_2\text{SiO}_5$ parameters are scaled and fitted to predict the hyperfine structure of the $^7\text{F}_0$ ground state of $\text{Eu}^{3+}:\text{Y}_2\text{SiO}_5$ (Site 1)

Spin Hamiltonian: $\mathcal{H} = \mu_B \mathbf{B} \cdot \mathbf{g} \cdot \mathbf{S} + \mathbf{I} \cdot \mathbf{A} \cdot \mathbf{S} + \mathbf{I} \cdot \mathbf{Q} \cdot \mathbf{I} - \mu_n g_n \mathbf{B} \cdot \mathbf{I}$

Contributions from

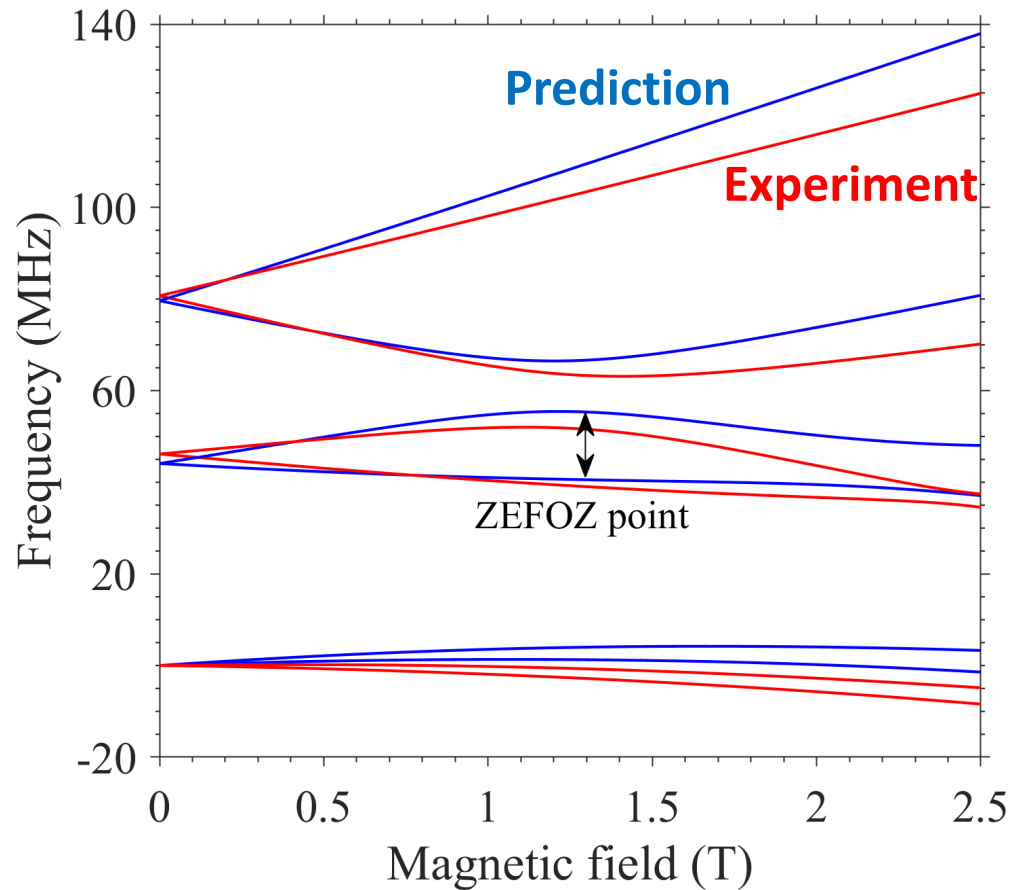
1. Electronic effects due to mixing of $^7\text{F}_2$ with $^7\text{F}_0$ by crystal field.
2. Direct interaction of lattice and magnetic field with nucleus.

See: Smith et al, Complete crystal-field calculation of Zeeman hyperfine splittings in europium.
Phys. Rev. B 105: 125141



In Progress: Predictions of the hyperfine structure of $^{151}\text{Eu}^{3+}:\text{Y}_2\text{SiO}_5$

Nuclear spin: $I=5/2$

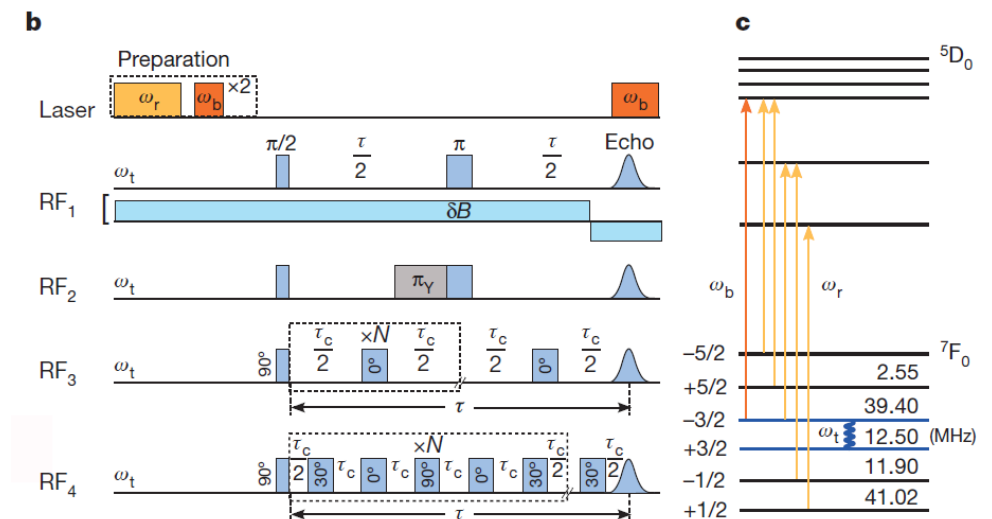


The $\text{Sm}^{3+}:\text{Y}_2\text{SiO}_5$ parameters were scaled to predict the hyperfine structure of the $^7\text{F}_0$ ground state of $\text{Eu}^{3+}:\text{Y}_2\text{SiO}_5$ (Site 1)

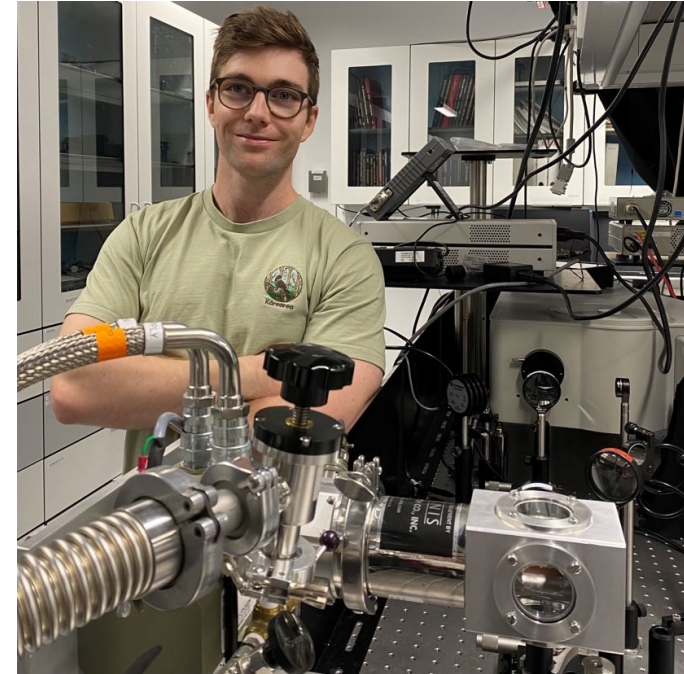
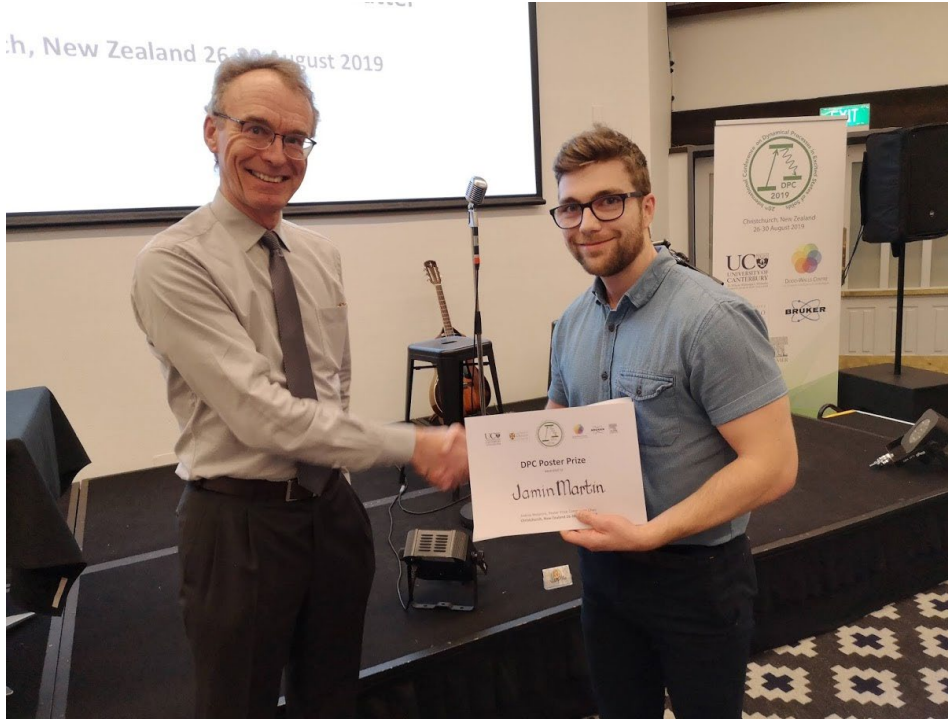
The experiment and prediction are for a magnetic field in the particular direction that gives the ZEFOZ point used in Zhong et al. Nature paper demonstrating six-hour coherence.

Contributions from:

1. Electronic effects due to mixing of $^7\text{F}_2$ with $^7\text{F}_0$ by crystal field.
2. Direct interaction of lattice and magnetic field with nucleus.



Magnetic field effects in nanoparticles - Jamin Martin

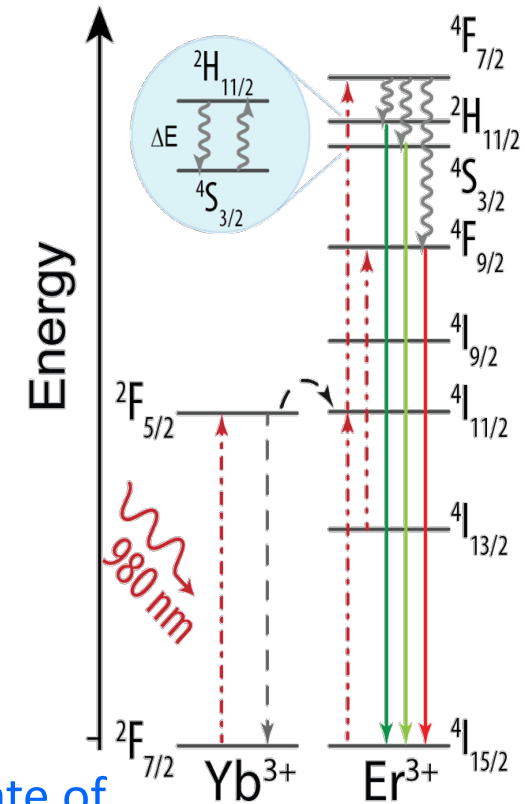
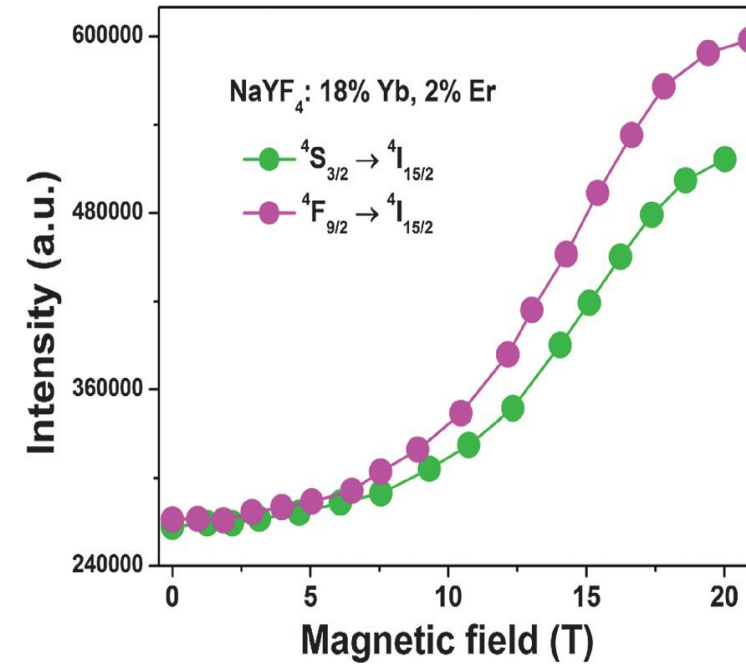
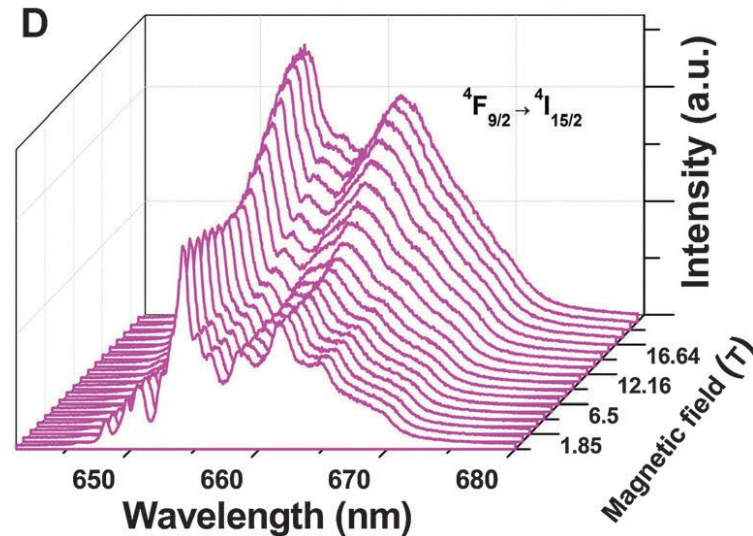
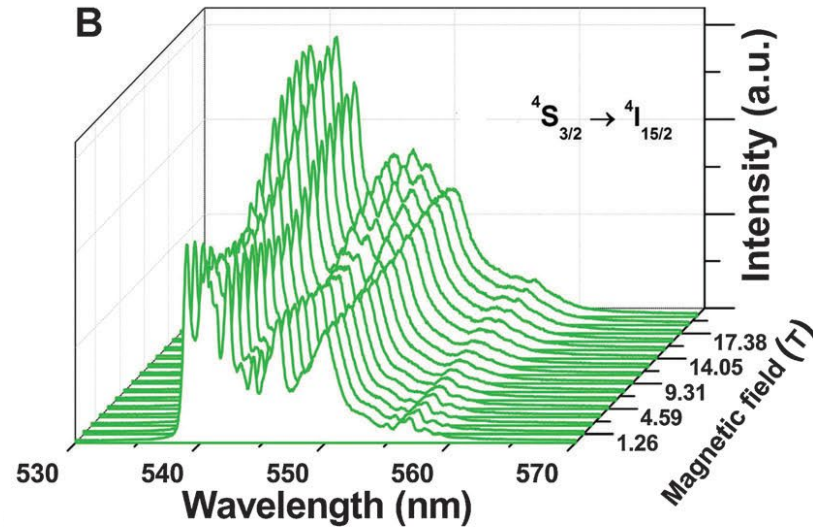


Review: Y. Luo, Z. Chen, S. Wen, Q. Han, L. Fu, L. Yan, D. Jin, J.-C. G. Bünzli, G. Bao, Magnetic regulation of the luminescence of hybrid lanthanide-doped nanoparticles, Coordination Chemistry Reviews 469 (2022) 214653

We use KY_3F_{10} , which has high symmetry (C_{4v}) and so calculations are possible of energy levels and intensities.

Magnetic Fields

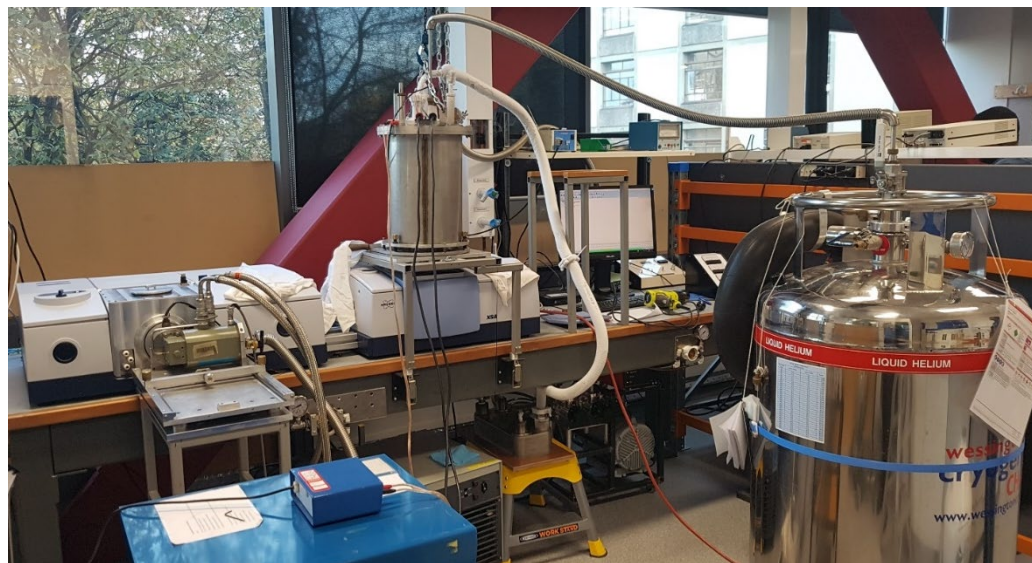
Yb/Er NaYF₄



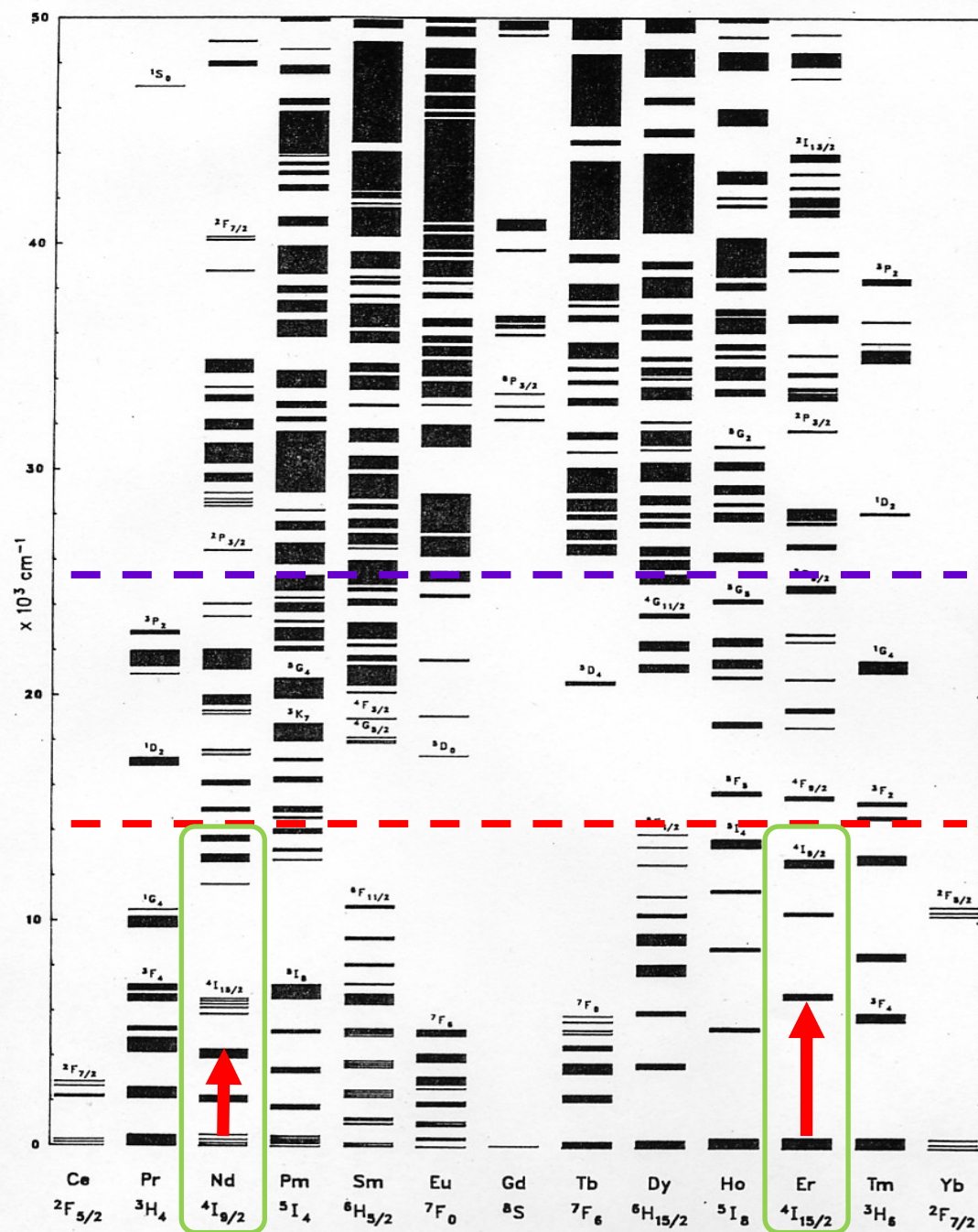
“... It is **highly possible** that the rate of excited state absorption of Er³⁺ is enhanced with magnetic field, because the energy level splitting **might** reduce the energy difference between the excitation light (975 nm) and the gap between the $4I_{11/2}$ and $4F_{7/2}$ levels of Er³⁺...”

$\text{Er}^{3+}/\text{Nd}^{3+} : \text{KY}_3\text{F}_{10}$

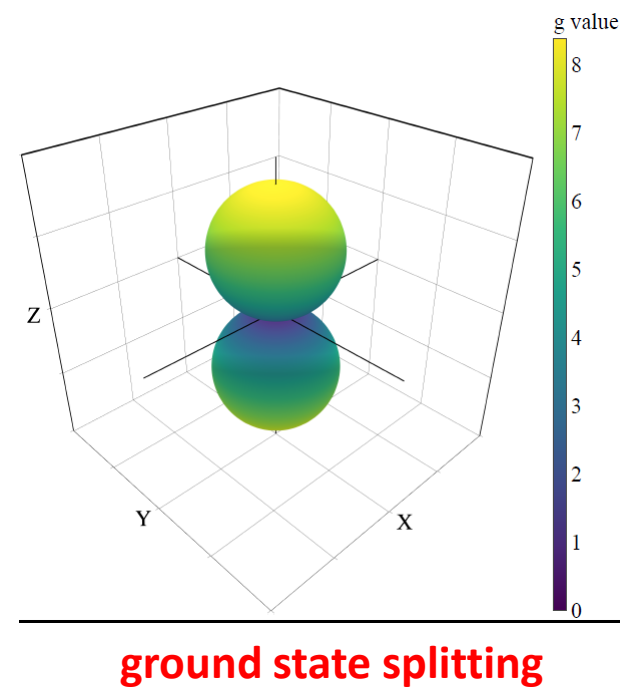
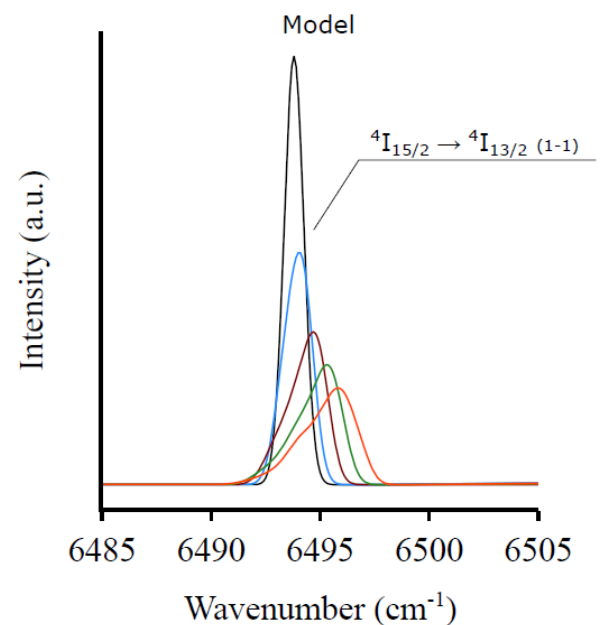
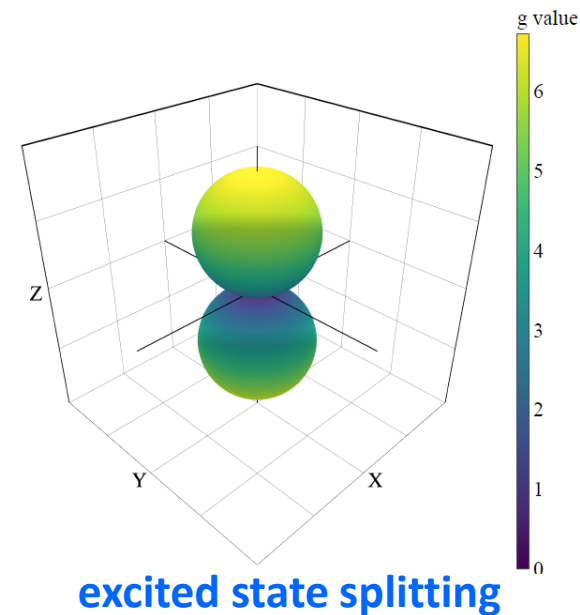
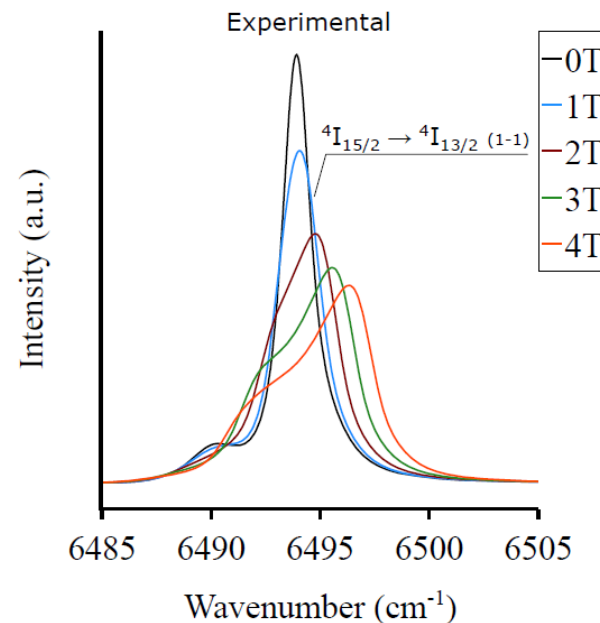
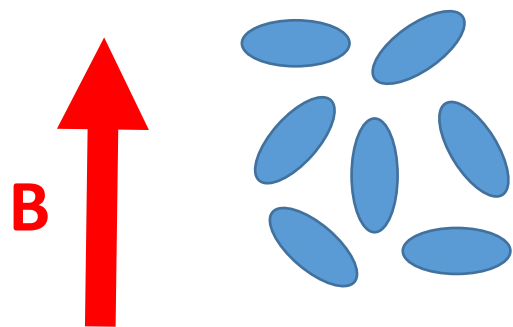
Jamin Martin



ENERGY LEVELS OF THE +3 LANTHANIDES IN LaF_3



Er³⁺:KY₃F₁₀ nanoparticles

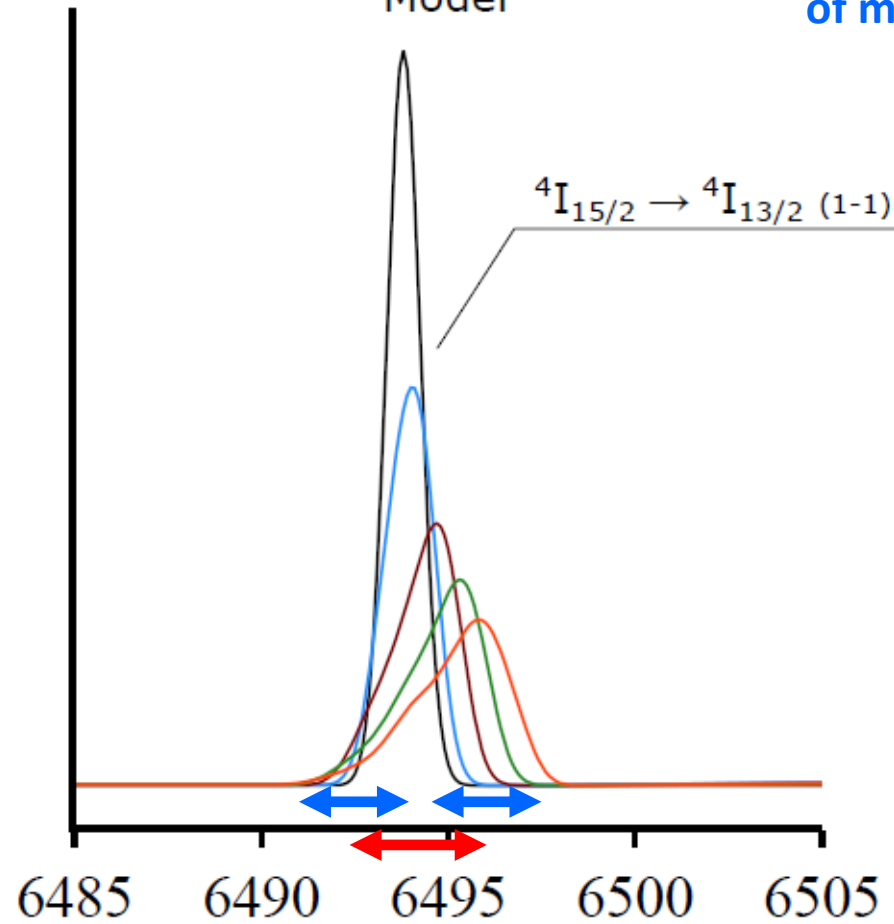


Not symmetrical: Transitions from lower ground state are more intense due to Boltzmann factors.





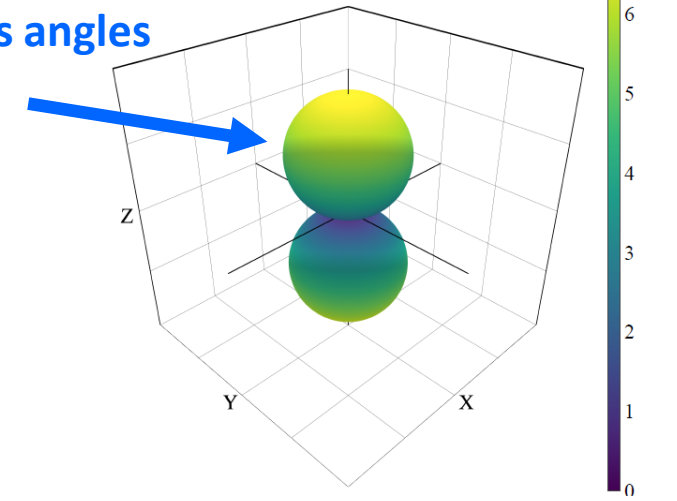
Model



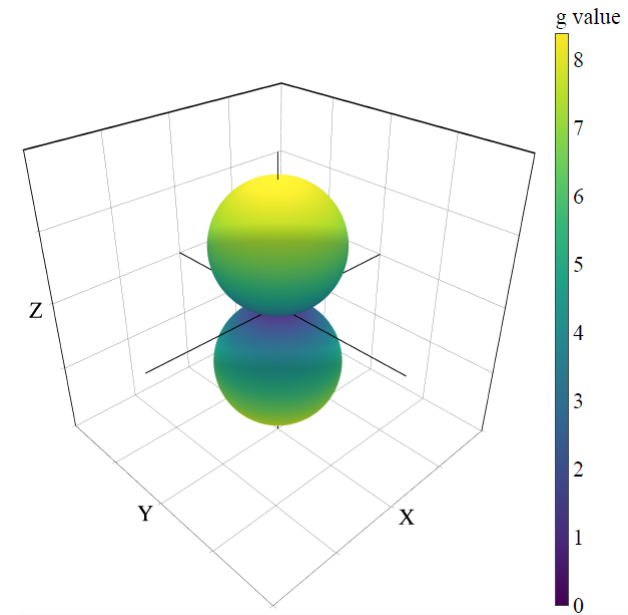
1 2 3 4

lower ground state –
higher population

Random orientation probes
populations at various angles
of magnetic field.



excited state splitting

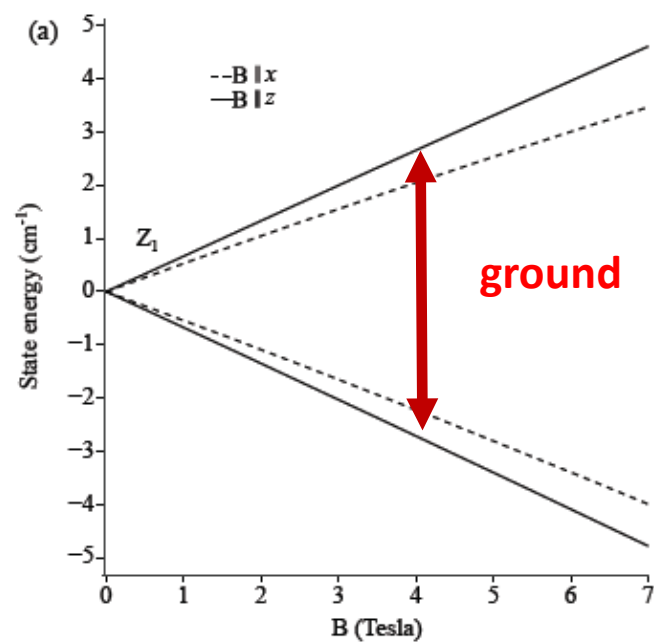
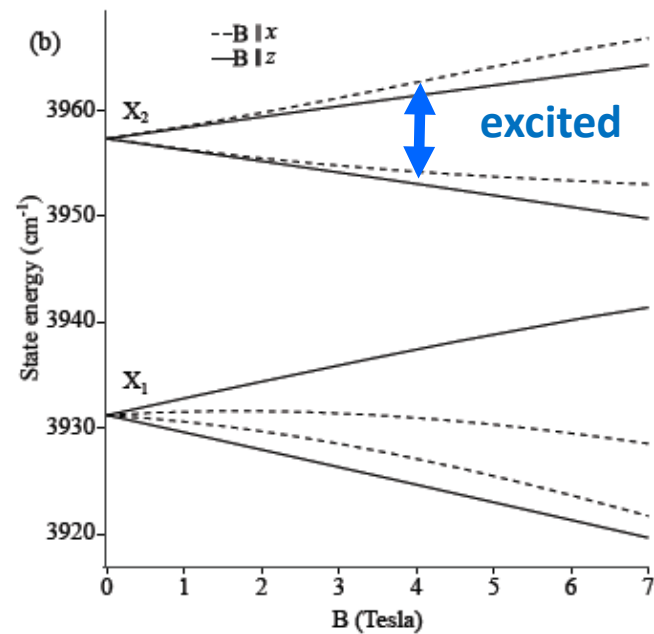
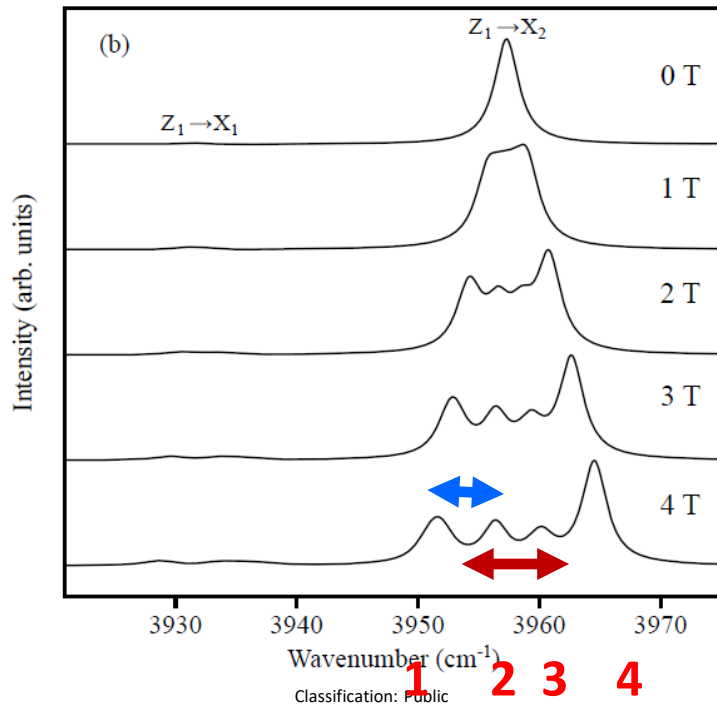
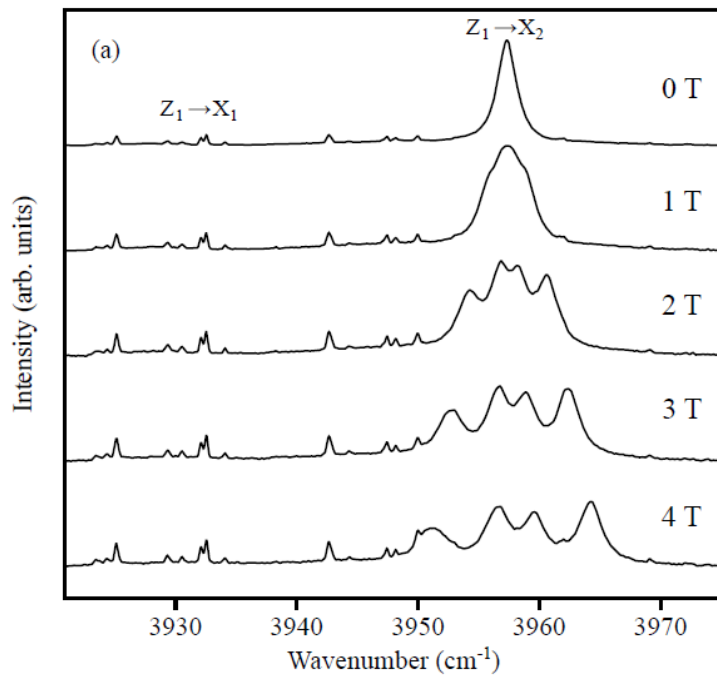
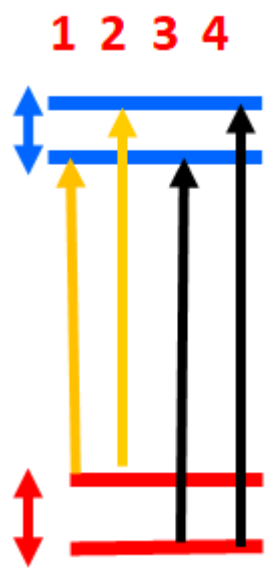
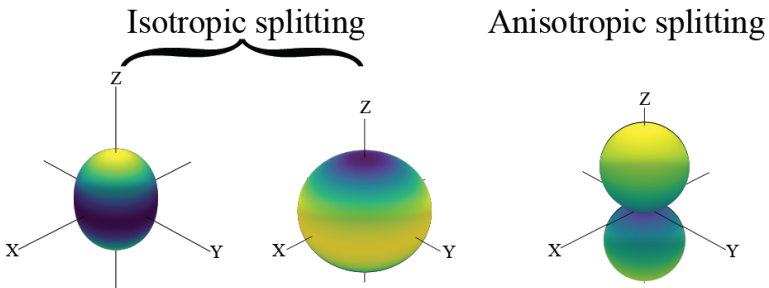


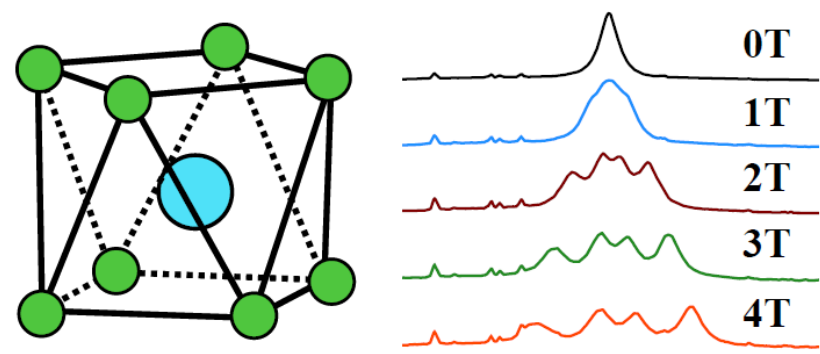
ground state splitting

Peak splitting not at maximum possible splitting.
This has to do with integral over solid angle of splitting function.

Nd³⁺:KY₃F₁₀

Transition selected for isotropic splitting





Fit including magnetic splittings gives a good reproduction in the splittings, including non-linear effects.

Jamin Martin et al.
Optical Materials X, 2022, 100181.

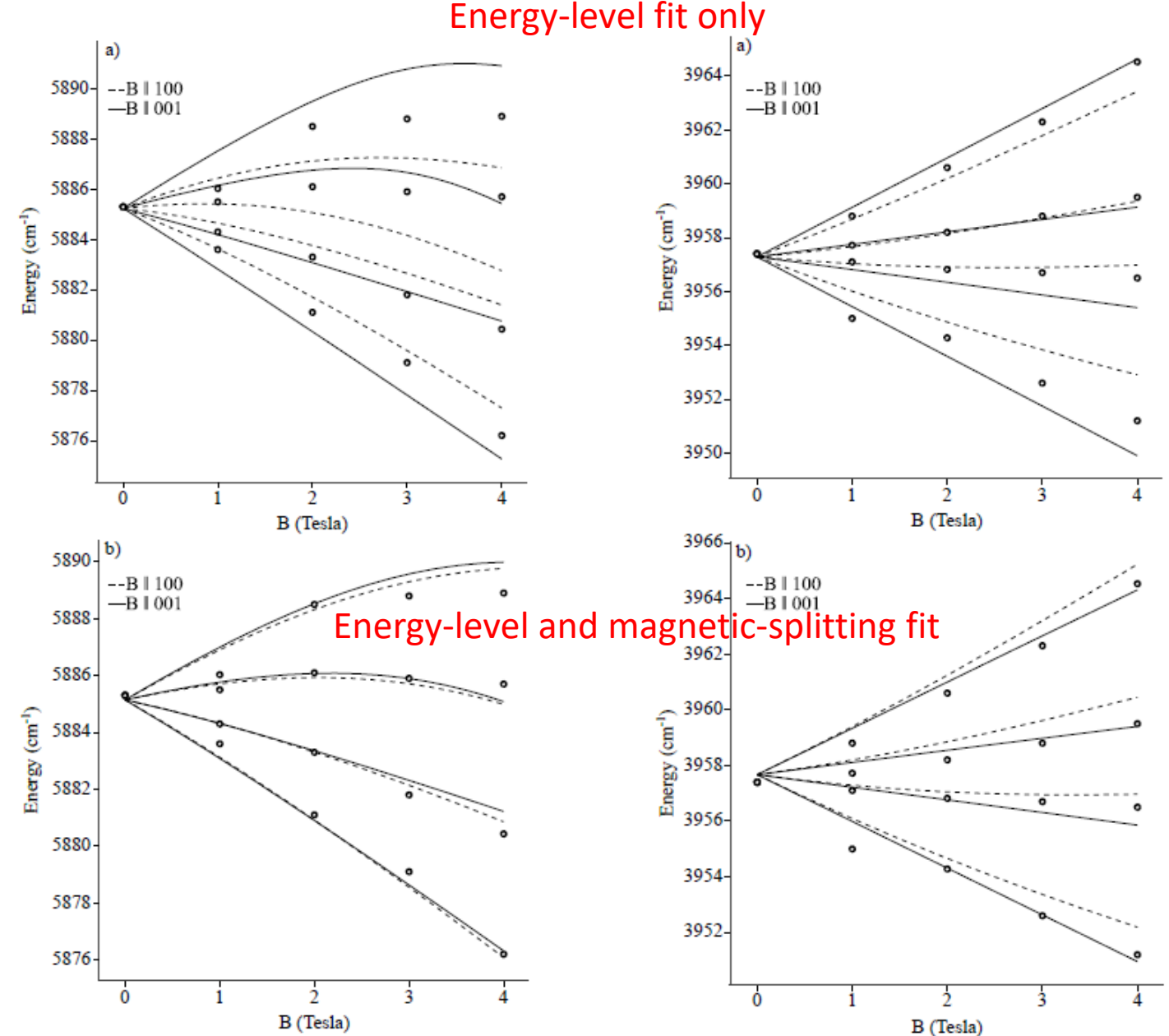


Figure 3: Calculated Zeeman splittings for the $Z_1\gamma_6 \rightarrow W_1\gamma_7$ transition. Energies only fit (a) and energies + splittings fit (b)

Figure 4: Calculated Zeeman splittings for the $Z_1\gamma_6 \rightarrow X_2\gamma_6$ transition. Energies only fit (a) and energies + splittings fit (b)

Conclusions

- Crystal-field modelling for several rare-earth ions: Ce^{3+} , Nd^{3+} , Sm^{3+} , Ho^{3+} , Er^{3+} in Y_2SiO_5 (YSO).
- Other groups include Yb^{3+} : Zhou et al. Inorganic Chemistry 59:13144 (2020).
- Due to the C_1 symmetry, directional magnetic data is required to determine unique sets of parameters. [May still not be unique!]
- Parameters can be scaled between ions.
- Prediction of polarization and high-field hyperfine structure for $\text{Er}^{3+}:\text{Y}_2\text{SiO}_5$.
- In progress:
 - Comparison with ab-initio calculations.
 - Micro and nanocrystals.
 - Prediction of magnetic-hyperfine structure for $\text{Eu}^{3+}:\text{Y}_2\text{SiO}_5$.
 - Work on other ions.



TE WHAI AO
DODD-WALLS CENTRE
for Photonic and Quantum Technologies



Tutorials on Electronic Structure

www2.phys.canterbury.ac.nz/~mfr24/

Google: **Mike Reid, Personal Home Page Canterbury**

mike.reid@canterbury.ac.nz



TE WHAI AO
DODD-WALLS CENTRE
for Photonic and Quantum Technologies

